UNIVERSITÀ DEGLI STUDI DI PADOVA

UNIVERSITÀ DEGLI STUDI DI PADOVA

INDUSTRIAL ENGINEERING DEPARTMENT

MASTER DEGREE COURSE IN
ENERGY ENGINEERING

Power to hydrogen to power: thermodynamic and economic assessment of an electrolyser - hydrogen turbine system

Supervisors:
PROF. PAUL LEAHY
PROF. ANNA STOPPATO

Graduating:
TOMMASO BRONDOLIN
2054793

Academic Year 2023/2024
Graduation Date 25/10/2024

Abstract

In the realm of sustainable energy solutions, the synergy of wind energy, hydrogen, and converted gas turbines could be an important combination to ensure a smooth transition towards a less polluting electricity grid. Wind turbines serve as a primary driver, converting the kinetic energy of the wind into renewable electricity, while the utilization of green hydrogen, produced from electrolysis powered by renewable energy, provides a versatile energy vector that can replace the fossil fuels. A noteworthy way to employ this vector to close the cycle from power to power, is the reconfiguration of gas turbines for hydrogen combustion. This entails the retrofitting of existing gas turbine infrastructure, adapting it for hydrogen fuel, thereby enabling a cleaner and more sustainable mode of energy production. This innovative approach aligns with the imperative of repurposing legacy systems in the pursuit of reduced carbon emissions. The integration of wind energy, hydrogen, and converted gas turbines will be analysed focusing on the thermodynamical and economical aspects in order to assess its feasibility in the near future.

However, the seamless implementation of this technical triad will be greatly affected by evolving technological standards, substantial infrastructure investments, and the formulation of adaptive policy frameworks.

Contents

List of Figures

List of Tables

Nomenclature

AE/AEL Alkaline Electrolysis

DLE Dry Low Emissions

DLN Dry Low NOx

EGR Exhaust Gas Recirculation

FLOX Flameless Oxidation

GHG Green House Gases

HER Hydrogen Evolution Reaction

HTE/HTEL High Temperature Electrolysis

LCOCH Levelized Cost of Compressed Hydrogen

LCOE Levelized Cost of Electricity

LCOE(C) Levelized Cost of Electricity for stored hydrogen

LCOH Levelized Cost of Hydrogen

MILD Moderately Intense Low Oxygen Dilution

NTP Normal Temperature and Pressure

OER Oxygen Evolution Reaction

P2P Power to Power

PEM/PEME Proton Exchange Membrane

PGP Power to Gas to Power

PHP Power to Hydrogen to Power

RQL Rich-Burn/Quick-Mix/Lean-Burn

rSOC Reversible Solid Oxide Cell

SEAI Sustainable Energy Authority of Ireland

SOE/SOEC Solid Oxide Electrolysis

Chapter 1

Introduction

Gas turbines are widely used for electricity generation due to their ability to produce high power within a compact space, their rapid start-up times, and their potential for integration with other power generation systems like Rankine cycles. Gas turbines are mainly employed in Brayton cycles, which consist of a compressor, combustor, and turbine. The overall thermodynamic performance of the system is heavily influenced by the dynamics of the combustion process, with the type of fuel burnt being a key factor in determining combustion efficiency and emissions.
Currently fossil fuels, such as oil and gas, are the primary propellants used in these combustors; due to this the major drawback of this technology is indeed the emission of greenhouse gases. To mitigate this issue, the use of alternative clean fuels such as biofuels and hydrogen have been suggested; the latter is particularly attractive for its high energy content of 120 MJ/kg, which is considerably higher than the conventional fuels, like gasoline or methane whom have 44-50 MJ/kg.
During October of last year the HyFlexPower consortium, with partners like ENGIE and Siemens [1], successfully operated the first gas turbine with 100% hydrogen content in real world conditions maintaining the NO_x emissions below the law limits. This goal was forerun by many tests under blended fuel condition that started in the year 2022 that employed a mix of 30% H_2 and 70% CH_4 on a mass basis. The project comprised a 1 MW electrolyser and a 1 ton storage tank with an estimate expense of 15.2 million euros, 2/3 funded by the European Union Horizon 2020 program [2].
To give meaning to this solution it is necessary to produce green hydrogen by renewable electricity, as a matter of fact producing H_2 from steam reforming for example, would just switch the time the CO_2 is emitted. To make the practice work it is advised to store the hydrogen produced when there is a surplus of renewable energy and use it in the turbine when there is an energy demand.
In order to enhance the green hydrogen production the European Union deviced the Hydrogen Bank program to award €720 million in total: "The seven selected projects were the winners of an oversubscribed auction which attracted 132 bids in total. Together, the winning bidders plan to produce 1.58 million tonnes of renewable hydrogen over ten years, avoiding more than 10 million tonnes of CO_2 emissions. The selected projects are located in 4 European countries. They submitted bids between **€0.37** and **€0.48 per kilogram** of renewable hydrogen produced, and also met the other qualification requirements.
The subsidy the seven projects will receive ranges from €8 million to €245 million." [3]

1. eNRG Lahti of Nordic Ren-Gas Oy (Finland)

2. El Alamillo H2 of Benbros Energy S.L. (Spain)
3. Grey2Green-II of Petrolgas S.A. (Portugal)
4. HYSENCIA of Angus (Spain)
5. SKIGA of Skiga (Norway)
6. Catalina of Renato PtxHoldco (Spain)
7. MP2X of Madoquapower 2x (Portugal)

Following the trend several other projects have been built or are in the planning phase regarding PEM and SOC systems. Some examples are:

- The 2.6 MW SOC Sunfire [4] electrolyser for the Multiphly project funded by the Horizon 2020 program [2] and built in 2023.
- The 4 MW SOC Bloom electrolyser built for the NASA facilities [5].
- The 10 MW PEM project by Shell installed in 2021 [6].
- The 8.75 MW PEM project commissioned by Siemens in Germany [7].

However most of the literature available focuses on systems with one or two coupled technologies or small complex systems in the kW size [8] while in this case there are three in the MW scale.
Consequently it is still not clear how a whole system "Power to Gas to Power" of this size should work, which are the technical problematics and the estimate expense to build it.
To summarize, the aim of this thesis is to study how a real "Power to Gas to Power" renewable system, in the MW range, can work in the republic of Ireland, by means of real data (the Mountlucas wind [9] farm and the gas turbine in Rhode [10], county Offaly) from the year 2022 that was obtained from the website of the national single electricity market operator Sem-o [11].
In particular the system in question focuses on the conversion of the gas turbine technology to hydrogen firing and connects together the mathematical models of an hydrogen turbine, an electrolyser (Solid Oxide or PEM) and renewable electricity supplied from a wind farm.

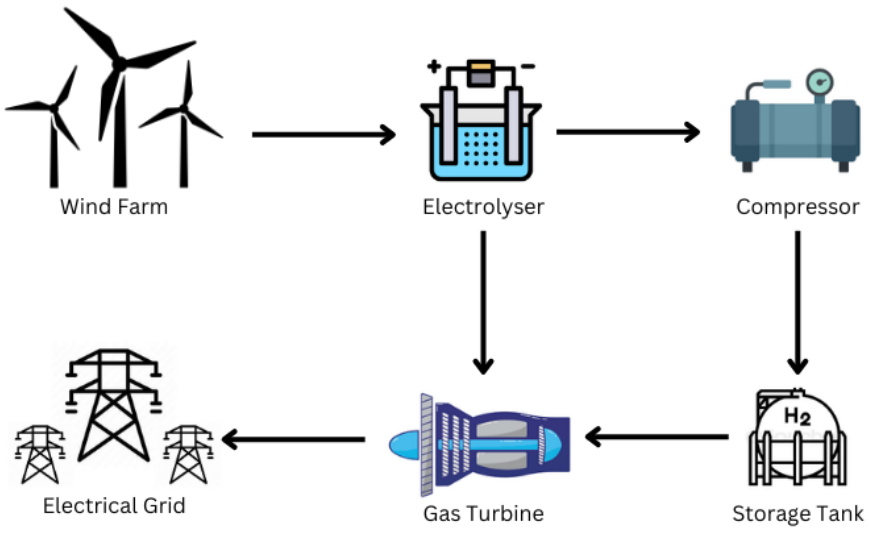

Figure 1.1: System layout design

Chapter 2

Literature review

In order to decide the thesis topic a wide literature review was performed. It was necessary to know if the coupling of a retrofitted gas turbine and an electrolyser system was already extensively described or not. The research of articles lead to the conclusion that it is a topic of increasing interest in the literature but still in the early stages in regards to publications available.
Aside from the topic as a whole, every subtopic that is part of the work has it is own sources of analysis; starting from the gas turbine reconversion to the wind farm with employment of electrolysers. For what regards the coupling of different technologies K. Jia [12] gives an idea of how renewables, gas turbines and energy storage can coexist together, improve the curtailment problem and reduce emissions; however these improvements are at the expenses of an high investment cost.

Electrolysers and Wind Farm Coupling

Multiple publications regarding the state of art of electrolysers were used in order to quantify the pros and cons of the different technologies available. The most interesting ones from S.Shiva Kumar [13], X. Liu [14] and S.Dermühl [15] give a good range of values for the technical characteristics of the system such as the materials, the current density, the temperature, the pressure and the efficiency as well as the plant size. Being more specific the authors bring attention to the favorable points, the cost and the problems that need to be solved in order to effectively deploy the technology on a large scale. To delve in more detail in the PEM and SOC systems a few modelling papers were employed, the PEM modelling has a clear approach in literature while for the SOC multiple studies were used to get a complete overview:

1. M.Nasser [16] performs a techno-enviro-economic analysis through hydrogen production models with different electricity sources such as PV panels, wind turbines, Rankine cycle based on waste heat recovery and electricity from grid. Afterwards the efficiency, the hydrogen production rate and the levelized cost, for both low and high temperature H_2O electrolysis, are evaluated for all systems showing that the wind related ones are the most expensive due to a low wind profile.

2. T.Egeland-Eriksen [17] simulates offshore hydrogen production via PEM electrolysis using real power production data from a 2.3 MW floating offshore wind turbine; the results show that the highest hydrogen production achieved in a 31-day period was 17242 kg using a 1.852 MW electrolyser (with an utilization factor of approximately 68%) while the lowest hydrogen production cost was 4.53 \$/kg$_{H_2}$ with a system efficiency of roughly 56%.

3. H.Groenemans [18] developed a model for the hydrogen production via offshore wind electrolysis and calculated the levelized cost of hydrogen, that is estimated to be 2.09 $/kg versus 3.86 $/kg from traditional electrolysis using wind power.

4. M.Pfennig [19] employs a simplified electrochemical model, that includes only ohmic and activation overpotentials, to describe the performance of a 100 MW PEM electrolyser plant; this size is the target that the European Union plans to establish in the upcoming years. The outcome is a comprehensive model of a PEM electrolyser plant, exemplarily adapted to the Siemens Silyzer 300 [20], which will later be used for the python script.

5. P.Mottaghizadeh [21] models an islanded microgrid system that integrates identical stacks of solid oxide fuel cell and electrolyser to achieve a thermally self-sustained energy storage system; it produces hydrogen thanks to a 18 MW wind farm in Palm Springs, then the system supplies the necessary energy to power an industrial building with a maximum load of 5.4 MW.

6. Y.Zhao [22] investigates the possibility of coupling external waste heat with a SOEC system. The results show that the recommended coupling location is at the water evaporator with temperature above $130°C$. In detail for a SOEC system of 1 MW electrolysis power input, the required external waste heat is about 200 kW when the stack operates at thermoneutral state; the specific energy consumption instead is 3.77 kWh/$Nm^3_{H_2}$ (84% electric power and 16% thermal power).

7. A.Chandrasekar [23] analysis of a 0.5 MWe HTE system coupled with a wind turbine is very important to understand the dynamic behaviour of such a configuration and gives an estimate of the maximum hydrogen produced to be about 6 tons/year in 2021.

8. A.Hauch [24] [25] gives a clear description of the recent advancement of the technology and the design of stacks, MW-sized systems of Topsoe SOEC electrolyser plants.

9. LA.Jolaoso [26] that focuses on the state-of-the-art SOEC component materials and their degradation mechanisms, SOEC modeling essentials and efficiencies, and the scalability of SOECs.

10. J.Laurencin [27], P.Kazempoor [28] and C.Wang [29] are interesting papers to model the characteristics of a cell such as overpotentials and thermal behaviour.

11. T.Chmielniak [30] focuses on the comparison between SOC and PEM technology electrolysers.

Retrofitted Gas Turbines

To develop the turbine model knowledge from both papers and previous modules of the master degree were used; in particular the work of P.Trawiński [31], S.Kim [32], AA.Sinha [33] and Y.Haseli [34] were useful sources to develop the thermodynamic cycle of the turbine and the obtained electrical power.
The paths and the problematics towards the blending or a 100% H_2 turbine system are well debated in the article by D. Cenere [35] in which the focus is to give an overview of the most promising fuel-flexible and clean combustion technologies to accomplish the 2030 target in emission reduction.
The most promising one appears to be the micro-mixing technology that enhances the mixing of air-fuel obtaining many small flames with low residence time and then low NO_x emissions; a real system example is the DLE Micro-Mix burner developed by the Kawasaki heavy industries [36].
Again regarding the conversion of turbines to H_2 firing G.Song [37] makes a life cycle model to quantify the impact of the NO_x and GHG pollution in a PHP system with the conclusion that it's an environmentally friendly technology. Another important point of view is shared in the article of S.Gülen [38] in which are underlined the most rational and effective ways to reduce GHG emissions in the near future, 3 out of 5 involve the utilization of green hydrogen in retrofitted turbines.
Furthermore it's important to report the achievement of R.Banihabib [39] to complete the first successful test on a micro gas turbine running on 100% hydrogen, with NO_x emissions below the limits.
So after the description of the papers related to the thesis' topic, the theory behind these systems will be revised to make the key points of the study clear from any misunderstanding.

Chapter 3

Water electrolysis

Water electrolysis is the process of using an electric current to split water molecules into hydrogen and oxygen gases involving two main reactions (Cathodic and Anodic).
The electrolysis process has slightly different reactions based on the catalyst and the operating conditions but for the most widespread technology nowadays (PEM) the chemical reactions consist of:

1. At the cathode (negative electrode), water is oxidized to produce hydrogen ions, oxygen and electrons:

$$2H_2O(l) \rightarrow 4H^+ + O_2(g) + 4e^- \tag{3.1}$$

2. At the anode (positive electrode), hydrogen ions are reduced to generate hydrogen gas:

$$4H^+ + 4e^- \rightarrow 2H_2(g) \tag{3.2}$$

The overall reaction for water electrolysis is:

$$2H_2O(l) \rightarrow 2H_2(g) + O_2(g) \tag{3.3}$$

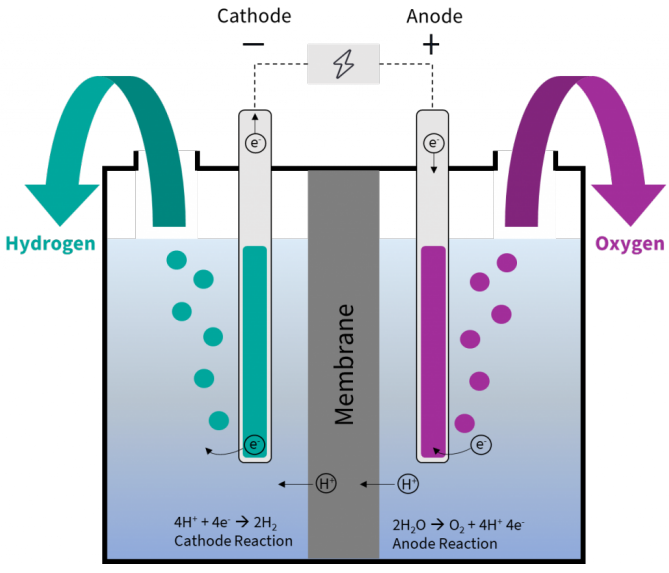

Figure 3.1: Electrolysis of water with proton exchange membrane [40]

3.1 Electrochemistry

Delving into the process itself it is important to speak about electrochemistry, the discipline that investigates the intricate relationship between electricity and chemical reactions, exploring how they interconnect. Central to this field is the study of redox reactions where electrons transfer between substances. To do so it is important to understand the reaction behaviour that is dictated by thermodynamics and kinetics.

3.1.1 Cell thermodynamics: Gibbs free energy and cell potential

The Gibbs free energy equation serves as a cornerstone in electrochemistry, linking changes in energy (ΔG) to temperature (T), enthalpy (ΔH), and entropy (ΔS). It is expressed as:

$$\Delta G = \Delta H - T\Delta S$$

Within electrochemistry, this equation helps determine if a reaction is energetically favorable or not based on energy release or absorption.
Indeed if $\Delta G < 0$ the reaction is spontaneous while if $\Delta G > 0$ it is not.
In electrochemical reactions, ΔG corresponds also to the electrical work, where:

$$\Delta G = -W_{\text{elec}} = -nFE \tag{3.4}$$

In a cell oxidation and reduction reactions happen at separate electrodes (anode and cathode), connected by an electrolyte; while the movement of electrons through an external circuit generates electrical current.

The driving force behind these reactions is the cell potential (E_{cell}), connected to the standard cell potential (E°_{cell}) via the Nernst equation:

$$E_{\text{cell}} = E^{\circ}_{\text{cell}} - \frac{RT}{nF} \ln Q \tag{3.5}$$

Here:

- R is the gas constant
- T is temperature
- n is the moles of electrons transferred
- F is Faraday's constant
- Q is the reaction quotient

In particular the reaction quotient serves as a tool in chemical thermodynamics for assessing the progress of a reaction under specific conditions: temperature, pressure, and concentrations. Unlike the equilibrium constant K, which characterizes a reaction's equilibrium state, Q provides insight into a reaction's status at any given moment, whether equilibrium has been attained or not.
To compute Q, concentrations (or partial pressures) of the reactants and products are utilized, each raised to a power equal to their stoichiometric coefficients in the balanced chemical equation.

For a typical reaction:

$$aA + bB \rightleftharpoons cC + dD \tag{3.6}$$

The reaction quotient Q is determined by:

$$Q = \frac{[A]^a[B]^b}{[C]^c[D]^d} \tag{3.7}$$

$$Q = \frac{(P_A)^a(P_B^b)}{(P_C)^c(P_D)^d} \tag{3.8}$$

[A],[B],[C],[D] represent the concentrations of substances A, B, C, D respectively, at a specific time. P instead is the partial pressure of reagents and products at a given time.
In particular for water electrolysis:

$$2H_2O(l) \rightarrow 2H_2(g) + O_2(g) \tag{3.9}$$

$$Q = \frac{[H_2]^2[O_2]}{[H_2O]^2} \tag{3.10}$$

$$Q = \frac{(P_{H_2})^2(P_{O_2})}{(P_{H_2O})^2} \tag{3.11}$$

Depending on how Q compares to K (the equilibrium constant), the reaction will proceed accordingly:

- If $Q < K$, the reaction will progress toward the product side.
- If $Q = K$, the reaction is at equilibrium.
- If $Q > K$, the reaction will shift toward the reactant side.

In essence, Q aids in predicting the direction a reaction will take to reach equilibrium based on the existing concentrations of reactants and products.

3.1.2 Cell kinetics: Current density and Overpotentials

There are mainly two types of charge transport produced on active surfaces: electronic and ionic. Electron transport occurs in the electrodes, according to mechanisms of electrical conduction, drived by the electric field (gradient of electric potential) which acts directly on the electric charges.
The transport of ions occur in the electrolyte according to different mechanisms, namely by the effect of various forces:

- Electrical conduction, produced by the electric field (gradient of electrical potential) which acts directly on electrical charges.
- Diffusion, both of charge and charge carriers, produced by the relative concentration gradient.
- Convection of the charge carriers, produced by the pressure gradient.

Almost always, the dominant forces on the ions are the electric ones, therefore the dominant mechanism is conduction; so it is essential to establish a relationship between the quantity of moving ions and

their electrical charge. The electrical charge associated with a molar quantity can be expressed as:

$$Q = zFN \tag{3.12}$$

Where:

- N is the moles of the reacting chemical species [mol].
- F is Faraday's constant (modulus of the charge of one mole of electrons, 96485 C/mol).
- z is the number of charges associated with the carrier (1 for H^+ and -2 for O_2^-).
  The product $z \cdot F$ is the electric charge of a mole of charge carriers of the chemical species and allows the transformation from chemical quantities to electrical quantities.

When that quantity moves, passing through a normal section A, it gives rise to electric current i [A] and molar flow dN/dt [mol/s].
Accounting that these quantities pass through a given surface the density of electric current j [A/m^2] and the specific molar flux J [mol/cm^2s] can be defined. The relation in vector form is therefore:

$$\frac{dt}{dQ} = \frac{dt}{dN} \cdot i = \frac{dA}{di} \cdot \frac{dt}{dN} = \frac{dA}{dJ} \tag{3.13}$$

And it is fundamental because it establishes the bridge between the chemical world and the electrical world in transport phenomena.

When delving into the water electrolysis process, the interplay between thermodynamics and kinetics defines the feasibility and pace of the reaction. While thermodynamic aspects establish the requirements for the reaction's occurrence, kinetics govern its speed and efficiency.
In the kinetics of water electrolysis, several key formulas and concepts elucidate the reaction rate: the **current density** (j) characterizes the rate of electron transfer per unit area at the electrodes. It is typically expressed as:

$$j = nFv \tag{3.14}$$

Where:

- n is the number of moles of electrons transferred in the reaction
- F is Faraday's constant
- v is the specific molar rate per unit of area

The **exchange current density**(j_0) represents the point where the forward and reverse reaction rates are equal at equilibrium. It relates to the kinetics of the reaction and is a crucial parameter in the **Butler-Volmer** equation; the equation describes the relationship between the activation overpotential (η), current density (j), exchange current density (j_0), and various kinetic parameters:

$$j = j_0 \cdot \left(e^{\frac{\alpha F \eta}{RT}} - e^{-\frac{(1-\alpha) \cdot F \eta}{RT}} \right) \tag{3.15}$$

Where:

- α is the charge transfer coefficient (0.5 when reaction is balanced)
- R is the gas constant (8.314 J / mol K)
- T is temperature
- F is Faraday constant
- η is the activation overpotential

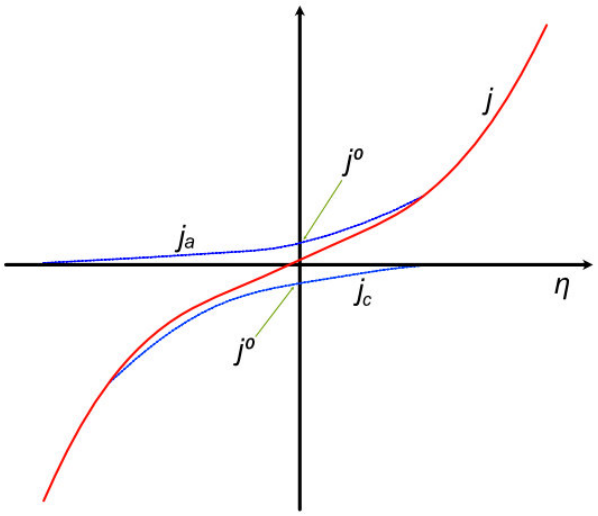

Figure 3.2: Butler Volmer curve [41]

The **cell overpotentials** (η) are other important parameters that are necessary to calculate in order quantify the cell performance. There are 3 different type of overpotentials that take place in a cell.

Activation Overpotential ($\eta_{\mathbf{act}}$)

This overpotential arises from the activation energy required for the reaction and, since they are statistical processes, their probability can be addressed as a function of the the specific molar rate v as:

$$v = c_r^* f p_{att} \tag{3.16}$$

Where:

- c_r^* is the concentration of the reactant species at the interface surface
- f is the reaction rate (rate at which reacted species are likely for react and form products)
- p_{att} probability that reactions species are in state of activation

$$p_{\text{att}} = e^{\frac{-\Delta G}{RT}} \tag{3.17}$$

the ΔG here is an important factor because its difference can determine if the reaction is going forward or backwards.

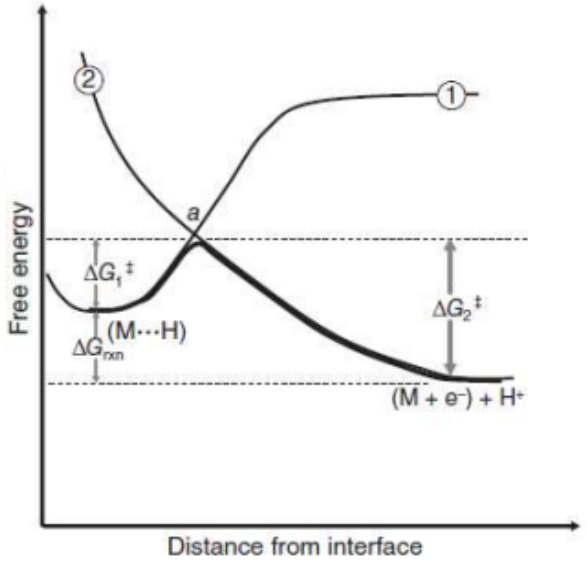

Figure 3.3: Activation energy function of interface distance [42]

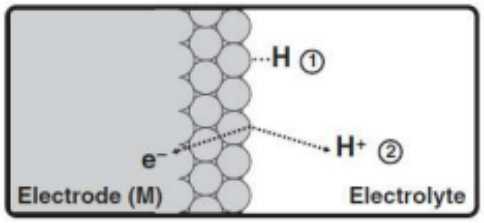

Figure 3.4: Electrode-electrolyte interface [42]

The activation overpotential is determined, for each electrode, by means of the Butler-Volmer equation.

$$\eta_{act} = \frac{RT}{\alpha F} \cdot \ln\left(\frac{j}{j_0}\right) \tag{3.18}$$

Given these formulas if the exchange current (j_0) varies keeping constant all the over parameters the activation overpotential decreases as the exchange current density increases.
In the case of electrolysis the overpotential is positive while in fuel cell operation is negative.

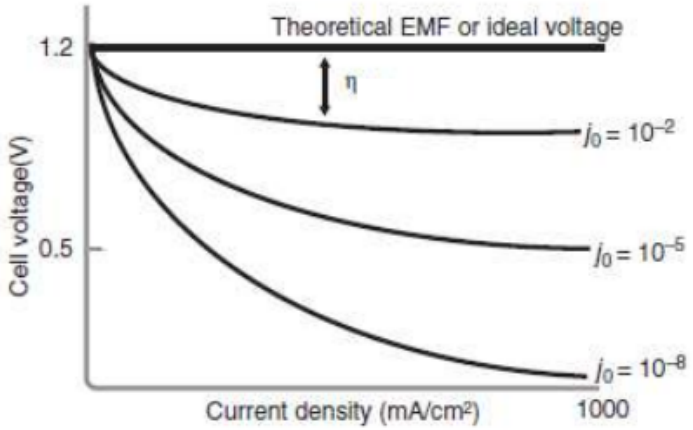

Figure 3.5: Example of j_0 influence on η_{act}:
exchange current variation in fuel cell mode [42]

To make it as high as possible the following methods can be employed:

- Increase the reactant concentration c_r^{*0}
- Increase the temperature T
- Decrease the activation barrier ΔG
- Increase the number of reaction sites (increase of surface roughness)

Ohmic Overpotential ($\eta_{\mathbf{ohm}}$)

Ohmic loss refers to the voltage decrease derived by the resistance encountered during charge transport. This encompasses both the electric charge transport in the electrodes and the flow of O_2^- ions through the electrolyte layer.
The transport of charge by conduction is governed by the constitutive law of conduction:

$$j = \sigma E \tag{3.19}$$

Where σ is the conductivity of the medium and it defines how well the medium allows the transport of charge:

$$\sigma = zFc\mu \tag{3.20}$$

With:

- c [mol/cm^3] molar concentration of the charge carriers present in the medium.
- μ [m^2/Vs] mobility in the medium, which links the drift velocity u of the carriers in viscous motion to the electric field applied to them E: $u = \mu E$

It is significant to point out that different materials have very different conductivities depending on the mobility of the medium.

Cation	μ[**cm**^{2}/**Vs**]	**Anion**	μ[**cm**^{2}/**Vs**]
H^+, (H_3O^+)	$3.63 \cdot 10^{-3}$	OH^-	$2.05 \cdot 10^{-3}$
K^+, (H_3O^+)	$7.62 \cdot 10^{-4}$	Cl^-	$7.91 \cdot 10^{-4}$
Na^+, (H_3O^+)	$5.19 \cdot 10^{-3}$	HCO_3^-	$4.61 \cdot 10^{-4}$

Table 3.1: Mobility of catalysts [42]

Then the conductivity in an electrolyser can be evaluated as:

$$\sigma = \sigma_0 \cdot \exp\left(\frac{-E_{\text{act,el}}}{RT}\right) \tag{3.21}$$

$$ASR_{\text{ohm}} = \frac{\delta_{\text{el}}}{\sigma_{\text{el}}} + r_{\text{sc}} \tag{3.22}$$

$$\eta_{\text{ohm}} = jASR_{ohm} \tag{3.23}$$

Where:

- E_{act} is the activation energy to start the reaction

- δ_{el} [m] is thickness of the electrolyte layer

- σ_0 $[1/\Omega m]$ is the conductivity at standard condition

- σ_{el} $[1/\Omega m]$ is the conductivity of the electrolyte

- r_{sc} is the constant term of ohmic resistance for one single repeating unit (SRU) at steady state

So to summarize the conductivity values are in the range of $\sigma = 10^{-2}$ to 100 $\Omega^{-1}m^{-1}$ that is various magnitudes smaller than that of metals ($\sigma = 10^6$ to 10^8 $\Omega^{-1}m^{-1}$) and that is why these losses need to be taken into consideration.

Concentration Overpotential ($\eta_{\mathbf{conc}}$)

The concentration overpotential emerges due to mass transport limitations, often associated with concentration gradients at the electrode surface. As a matter of fact there are different concentrations, due to the diffusion and convection of the species, between the bulk condition and the catalyst layer. If the diffusion and convection of species are too slow this can hinder the performance of the electrolyser so this phenomena needs to be analyzed with **Fick's law** to quantify its relevance.

$$J = -D \cdot \frac{\partial C}{\partial x} \tag{3.24}$$

Where:

- J is the flux of the species.

- D is the diffusion coefficient.

- C is the concentration of the species

- x is the direction of mass transport

We can analyse the stationary and dynamic conditions with the first and the second law. In stationary condition the diffusivity can be expressed as:

$$D = \frac{\Delta x^2}{2\Delta t} \tag{3.25}$$

So the law can be written as:

$$\frac{\partial C}{\partial x} = -\frac{J}{D} \tag{3.26}$$

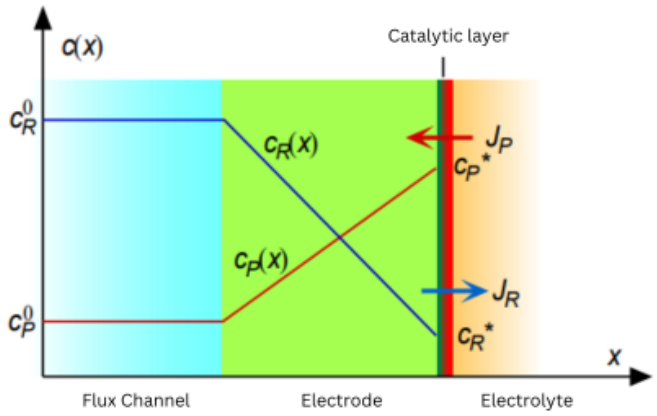

Figure 3.6: Linear distribution in diffusion layer to change [42]

In dynamic condition instead the non constant nature of the equations give birth to this situation:

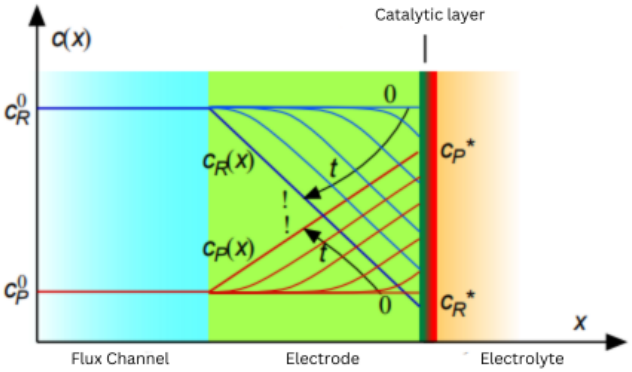

Figure 3.7: Non linear distribution in diffusion layer to change [42]

Now it is important to introduce the **limiting current** (J_L) that is the maximum value of current obtainable in a cell (last value in which there are still reactants in the diffusion layer):

$$J_{\mathrm{L}} = nFD_{\mathrm{eff}} \cdot \frac{c_r^0 - c_r^*}{\delta} \tag{3.27}$$

Given that D_{eff} can be calculated as:

$$D_{eff} = \frac{\tau}{\xi} \cdot \left(\frac{1}{D_{i,k}} + \frac{1}{D_{i,j}} \right) \tag{3.28}$$

With $D_{i,k}$ as the Knudsen term that describes the diffusion in porous media and $D_{i,k}$ as the binary diffusion coefficient that describes the diffusivity of two species within each other.

$$D_{i,k} = \frac{2}{3} r_p \cdot \sqrt{\frac{8RT}{\pi M_i}} \tag{3.29}$$

$$D_{i,j} = \frac{10^{-3} \cdot T^{1.75} \sqrt{\left(\frac{1}{M_i} + \frac{1}{M_j}\right)}}{p \cdot \left(V_i^{\frac{1}{3}} + V_j^{\frac{1}{3}} \right)^2} \tag{3.30}$$

Finally the concentration overpotential can be written as:

$$\eta_{conc} = \frac{RT}{nF} \cdot \ln\left(\frac{J_L}{J_L - J}\right) \tag{3.31}$$

Each of these overpotentials contributes to the overall voltage necessary for the electrolysis process. Here we can see a typical characteristic curve of a SOC electrolyser.

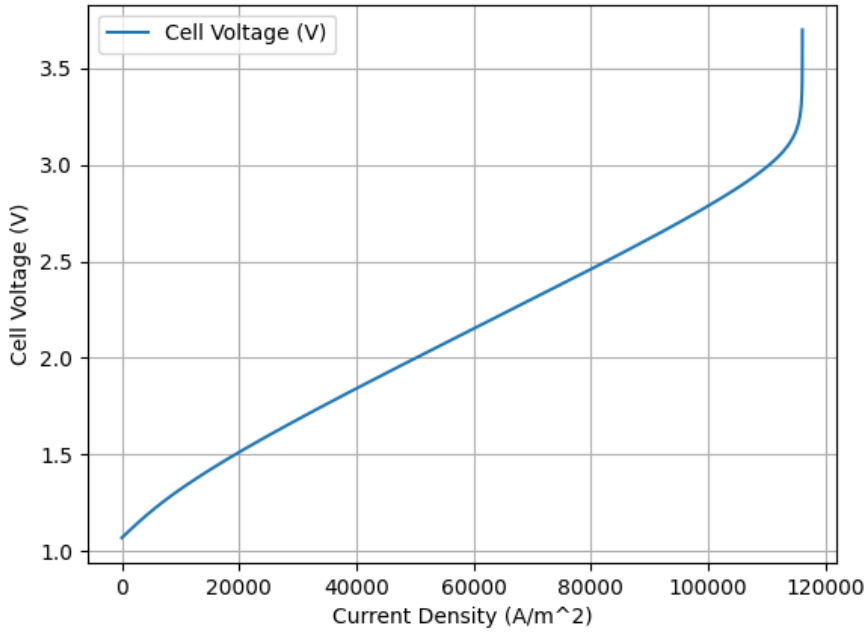

Figure 3.8: Cell Voltage vs Current Density, polarization curve of a SOC electrolyser

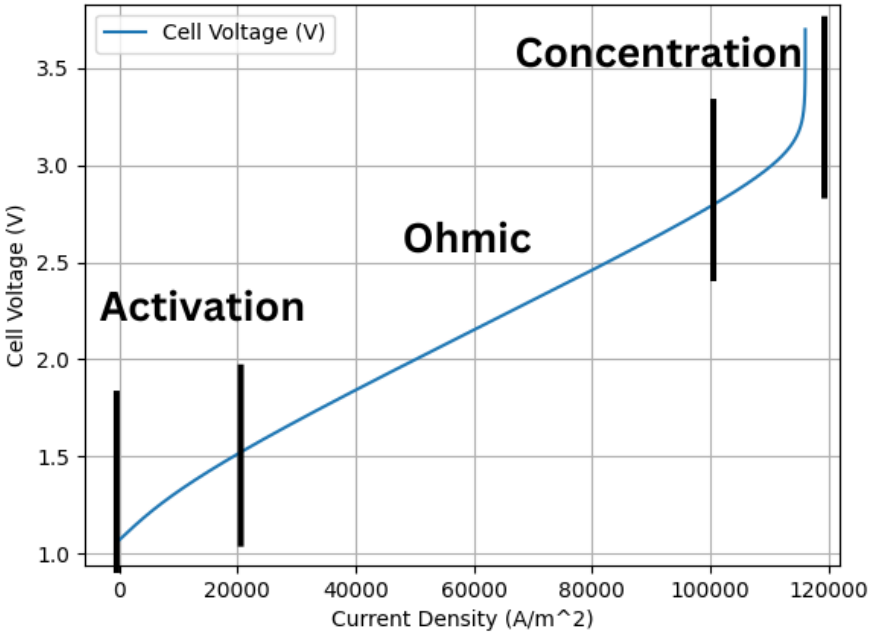

Figure 3.9: Dominating overpotential for each current density range

The change of the operating conditions enable the optimization of water electrolysis kinetics. Adjusting electrode materials, electrolyte concentration, temperature, and applied voltage helps control these parameters, ultimately enhancing the reaction rate and efficiency of hydrogen and oxygen production.

3.2 Type of electrolysers

There are three main types of electrolysis cells:

- Alkaline Electrolysis (AE)
- Proton Exchange Membrane Electrolysis (PEME)
- Solid Oxide Electrolysis Cells (SOEC)

3.2.1 Alkaline Electrolysis

Alkaline water electrolysis, originating from Troostwijk and Diemann's work in 1789, has become a widely adopted method for hydrogen production, with applications scaling up to the megawatt level globally. In this process, alkaline solutions like KOH or NaOH undergo electrolysis at the cathode (negative electrode). Here, two molecules of the alkaline solution are reduced to yield one molecule of hydrogen (H_2) and two hydroxyl ions (OH^-).

$$2H_2O(l) + 2e^- \rightarrow H_2(g) + 2OH^-(aq) \tag{3.32}$$

The hydrogen is then released from the cathode surface, while the hydroxyl ions migrate through a porous diaphragm to the anode (positive electrode). At the anode, they combine to form oxygen (O_2) and water (H_2O).

$$4OH^-(aq) \rightarrow O_2(g) + 2H_2O(l) + 4e^- \tag{3.33}$$

The overall reaction is:

$$2H_2O(l) \rightarrow 2H_2(g) + O_2(g) \tag{3.34}$$

Alkaline electrolysers have efficiencies ranging from 63% to 70% as reported by S.Dermühl [15], operate within a relatively low temperature range (30−80°C) and utilizing aqueous electrolytes with concentrations typically between 20% to 30% (S. Shiva Kumar [13]). This electrolysis relies on materials that are not rare nor expensive, such as asbestos diaphragms and nickel electrodes. These diaphragms play a crucial role in separating the cathode and anode, as well as the gases produced, to avoid the intermixing of species.
Despite its widespread use, alkaline electrolysis does have its limitations, such as the complexity of the potassium hydroxide cycle and its corrosive nature; however the most important is for sure the restricted range of current densities employable (0.2−0.6 A/cm^{-2}) [15]; this limits the system scalability and requires larger electrode surface areas for higher production rates.

Pros: Mature with long lifetime.
No expensive or rare catalyst required.

Cons: Rather low current densities.
System complexity (KOH cycle, corrosivity)

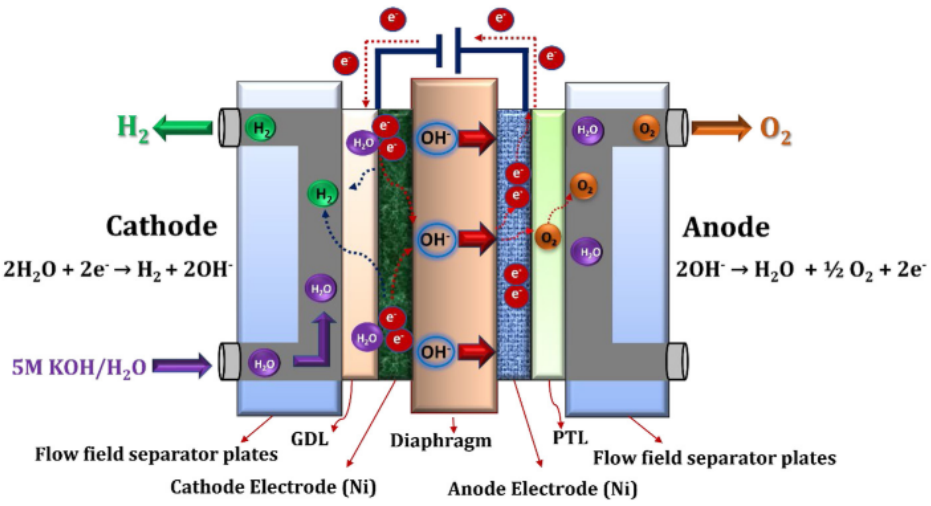

Figure 3.10: Schematic illustration of alkaline water electrolysis working principle [13]

3.2.2 Proton Exchange Membrane Electrolysis

Grubb's initial work in the early 1950s laid the foundation for Proton Exchange Membrane (PEM) water electrolysis, a concept further developed by General Electric Co. in 1966 to address the limitations of alkaline water electrolysis.

PEM water electrolysis utilizes solid polysulfonated membranes such as Nafion and fumapem as electrolytes (proton conductors). These membranes offer distinct advantages, including reduced gas permeability, high proton conductivity (0.1 ± 0.02 S/cm), thinner profiles ($20-300$ μm), and suitability for high-pressure operations.
In this type of electrolysis, water is electrically separated into hydrogen at the cathode (negative electrode) and oxygen at the anode (positive electrode). The process initiates with water being directed to the anode, where it undergoes splitting into oxygen (O_2), protons (H^+), and electrons (e^-). These protons then migrate through the proton-conducting membrane to reach the cathode.

$$2H_2O(l) \rightarrow 4H^+ + O_2(g) + 4e^- \tag{3.35}$$

Concurrently, electrons depart from the anode through the external power circuit, supplying the necessary driving force (cell voltage) for the reaction. Upon arrival at the cathode, protons and electrons reunite to generate hydrogen gas.

$$4H^+ + 4e^- \rightarrow 2H_2(g) \tag{3.36}$$

The overall reaction is:

$$2H_2O(l) \rightarrow 2H_2(g) + O_2(g) \tag{3.37}$$

PEM electrolysis plants offer remarkable dynamism, making them well-suited for integrating with fluctuating renewable energy sources; these systems exhibit fast response times, operating efficiently even at varying power inputs.
It has a respectable efficiency of around 56% to 65% [15], compact design, high current density (up to 3 A/cm^2) [15], rapid response, small footprint, operation at lower temperatures ($20-80$°C), and the

production of very pure hydrogen/oxygen as byproducts make it appealing for diverse applications.

However, the use of expensive electrocatalysts such as noble metals like Pt/Pd for the hydrogen evolution reaction (HER) at the cathode and IrO_2/RuO_2 for the oxygen evolution reaction (OER) at the anode contributes to higher costs compared to alkaline water electrolysis. Thus, a significant challenge in PEM water electrolysis lies in reducing production costs while maintaining high efficiency.

Pros: High current densities.
RE compatible.
Low system complexity

Cons: Expensive and rare catalyst required.
System durability

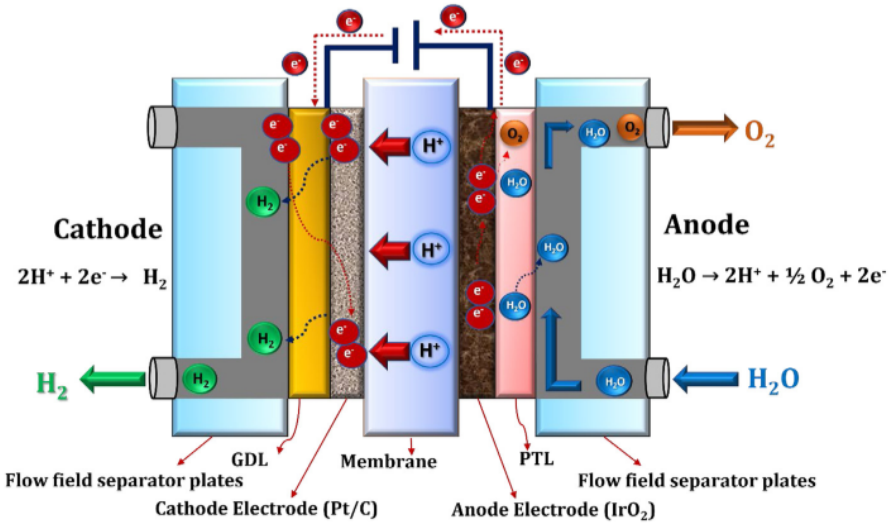

Figure 3.11: Schematic illustration of PEM water electrolysis working principle [13]

3.2.3 Solid Oxide Electrolysis

In the 1980s, Donitz and Erdle introduced solid oxide electrolysis (SOE), which has since garnered significant attention for its ability to convert electrical energy into chemical energy while producing ultra-pure hydrogen with exceptional efficiency. High-temperature electrolysers represent thus a promising avenue for efficient hydrogen production, particularly suitable for industries with high-temperature waste streams like steel or chemicals. With an impressive electrical efficiency range of 74% to 84% [15], HTE systems require less electricity per unit of hydrogen produced compared to their low-temperature counterparts; this is due to the heat that reduces the necessary energy to break the bonds on a water molecule. Furthermore the reversible solid oxide cell (rSOC) feature enables grid balancing services, versatility and co-electrolysis with CO_2 for hydrocarbon production.
The reaction involved in the electrodes are:
At the cathode (negative electrode), water is reduced to produce hydrogen gas and oxygen anions:

$$2H_2O(l) + 4e^- \rightarrow 2H_2 + 2O^{2-} \tag{3.38}$$

At the anode (positive electrode), oxygen anions are oxidized to generate oxygen gas:

$$2O^{2-} \rightarrow O_2(g) + 4e^- \tag{3.39}$$

The overall reaction is:

$$2H_2O(l) \rightarrow 2H_2(g) + O_2(g) \tag{3.40}$$

Coming back on the operating conditions this technology harness high pressures and temperatures ranging from 500°C to 850°C and utilizes water in the form of steam. Traditionally, SOE relies on O_2 conductors, primarily composed of nickel/yttria-stabilized zirconia; however, recent advancements have prompted a shift towards ceramic proton-conducting materials, originally studied in solid oxide fuel cells, due to their superior efficiency and ionic conductivity compared to O_2 conductors at temperatures ranging from 500°C to 700°C. This transition reflects the evolving emphasis on enhancing SOE technology.

HTE technology however is still in the early stage of commercialization, with limited scalability and sluggish dynamics. The need for high-temperature-resistant materials, the stability issues and the degradation adds to manufacturing costs and presents technical challenges, necessitating further research and development to overcome these limitations. These concerns underscore the need for further research and development efforts to optimize SOE for widespread adoption however the degradation problem seems to be improving according to a recent study reported by A.Hauch [43] and there are the first systems scaling up to MW power coupled with renewable energy (P.Mottaghizadeh [21]).

Pros: High electrical efficiency.
Reverse mode (rSOC)
Co-electrolysis mode

Cons: Less developed.
Sluggish dynamics High temperature resistant materials

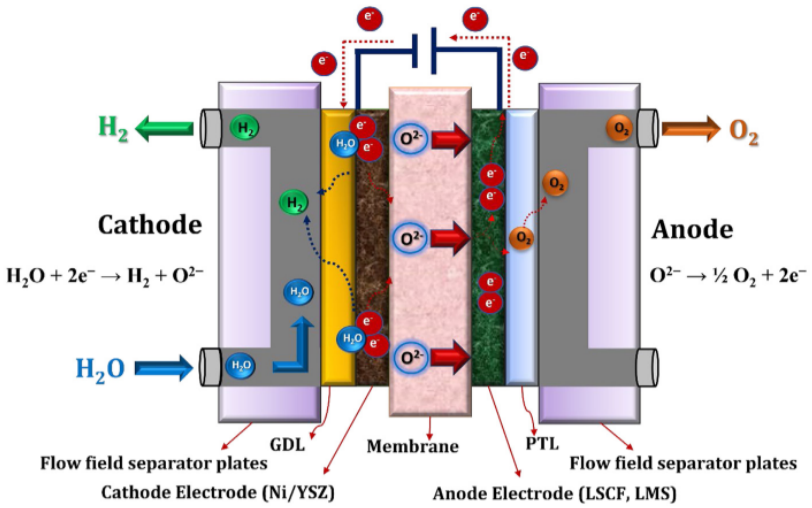

Figure 3.12: Schematic illustration of solid oxyde water electrolysis working principle [13]

3.2.4 Summary of technologies

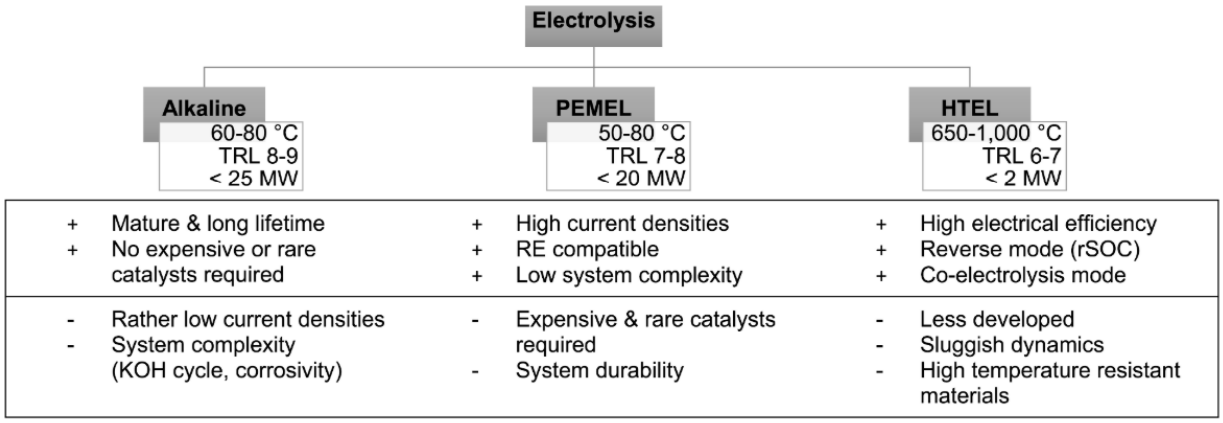

Figure 3.13: Comparison of the advantages and disadvantages of the electrolysis technologies AEL, PEMEL and HTEL. [15]

	AEL	**PEMEL**	**HTEL**
System efficiency % (LHV)	63 - 70	56 - 65	74 - 84
Current density [A/cm^2]	0.2 - 0.6	0.6 - 3.0	0.3 - 1.0
Electricity consumption [kWh/Nm^3]	4.3 - 4.8	4.6 - 5.3	3.6 - 4.0

Table 3.2: Comparison of electrolysis properties [15]

In summary, each electrolyser type offers distinct advantages and challenges, however the most promising technologies are for sure the PEM due to the modularity and fast response to current variation, the SOC due to the very high efficiency achievable and the possibility to couple it with waste heat sources.

Chapter 4

Gas turbine

Gas turbines are crucial for power generation, offering efficiency and versatility. This work focuses on the types employed for power generation, briefly summarizing the Brayton-Joule cycle characteristics and evaluating the performance of critical components such as compressors, combustion chambers, and turbines. Formulas delineating the thermodynamic processes and component behaviors are included, illuminating operational principles and strategies for optimization.

Gas turbines are widely deployed in power generation due to their efficiency, quick startup times, and environmental advantages. A comprehensive understanding of their operation, from the theoretical Brayton-Joule cycle to the behavior of individual components, is compulsory for enhancing their performance and efficiency.

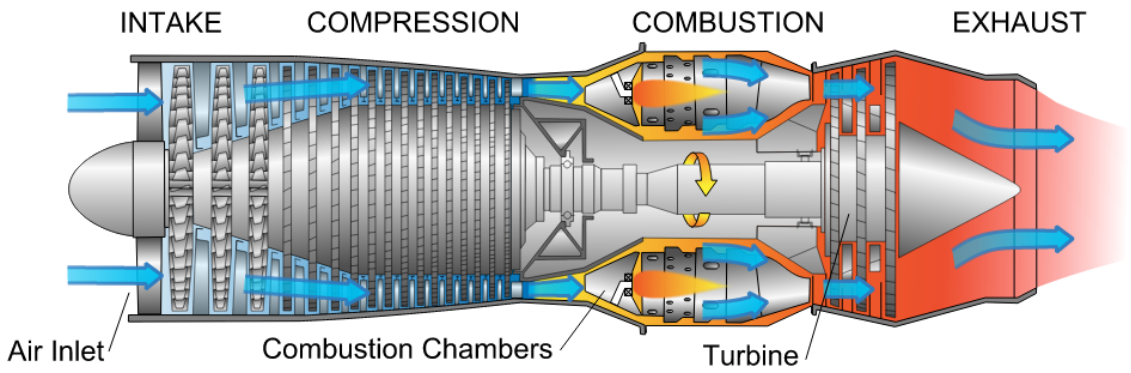

Figure 4.1: Gas Turbine simple representation [44]

4.1 Brayton-Joule Cycle Analysis

The **Brayton-Joule** cycle comprises four primary processes: compression, combustion, expansion, and exhaust. It can be open or closed depending on the application:

- it is defined as **OPEN** when the gases after the turbine are released in the ambient. This type of cycle is the most used both for small-big turbines and aircraft or power generation purposes. In the case of big units where the efficiency becomes crucial is usually present and heat exchanger to recover heat from the exhaust gases; this type of application is called combined cycle.

- it is defined as **CLOSED** when the gases after the turbine are reused in the system, cooling them by means of an heat exchanger. This type of cycle is rarely employed in practice and the majority of the existing ones have small dimensions.

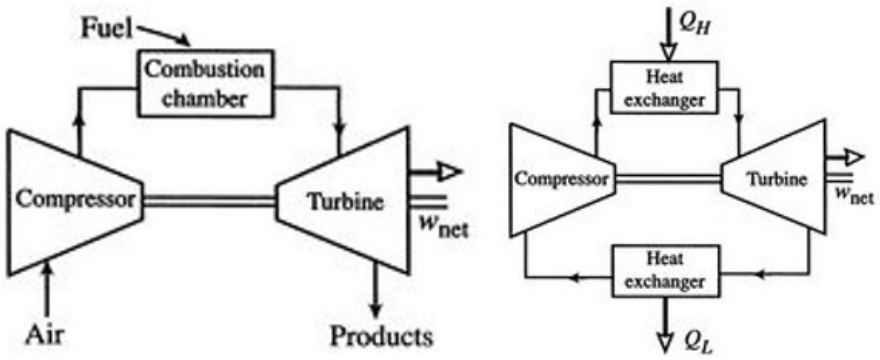

Figure 4.2: Typical Open and Closed configuration of Brayton-Joule cycles [45]

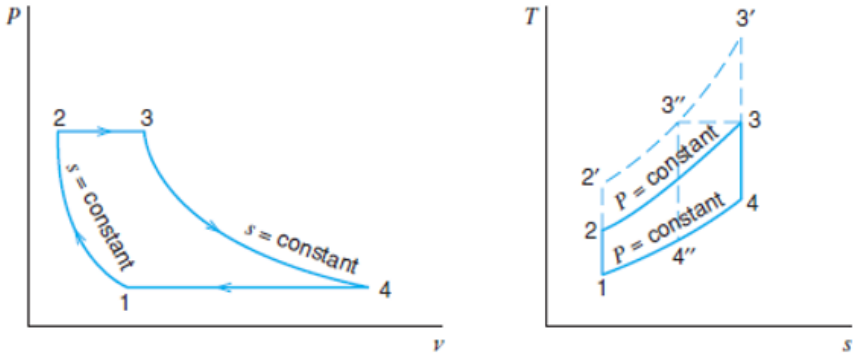

Figure 4.3: Typical diagrams of a Brayton-Joule Cycle [45]

4.1.1 Compression

Air is compressed to high pressure and temperature via an isentropic, adiabatic and reversible process:

$$P_2 = P_1 \cdot PR \tag{4.1}$$

$$\frac{T_2}{T_1} = \left(\frac{P_2}{P_1}\right)^{\frac{\gamma_{air}-1}{\gamma_{air}}} \tag{4.2}$$

$$\gamma_{air} = c_{p_{air}}/c_{v_{air}} \tag{4.3}$$

where T_1 and T_2 denote the temperatures at the compressor inlet and outlet respectively, P_1 and P_2 represent the pressures at the compressor inlet and outlet with their ratio as PR, and γ is the specific heat ratio between the one at constant pressure and the one at constant volume.
The performance of the compressor in the real case is less than the ideal due to the presence of losses (entropy production) in the component called irreversibilities.
So to calculate the real temperature at the exit is necessary to introduce the term to take them into account as η_{comp} :

$$T_2 = T_1 + (T_{2s} - T_1)/\eta_{comp} \tag{4.4}$$

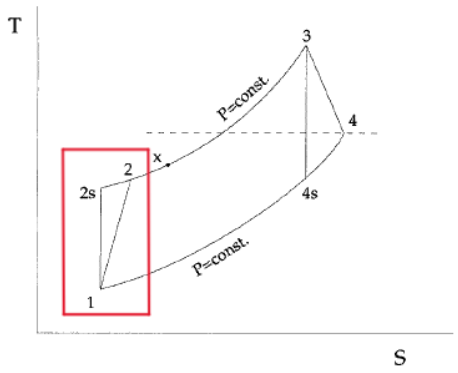

Figure 4.4: Compressor irreversibilities due to entropy generation [46]

4.1.2 Combustion

High-pressure air is fed into a combustion chamber where fuel is added and ignited, the process can be analysed with the first law of thermodynamic:

$$\Delta h = Q - W \tag{4.5}$$

where Δh signifies the change in enthalpy, Q represents the heat added, and W denotes the work done. In our case we have that difference in enthalpy is basically given by the LHV of the fuel.
To calculate the temperature (K) after the combustion the following correlation, obtained by an energy balance, can be used:

$$m_{gas} \cdot c_{p_{gas}} \cdot (T_3 - T_0) = m_{air} \cdot c_{p_{air}} \cdot (T_2 - T_0) + (\eta_{comb} \cdot m_{fuel} \cdot LHV_{fuel}) \tag{4.6}$$

$$T_3 = \frac{(m_{air} \cdot c_{p_{air}} \cdot (T_2 - T_0)) + (\eta_{comb} \cdot m_{fuel} \cdot LHV_{fuel})}{m_{gas} \cdot c_{p_{gas}}} + T_0 \tag{4.7}$$

Where:

- with $m_{gas} = m_{air} + m_{fuel}$ mass flow rate of the gas is the sum of the air and fuel one
- $c_{p_{air}}$, $c_{p_{gas}}$ specific heats at constant pressure
- LHV_{fuel} lower heating value of the fuel
- $T_0 = 298.15$ reference temperature of the system in K

$$p_3 = (1 - \eta_p) \cdot p_2 \tag{4.8}$$

The heat $(1 - \eta_{comb})$ and pressure $(1 - \eta_p)$ losses in the combustion are usually 1-2 % of the total.

4.1.3 Turbine

High-temperature gases from the combustion chamber expand in the turbine in an isentropic process, producing mechanical work:

$$P_3 = P_4 \cdot ER \tag{4.9}$$

$$\frac{T_3}{T_4} = \left(\frac{P_3}{P_4}\right)^{\frac{\gamma_{gas}-1}{\gamma_{gas}}} \tag{4.10}$$

$$\gamma_{gas} = c_{p_{gas}}/c_{v_{gas}} \tag{4.11}$$

where T_3 and T_4 denote the temperatures at the turbine inlet and outlet respectively, P_3 and P_4 represent the pressures at the turbine inlet and outlet with their ratio ER, and γ is the specific heat ratio between the one at constant pressure and the one at constant volume.
The performance of the turbine in the real case is less than the ideal due to the presence of losses (entropy production) in the component called irreversibilities.
So to calculate the real temperature at the exit is necessary to introduce the term to take them into account as η_{turb} :

$$T_4 = T_3 - \eta_{turb} \cdot (T_3 - T_{4s}) \tag{4.12}$$

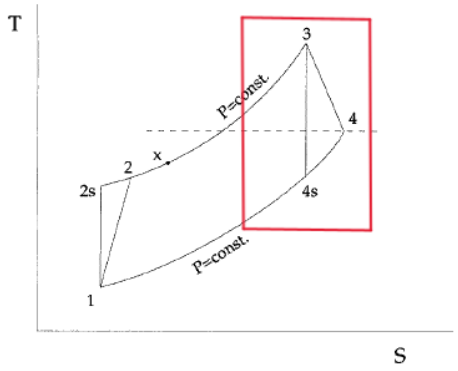

Figure 4.5: Turbine irreversibilities due to entropy generation [46]

4.1.4 Power generation and efficiency

The net power, or electrical, can be obtained subtracting the power used for the compressor to the one obtained by the turbine:

$$P_{el} = P_{turb} - P_{comp} \tag{4.13}$$

Then to define these powers:

$$P_{comp} = m_{air} \cdot c_{p_{air}} \cdot (T_2 - T_1) \cdot \eta_{gen} \tag{4.14}$$

$$P_{turb} = m_{gas} \cdot c_{p_{gas}} \cdot (T_3 - T_4) \cdot \eta_{gen} \tag{4.15}$$

- with $m_{gas} = m_{air} + m_{fuel}$ mass flow rate of the gas is the sum of the air and fuel one
- $c_{p_{air}}, c_{p_{gas}}$ specific heats at constant pressure
- η_{gen} the yield of the electrical conversion

The efficiency of the Brayton cycle (η_{Brayton}) can be assessed using the formula:

$$\eta_{\text{Brayton}} = \frac{P_{el}}{m_{fuel} \cdot LHV} \tag{4.16}$$

where P_{el} represents the electrical power output of the gas turbine, m_{fuel} denotes the fuel mass flow rate, and LHV signifies the lower heating value of the fuel.

4.2 Gas Turbine theory

4.2.1 The compressor and the turbine

The compressor is a mechanical device designed to increase the static pressure of a gas by means of a decrease of its volume. On the other hand the turbine is a device designed to convert the kinetic energy of a fluid into mechanical energy, typically to generate electricity or drive machinery.
There exist two primary types of compressors-turbines: **axial** and **radial**.

Axial Machines

Axial compressors are dynamic compressors where the gas flows in parallel with the axis of rotation. They comprise alternating rows of rotating blades (rotors) and stationary blades (stators); in which the gas velocity is increased by the rotor blades and subsequently its pressure by the stator blades.
Axial turbines are made of alternating rows of stationary vanes (nozzles) and rotating blades where the fluid's kinetic energy is converted into mechanical energy as it passes through the turbine, driving the rotor blades and causing rotation. Also for them the gas flows parallel to their axis of rotation.
These devices work with a high value of specific velocity (2.5-20), high mass flow rates and low specific energy transfer (pressure-expansion ratio of one stage is 1.1-1.3). Due to their efficiency and capacity to handle high flow rates, axial compressors-turbines are commonly employed in power plants, and turbochargers.

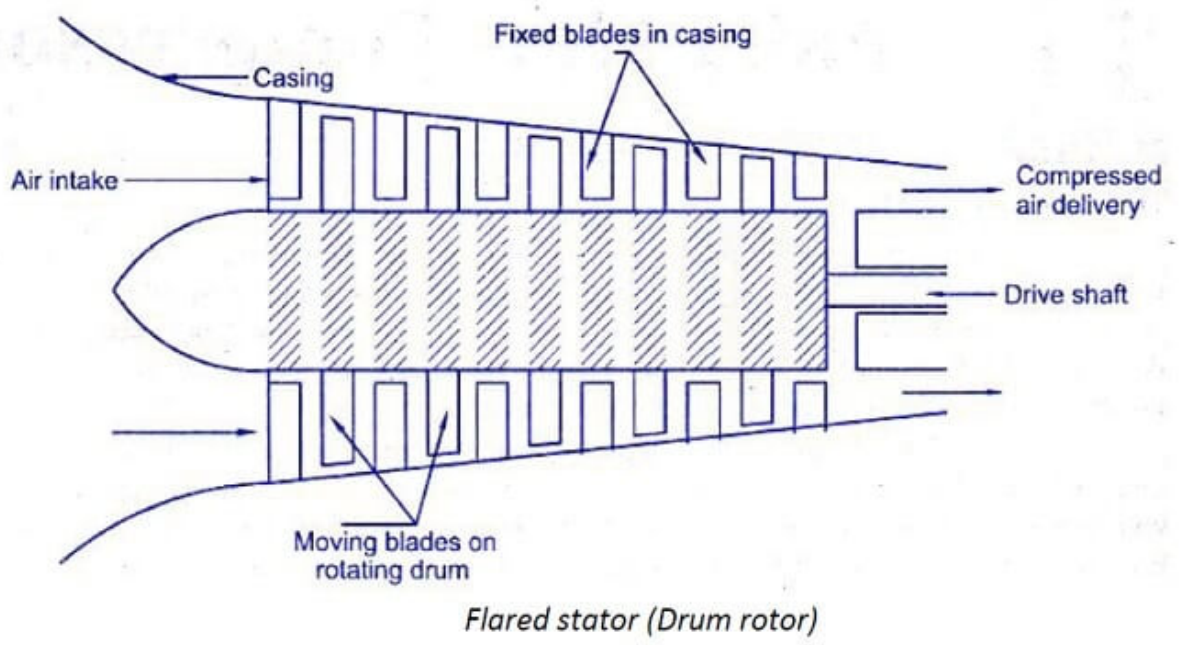

Figure 4.6: Multi stage axial compressor scheme [47]

Radial Machines

Radial compressors, also dynamic, differ in operation from axial compressors. The gas enters the compressor housing and is accelerated by a high-speed rotating impeller, then the kinetic energy imparted to the gas by the impeller is converted into pressure energy as the gas is forced outward by centrifugal force against a diffuser.

In radial turbines instead the fluid enters the turbine housing and is directed onto a rotating impeller that imparts kinetic energy to the fluid, which is then converted into mechanical energy as the fluid is forced outward by centrifugal force.
This outward flow drives the turbine rotor, generating mechanical energy.
Those devices work with low value of specific velocity (0.2-0.8), low mass flow rates and high specific energy transfer (pressure-expansion ratio of one stage is 4-5).

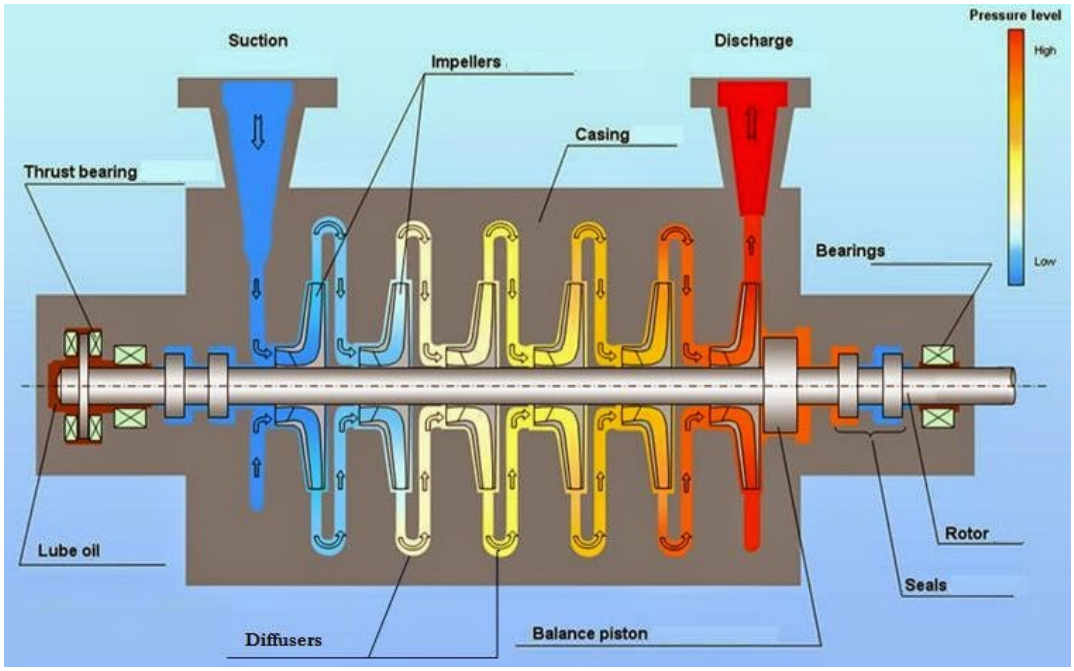

Figure 4.7: Multi stage radial compressor scheme [48]

In both types, compression-expansion is often split into multiple stages, each comprising rotating and stationary blades. Such staging enables enhanced efficiency, control, and management of high-pressure differentials. The number of stages is determined by factors such as desired pressure-expansion ratio, gas properties, and specific application requirements.
The higher pressure-expansion ratios or the greater the flow rates are, the more effective is the employment of more stages for the compression-expansion of the operating fluid.

4.2.2 The combustion process: CH_4 and H_2

Key points

The main focus when dealing with a gas turbine is on the combustion process, this seeks to reach the best compromise possible with the usage of the fuel available and the emissions.
The point can be summarized as follows:

- Use the correct surplus of air to ensure a complete combustion, limiting the CO emissions and exploiting all the fuel available.

- Limiting the NO_x emissions by controlling the temperature, the residence time and the pressure. However those emissions have an exponential dependence on the flame temperature that makes the reduction of the combustion temperature the key strategy for low NO_x combustion.

Lean Premixed Burners

Currently the main combustion technique employed in the gas turbines is the premixing one that enable to reduce the emissions of NO_x with a careful management of the mixture and flame temperature. This technique named "Dry Low NOx" (DLN) or "Dry Low Emission" (DLE) operates in lean premixed or partially premixed conditions; it is very useful in terms of reducing pollution but it needs to be designed carefully to avoid flashback, self-ignition and thermo-acustic instabilities.
An example of this technologies can be seen in the following image:

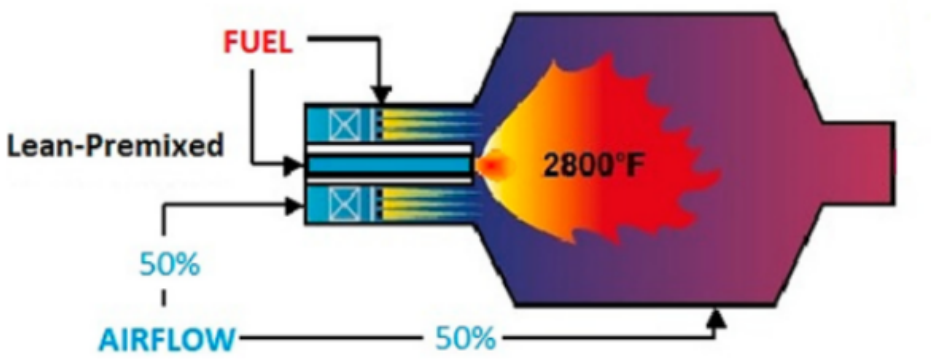

Figure 4.8: Operating scheme of a lean premix type combustor [35]

Conversion to H_2 firing

This technology however cannot handle the shifting of gas turbines to H_2 firing, essential to reduce CO_2 emissions, due the to different nature of the fuel:

- Higher adiabatic flame temperature than methane that defines the combustion efficiency, the cooling requirements of the liner and a possible increase in NO_x emissions
- The lower calorific value of hydrogen, in terms of volume, is approximately 3 times lower than that of natural gas, due to the lower density; therefore, fuel supply systems capable of providing a higher volumetric flow rate are required.
- Hydrogen's reactivity is around a hundred times greater than natural gas and it has a flame speed that is about an order of magnitude higher.
- The ignition delay time decreases with the H_2 addition. Designing the premixer to prevent autoignition requires knowledge of the fuel-mixture ignition delay time and the local conditions relative to a premixing time scale.
- The higher flame speed increases the risk of dynamic instabilities (i.e., flashbacks where turbulent flame speed exceeds the flow velocity, typically in the flow boundary layer, allowing flame propagation inside the mixer, with obvious problems of material resistance and safety).
- High H_2 content increases the risk of thermo-acoustic instabilities characterized by large amplitude pressure oscillations that are driven by unsteadiness in the phase heat release, which strongly alters the combustion process.
- The combustion of hydrogen produces flames that are not very bright; therefore, most of the energy is transmitted by convection, by the sensible heat in the exhausted gas decreasing the yield.

	H_2	CH_4
Molecular Weight [g/mol]	2.016	16.04
Density at NTP [Kg/m3]	0.0838	0.6512
Self Ignition T [K]	845-858	813-905
Minimum Ignition Energy [mJ]	0.02	0.29-0.33
Flammability range in Air [vol%]	4-75	5-15
Flammability range [ϕ]	0.1-7.1	0.4-1.6
Stoich. Composition in air [vol%]	29.53	9.48
Adiabatic Flame Temperature [K]	2318-2400	2158-2226
Lower Heating value [MJ/Kg]	118.8-120.3	50
Higher Heating Value [MJ/Kg]	141.75	55.5
Lower Heating value [MJ/m3]	10.78	35.8
Higher Heating Value [MJ/m3]	12.75	39.72
Lower Wobble Index [MJ/m3]	40.7	47.94

Table 4.1: Properties of H_2 compared with Methane (CH_4) [35]

The following sections report the combustion technologies developed to reduce NO_x formation in the pathway to increase the fuel flexibility in gas turbines, i.e., increasing the range of H_2 content in natural gas-hydrogen mixtures.
These systems can be divided into four categories, depending on the strategy adopted for stabilizing combustion.

1) Combustion aerodynamically stabilized by propagation;

2) Combustion stabilized by self-ignition;

3) Staged combustion, stabilized with different methodologies (by propagation and/or self-ignition);

4) Micro-mixing combustion, with many small premixed, partially premixed or diffusive flames.

1) Aerodynamically Stabilized Burners (Swirled Jets)

Swirled jet combustion technology harnesses the aerodynamic effects of swirling airflow to enhance mixing between fuel and air, promoting efficient combustion. By creating a strong rotational flow, swirled jets facilitate the formation of recirculation zones, leading to improved flame stability and shortening the reaction zone. However, achieving the ideal swirl number for optimal performance requires careful design considerations, and intricate burner geometries may be necessary to achieve desired combustion characteristics.

Pros: Utilizes swirled jets to create strong rotational flow for flame stabilization.
Improves combustion quality and shortens the reaction zone.
Suitable for a wide range of fuel compositions.

Cons: Limited to certain swirl numbers for optimal performance.
May require complex burner designs.

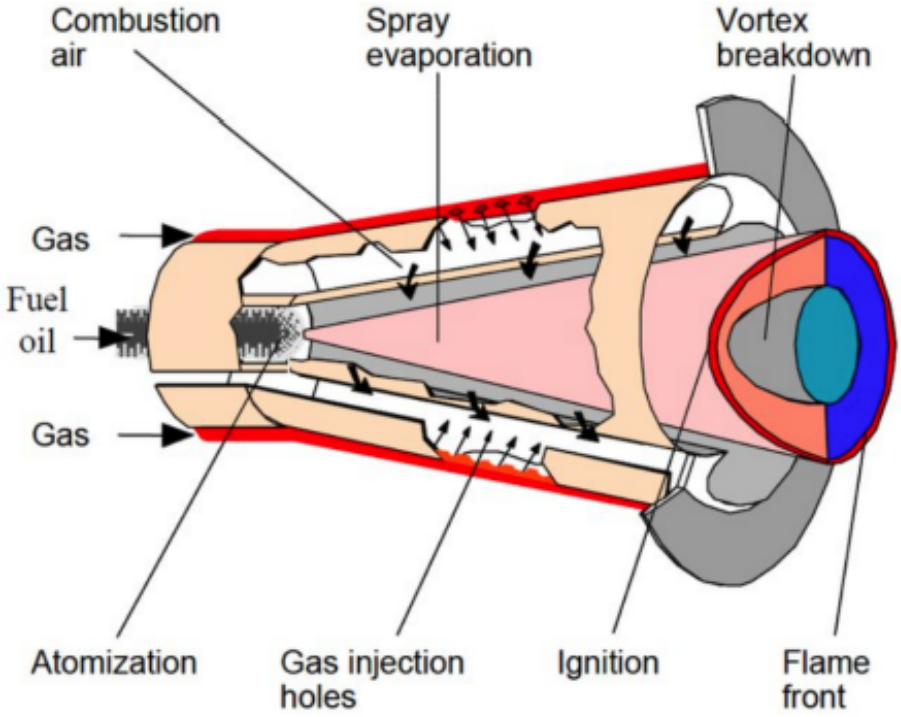

Figure 4.9: Example of aerodynamic stabilized burner [35]

2) Stabilized Combustion for Self-Ignition

Self-ignition combustion technologies, such as Flameless Oxidation (FLOX™) and Moderately Intense Low Oxygen Dilution (MILD), rely on preheating and recirculation to achieve self igniting combustion with reduced emissions. By maintaining uniform temperature distributions and minimizing peak flame temperatures, these techniques mitigate NO_x formation while facilitating stable and efficient combustion. The flameless combustion technology is commercially available for reheating furnaces in the steel sector, with devices already able to operate with natural gas and hydrogen mixtures up to 100% H_2, while in the gas turbine sector, there are only some numerical and experimental examples like the one of Banihabib et al. [39] that conducted modifications on a 100 KW AE-T100 PH micro-gas turbine swirl-type combustor, repurposed from its original natural gas usage configuration.
This technology however is still far from being mature as achieving optimal performance requires precise control of operating conditions, including temperature, pressure, and fuel-air ratios, which may necessitate sophisticated control systems.

Pros: Generates uniform temperature distribution with reduced NO_x formation.
Suitable for a wide range of fuels, including hydrogen-rich mixtures.

Cons: Limited by specific temperature and pressure conditions for optimal performance.
May require additional control mechanisms for stability.

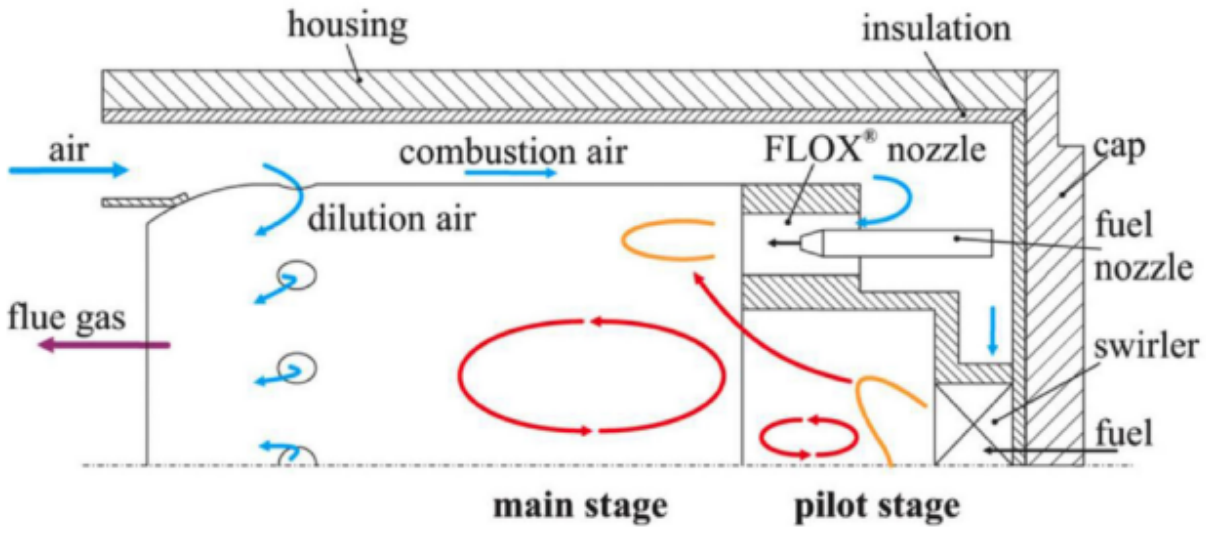

Figure 4.10: Example of a Stabilized Combustion for Self-Ignition burner [35]

3) Staged Combustion

Staged combustion techniques, such as Rich-Burn/Quick-Mix/Lean-Burn (RQL), employ sequential fuel injection to create distinct combustion zones with varying air-fuel ratios. By dividing the combustion process into stages, these technologies mitigate NO_x formation by reducing peak flame temperatures and promoting more complete fuel oxidation. However, transition regions between rich and lean combustion zones present challenges in minimizing thermal NO_x production necessitating careful design and control strategies to optimize performance while meeting emissions targets. Such as the controls for the mixing with the secondary air that must be very rapid and uniform to reduce the residence time in the transition zone.

Pros: Divides the reaction zone to control NO_x formation.
Offers flexibility in fuel-air mixing for emissions control.

Cons: Transition zones between rich and lean combustion may increase thermal NO_x production.
Requires careful design and control for optimal performance.

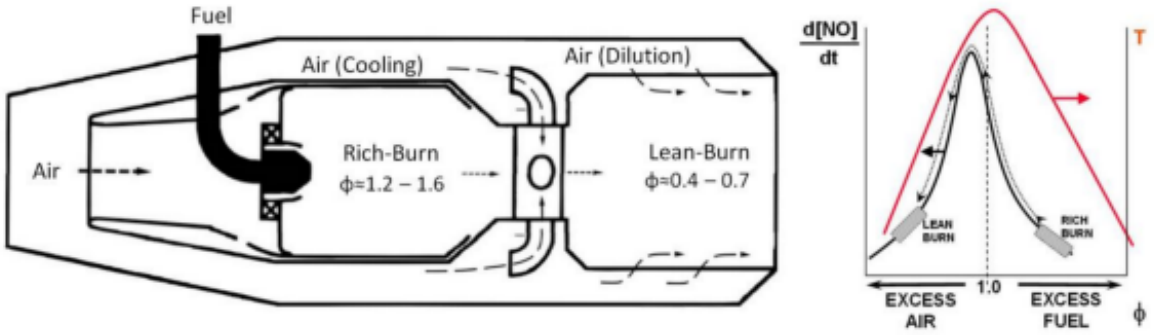

Figure 4.11: Example of an RQL combustor and NO_x formation rate, temperature trend as a function of the equivalence ratio [35]

4) Micro-Mixing Combustion

Micro-mixing combustion focuses on enhancing the mixing of fuel and oxidizer at a small scale, typically through the use of intricate injector designs or microfluidic channels. By promoting rapid and thorough mixing, this technology facilitates more uniform combustion, which helps reduce NO_x emissions. The basic idea is to distribute the heat release inside the turbine combustor, through a large number of very small flames, instead of a single conventional flame allowing a great scalability and flexibility that makes this technology suitable for various turbine sizes and operating conditions. However, the complexity of the fuel and air supply systems, as well as the need for optimization based on fuel compositions and turbine configurations, can pose challenges in implementation and increase manufacturing costs. The main exponent of this technology is the KAWASAKI Heavy Industries burner, based on the Aachen University prototype, that is proven to run on up to 100% hydrogen in the GPB17MMX [49] gas turbine under commercial operating conditions. It seems that the machine supplied 1.1 MW_e of power, instead of the nominal natural gas power of 1.8 MW_e, with about 2.8 MW_t of available thermal power, thus with an electrical efficiency of 27%. The NO_x production with this combustor (at two bar condition) remains below 20 ppm at 15% O_2 for any workload. The load variation is obtained through the ignition of the different rings (from idle to 30% load conditions, inner two hydrogen rings were used and from 30% load to full load conditions, all three rings were used).

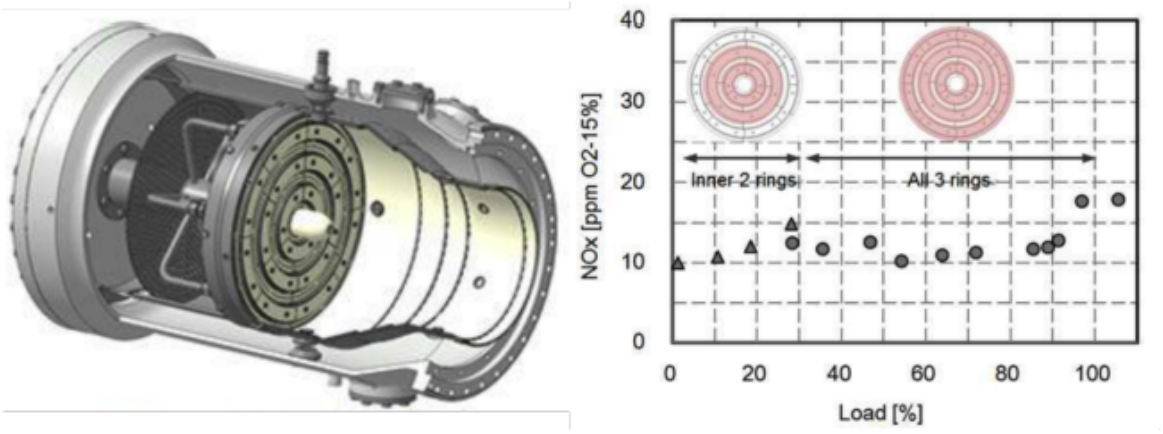

Figure 4.12: Micro mixing combustion, scheme of KAWASAKI M1A-17 gas turbine combustor and related NO_x emissions [36]

It has been found that the two key parameters that influence the flame shape and length, and then NO_x formation, are the air flow blockage ratio and the depth of the fuel jet penetration into the air stream. The advantages of this technology are the safety in relation to the possibility of flashback, and the low NO_x emission thanks to the very short residence times of the reactants in the micro-flames area.

Pros: Utilizes rapid mixing between fuel and oxidant to reduce NO_x emissions.
Offers scalability and flexibility in design.

Cons: Complex fuel and air supply systems may increase manufacturing costs.
Optimization required for different fuel compositions and turbine sizes.

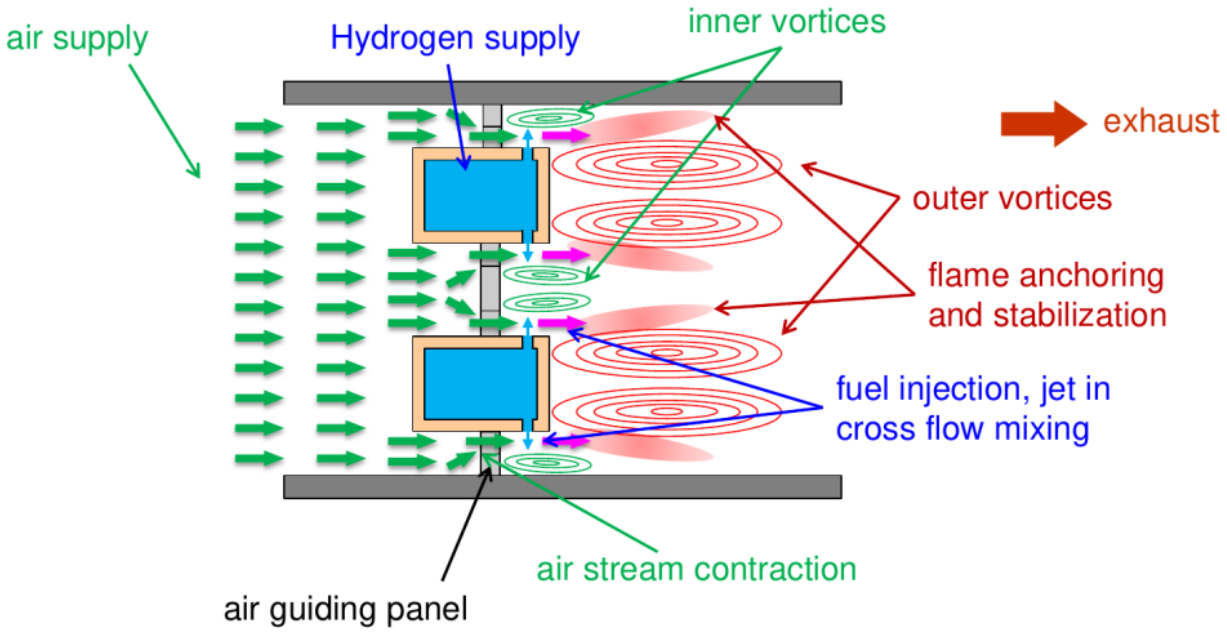

Figure 4.13: Operating principle of KAWASAKI micro-mixing type combustor [36]

Exhaust Gas Recirculation

All the technologies described above can be integrated with flue gas recirculation. Exhaust Gas Recirculation (EGR) involves reintroducing a portion of exhaust gases into the combustion chamber to dilute the fresh air and lower the combustion temperature. By reducing the oxygen concentration and suppressing temperature peaks, EGR helps mitigate NO_x formation while improving combustion stability. Additionally, EGR enhances operational flexibility by allowing adjustments to the recirculation rate based on load demands. However, its application in gas turbine systems may be limited, especially in highly flexible operating conditions where maintaining combustion stability can be challenging. Effective implementation of EGR requires meticulous control systems to achieve desired emissions reduction without compromising turbine performance.

Pros: Reduces local temperature peaks and slows down NOx formation.
Enhances operational flexibility and efficiency.

Cons: Limited application in gas turbine systems, particularly in flexible operating conditions.
Requires careful control and optimization for effective emissions reduction.

4.2.3 The design point

In order to select the operational design point for a gas turbine various factors need to be taken into account to ensure the best performance. This process revolves around identifying the operating conditions that align with the desired power output while meeting specific criteria such as fuel usage, emissions control, and operational adaptability.

The following topics need to be taken into account during this decision-making process:

- **Power Output Needs:** Determining the required power output sets the groundwork for defining the operational conditions of the gas turbine system.

- **Efficiency Optimization:** Obtaining the best efficiency possible is crucial to minimize operational costs and environmental impact. Operating the turbine at its peak efficiency point ensures the highest power output for the energy input.
- **Environmental Compliance:** The respect of the emission limits is one of the most important points nowadays. In particular very strict regulation is applied to nitrogen oxides (NOx), carbon monoxide (CO) and carbon dioxide (CO_2) that are quite dangerous for human health and the atmosphere.
- **Component Longevity:** Operating conditions significantly affect the lifespan of turbine components. Designing the operational point to reduce stress on critical components, such as blades and combustors, helps ensure their durability and reliability.
- **Fuel Choice Impact:** The selection of fuel influences the design point. Different fuels possess distinct combustion characteristics and energy densities, which impact turbine performance and emissions.
- **Cost Management:** Balancing performance needs with budgetary constraints is crucial. Optimal design points often strike a balance between upfront capital expenditures and long-term operational costs, considering factors such as fuel prices, maintenance expenses, and potential revenue streams.

To sum up the selection of the design point for a gas turbine demands careful assessment, modeling, and refinement to obtain the best compromise between performance, efficiency, and sustainability throughout the turbine's operational lifespan.

4.2.4 The off-design condition

In the off-design condition the power varies to satisfy a variable demand thus varying the operational condition of the system. In particular control on the power obtained can be done changing:

- The **quantity of fuel** and so the temperature of the operating points
- The **rotational speed of the machines** and the flow rates keeping the **same fuel/air ratio**
- The **blade angle** of the machines to impact the flow in a better way

This process revolves around identifying the operational parameters that allow the turbine to maintain acceptable performance levels while accounting for deviations in component efficiency and smooth operation.

The aspects to be taken into account can be summarized in:

- **Operating Range:** Gas turbines must operate efficiently across a range of conditions and transient operation.
- **The Component Efficiency Variation:** Various components within the gas turbine, such as compressors, combustors, and turbines, may experience efficiency variations under off-design conditions. These variations can result from factors like changes in inlet conditions, ambient temperature, and operating speeds. Usually compressor and turbine maps are used to quantify their off-design performance.

- **Performance Trade-offs:** Off-design operation often involves trade-offs between different performance parameters, such as efficiency, power output, and emissions. It is thus essential to find the best condition of operation based on the needs.
- **Stability and Reliability:** Maintaining stable and reliable operation is paramount, particularly during off-design conditions. Turbine control systems and operating strategies must be robust enough to handle variations in component efficiency without compromising safety or reliability.
- **Emissions Control:** Off-design operation can impact emissions performance, particularly under transient conditions. Designing the off-design condition to minimize emissions while maintaining acceptable performance levels is essential for regulatory compliance and environmental responsibility.
- **Flexibility Requirements:** Gas turbines often need to respond quickly to changes in demand or operating conditions. Designing for flexibility ensures that the turbine can adapt efficiently to varying load profiles and operational scenarios while maintaining performance and reliability.

To sum up the choice of the off-design condition involves careful analysis, modeling, and optimization to ensure reliable and efficient operation across a range of operating conditions while meeting performance, emissions, and reliability objectives.

Chapter 5

System Design

To develop the models necessary to carry out the analysis it was chosen to employ Python 3.11 coding language so that it could be read by various devices without the need of a license. In order to configure the system multiple libraries were imported to do the calculations, print graphs, read excel data and harness the thermodynamic properties of fluids directly from databases. In particular these are:

- **Numpy 1.26.4**, used to compute all basic calculations
- **Matplotlib 3.8.3**, used to print the graphs
- **Pandas 2.2.1**, used to import data from excel files
- **Coolproop 6.6.0**, used to harness thermodynamic properties
- **Cantera 3.0.0**, used to harness thermodynamic properties

The purpose of the simulation is to assess the feasibility of a gas turbine peaker, powered by H_2, both from technical and economical points of view. In particular the model comprises an already existing wind farm that supplies the electricity to a solid oxide or proton exchange membrane electrolyser; this then produces the hydrogen necessary to fuel the converted gas turbine when the electricity is requested from the grid during peak times. The model is based on the **Rhode** power station [10] that is one of the peaker plants operating in Ireland; it is comprised of **2 units of 52 MW** each, powered by natural gas. For the wind energy the nearly wind farm of **Mountlucas** [9] was used, it has a nominal power of **84 MW** and is comprised of 28 Siemens 3.0DD-101 turbines. For the solid oxide electrolyser the model was based on literature [21], referring to a real electrolyser built for a refinery in Rotterdam by **Multiplhy** [4] and another for the NASA by **Bloom Energy** [5]. The same was done for the PEM electrolyser, this time with the **Siemens Silyzer 300** [50].
Furthermore the script has the possibility to analyse turbine performance in blending conditions choosing the quantity of methane and hydrogen to be employed.

5.1 Gas Turbine modeling

5.1.1 Thermodynamic cycle

The Gas Turbine theory presented before {4} was implemented in a code to assess the performance of the system. The script was given the following inputs:

- P_{el}, desired electric power (52 MW)
- Mass fraction of the fuels (Methane or Hydrogen)
- Molar mass of all the substances involved
- Excess air of the system (fixed to obtain $750°C$ after the turbine)
- T_{inlet}, inlet temperature of the air (298.15 K)
- P_{inlet}, inlet pressure of the air (0.101325 MPa)
- Pressure ratio of the compressor (PR fixed at 15.9)
- Isentropic efficiency of the compressor ($\eta_{is} = 0.85$)
- Isentropic efficiency of the turbine ($\eta_{is} = 0.89$)
- Pressure and heat losses in the combustion chamber (5 %, 1 %)
- η_{gen}, conversion efficiency of the generator ($\eta_{gen} = 0.98$)

Compute the following desired outputs:

- Equivalence ratio of the combustion (ϕ)
- Temperature at the outlet of every component (Compressor, Combustion Chamber, Turbine)
- Pressure at the outlet of every component (Compressor, Combustion Chamber, Turbine)
- Mass flow rate of the air ($\dot{m}_{air}$), fuel ($\dot{m}_{fuel}$) and gas ($\dot{m}_{gas}$) at the inlet-outlet of the cycle
- Volumetric flow rate of the air ($\dot{V}_{air}$), fuel ($\dot{V}_{fuel}$) and gas ($\dot{V}_{gas}$) at the inlet-outlet of the cycle
- Yield of the cycle (η)

From the initial variables the model starts calculating the molar mass of the air and the gas, as they are a mix of different substances. Then the fuel to air ratio is computed knowing the excess air involved in the process:

$$Fuel/Air = \frac{\dot{m}_{fuel}}{\dot{m}_{air}} \tag{5.1}$$

From this the equivalence ratio ϕ is obtained as the ratio between the real and stoichiometric value:

$$\phi = \frac{\dot{m}_{fuel}/\dot{m}_{air}}{\dot{m}_{fuel_{stoich}}/\dot{m}_{air_{stoich}}} \tag{5.2}$$

At this point the calculation of the operating points of the cycle begins, in particular the pressure p_2 from the pressure ratio of the compressor and T_2. The Cantera database [51] is used to obtain the entropy S_1 (as pressure and composition of the air are known) then the point T_{2is} can be obtained with the new pressure p_2. From T_{2is} the real temperature can be obtained knowing the isentropic efficiency of the compressor:

$$T_2 = \left(\frac{(T_{2s} - T_1)}{\eta_{comp}}\right) + T_1 = 435°C \tag{5.3}$$

Then again knowing temperature, pressure and composition of the air the entropy S_2 is calculated. Now pressure and temperature after the combustion are computed taking into account the losses, for

the pressure by simply multiplying by the coefficient while for the temperature with a balance of mass.

$$p_3 = (1 - \eta_p) \cdot p_2 = 1.53MPa \tag{5.4}$$

Given:

- LHV_{CH_4} = 50000 kJ/kg (Lower Heating Value)
- LHV_{H_2} = 120000 kJ/kg (Lower Heating Value)
- A = Hydrogen fraction of mass
- B = Methane fraction of mass
- $T_0 = T_1$ (Reference Temperature)

$$T_3 = \frac{c_{p_{air}} \cdot (T_2 - T_1) + \eta_{comb} \cdot Fuel/Air \cdot (LHV_{H_2} \cdot A + LHV_{CH_4} \cdot B)}{Fuel/Air \cdot c_{p_{gas}}} + T_1 = 1470°C \tag{5.5}$$

With $c_{p_{air}}$ and $c_{p_{gas}}$ calculated by means of the CoolProp library and in the $c_{p_{gas}}$ case with an iterative method, to ensure the best precision in the calculations (input the first value of calorific value to calculate the temperature and repeat until the previous and following calorific values difference is below a threshold). At this point the composition of the gas is derived from the chemical reaction, knowing the fuel composition and the entropy after the combustion S_3, is calculated with the Cantera library, as the temperature T_3 is also known. Then with the constraint of $p_1 = p_4$, the gas composition and the entropy, it is possible to calculate T_{4s} and then T_4.

$$T_4 = T_3 - \eta_{turb} \cdot (T_3 - T_{4s}) = 750°C \tag{5.6}$$

To compute the desired temperature at the outlet of the cycle an iterative approach is adopted by means of adjusting the inlet air, in this case 750^{o}C was used as it is the correct temperature to recover the heat. After obtaining T_4 it is possible to calculate the entropy S_4 to obtain all the values for each point.
Furthermore it's important to point out that the desired power of the turbine is an input to the script. As a matter of fact this value is given by the data obtained from Sem-o [11], the national single electricity market operator, while the mass flow rates of both fuel and air are outputs.

To do so the power of the compressor and turbine are calculated in specific terms:

$$\frac{P_{comp}}{\dot{m}_{air}} = \Delta h_c = c_{p_{air}} \cdot (T_2 - T_1) \tag{5.7}$$

$$\frac{P_{turb}}{\dot{m}_{gas}} = \Delta h_t = c_{p_{gas}} \cdot (T_3 - T_4) \tag{5.8}$$

Them the specific electric power is derived from:

$$P_{el} = \eta_{gen} \cdot \left(\frac{P_t}{\dot{m}_{air}} - \frac{P_c}{\dot{m}_{air}} \right) \tag{5.9}$$

$$\frac{P_t}{\dot{m}_{air}} = \frac{P_t}{\dot{m}_{air}} \cdot \frac{\dot{m}_{fuel}}{\dot{m}_{air}} = \frac{P_t}{\dot{m}_{gas}} \cdot \left(\frac{\dot{m}_{fuel}}{\dot{m}_{air}} + 1 \right) \tag{5.10}$$

$$\frac{P_t}{\dot{m}_{air}} = c_{p_{gas}} \cdot (T_3 - T_4) \cdot \left(\frac{\dot{m}_{fuel}}{\dot{m}_{air}} + 1 \right) \tag{5.11}$$

So that:

$$\frac{P_{el}}{\dot{m}_{air}} = \eta_{gen} \cdot \left(\frac{P_t}{\dot{m}_{gas}} \cdot \left(\frac{\dot{m}_{fuel}}{\dot{m}_{air}} + 1 \right) - \frac{P_c}{\dot{m}_{air}} \right) \tag{5.12}$$

In the end the flow rates can be calculated as:

$$\dot{m}_{air} = \frac{P_{el}}{P_{el}/\dot{m}_{air}} \tag{5.13}$$

$$\dot{m}_{fuel} = Fuel/Air \cdot \dot{m}_{air} \tag{5.14}$$

$$\dot{m}_{H_2} = \dot{m}_{fuel} \cdot A \tag{5.15}$$

$$\dot{m}_{CH_4} = \dot{m}_{fuel} \cdot B \tag{5.16}$$

$$\dot{m}_{gas} = \dot{m}_{air} + \dot{m}_{fuel} \tag{5.17}$$

The results obtained with fuel 100% hydrogen, considering fixed excess air and $\dot{m}_{air}$, are:

- An equivalence ratio of 0.48 (lean mixture)
- A mass flow of air of 85 kg/s
- A mass flow of fuel of 1.2 kg/s
- A power of 35 MW for the compressor
- A power of 87 MW for the turbine

On the other hand only with methane the results are:

- An equivalence ratio of 0.27 (lean mixture)
- A mass flow of air of 94 kg/s
- A mass flow of fuel of 2.9 kg/s
- A power of 39 MW for the compressor
- A power of 91 MW for the turbine

If we consider instead a blend made of 50/50 % by mass, the following results are obtained:

- An equivalence ratio of 0.25 (lean mixture)
- A mass flow of air of 93 kg/s
- A mass flow of fuel of 1.7 kg/s
- A power of 38 MW for the compressor
- A power of 90 MW for the turbine

Then CoolProp library is used to calculate the density of the fluid and obtain all the volumetric flow rates.

Finally the yield of the cycle is calculated:

$$\eta = \frac{P_{el}}{(m_{H_2} \cdot LHV_{H_2}) + (m_{CH_4} \cdot LHV_{CH_4})} \tag{5.18}$$

So it is possible to say that for the H_2 turbine:

- 85 kg/s of air correspond to 72 m^3/s
- 1.2 kg/s of hydrogen corresponds to 1.7 m^3/s
- A cycle yield of **36%** assuming that the hydrogen technology would be as "efficient" as the methane one (the best obtained so far given the literature is 27 % [35])

So it is possible to say that for the gas turbine:

- 94 kg/s of air correspond to 79 m^3/s
- 1.2 kg/s of hydrogen correspond to 0.5 m^3/s
- A cycle yield of **35.6%** for a traditional gas turbine

For the blended turbine:

- 93 kg/s of air correspond to 78 m^3/s
- 0.85 kg/s of hydrogen corresponds to 1.2 m^3/s
- 0.85 kg/s of methane corresponds to 0.15 m^3/s
- A cycle yield of **35.7%** assuming that the hydrogen technology would be as "efficient" as the methane one

So now it is possible to confirm the qualitative shape of the Brayton-Joule cycle in a T-S diagram to check for irregularities.
For example with a power of 52 MW burning hydrogen, methane or in blended operation the only difference is related to the composition of the gases after the combustion that slightly varies the entropy of the system:

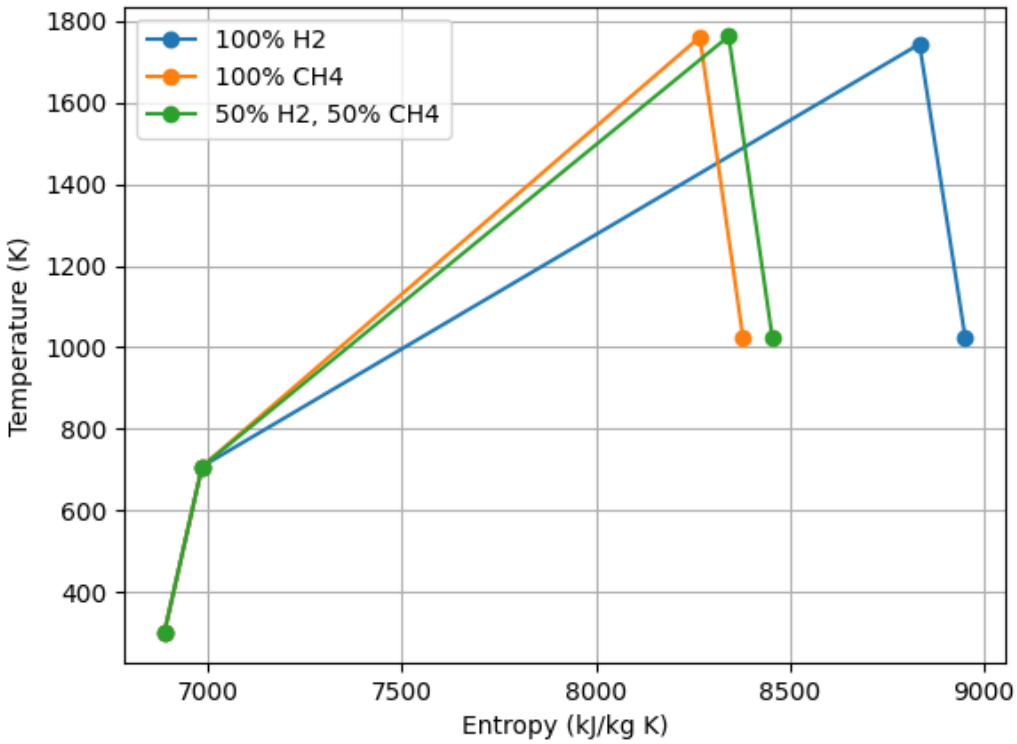

Figure 5.1: T-S diagram for a 52 MW turbine at design point with three fuel configurations

5.1.2 The emissions in blending conditions

The code is able to compute different fuel compositions to see how emissions are correlated with the mass fractions. In particular it varies A, B (percentage of H_2 and CH_4) accordingly for 100 runs and calculates all the previous employed variables with a focus on the gas composition:

- Molar mass of air and gas
- Excess air
- Fuel/Air ratio
- Temperature, pressure and entropy in all operating points
- Gas composition after combustion (Employment of Cantera library)
- Mass flow rate of the air, fuel and gas at the inlet-outlet of the cycle
- Volumetric flow rate of the air, fuel and gas at the inlet-outlet of the cycle
- Yield of the cycle

The results indicate the quantity of CO_2 emitted for each kWh produced and for each kg of fuel employed. The results are compared with the literature to ensure their veridicity.

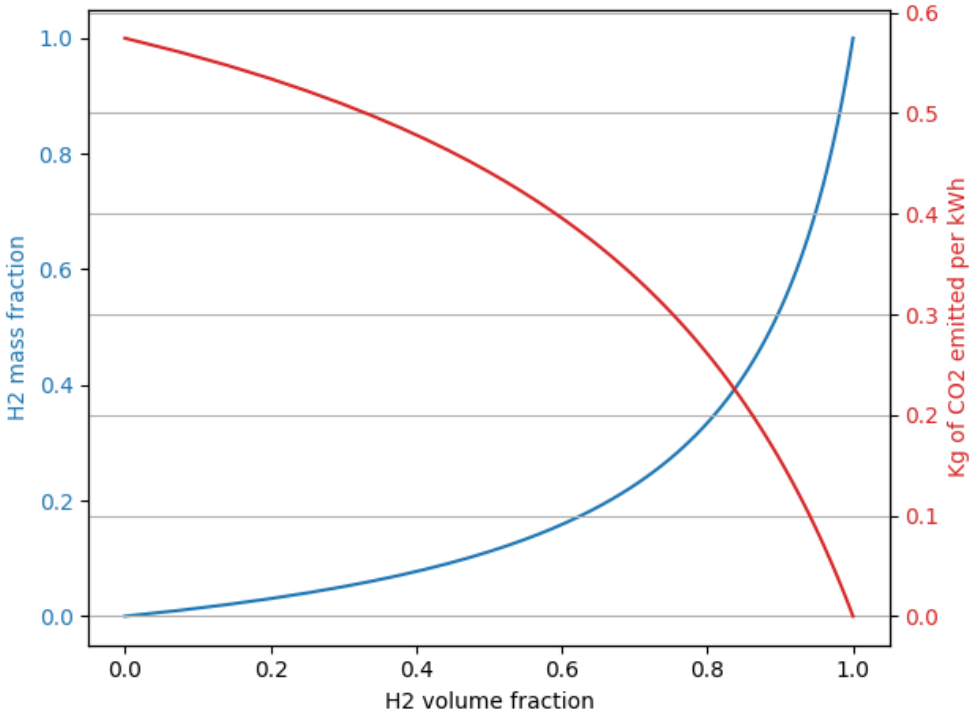

Figure 5.2: H_2 Volume fraction vs kg of CO_2 per kWh produced

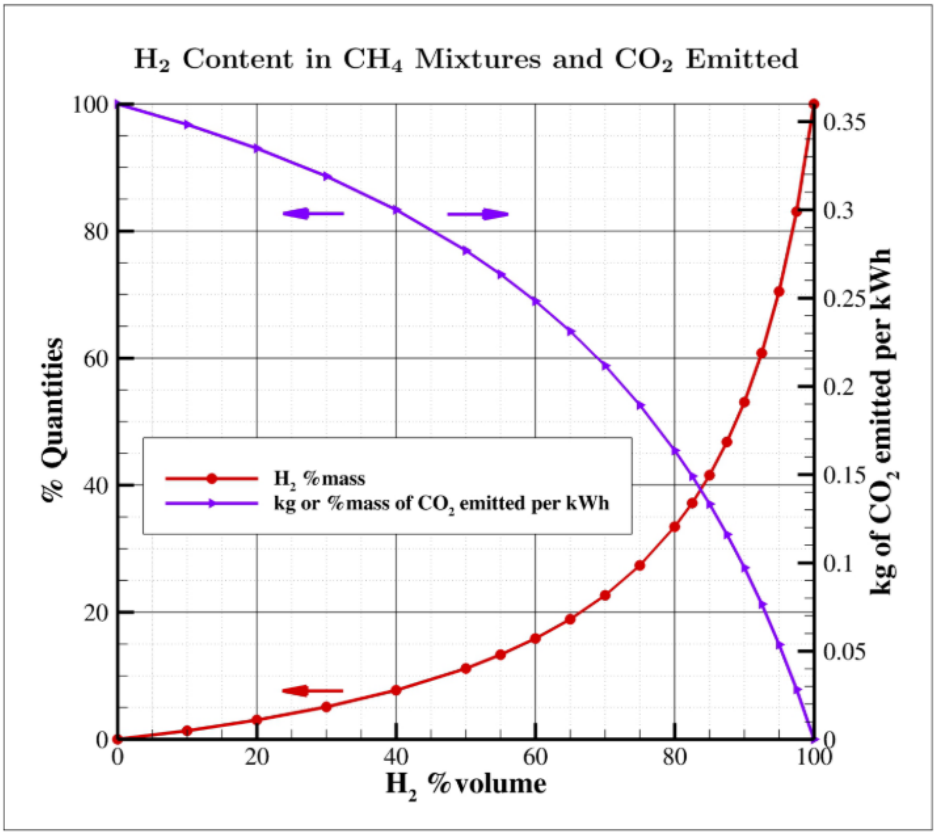

Figure 5.3: H_2 Volume fraction vs kg of CO_2 per kWh produced as reported in article [35]

As we can see from the figures the trend is the same but the values are slightly different due to the different emission impact that a kWh has for the systems. This is because the considered efficiency is different in the simulation by D. Cenere [35]. Indeed the script design point efficiency is around

35-36% while in the publication it's 55% leading to less fuel consumption therefore less CO_2 emitted; the value used in the article is feasible for a combined cycle while the value in the script is meant for a peaker plant.

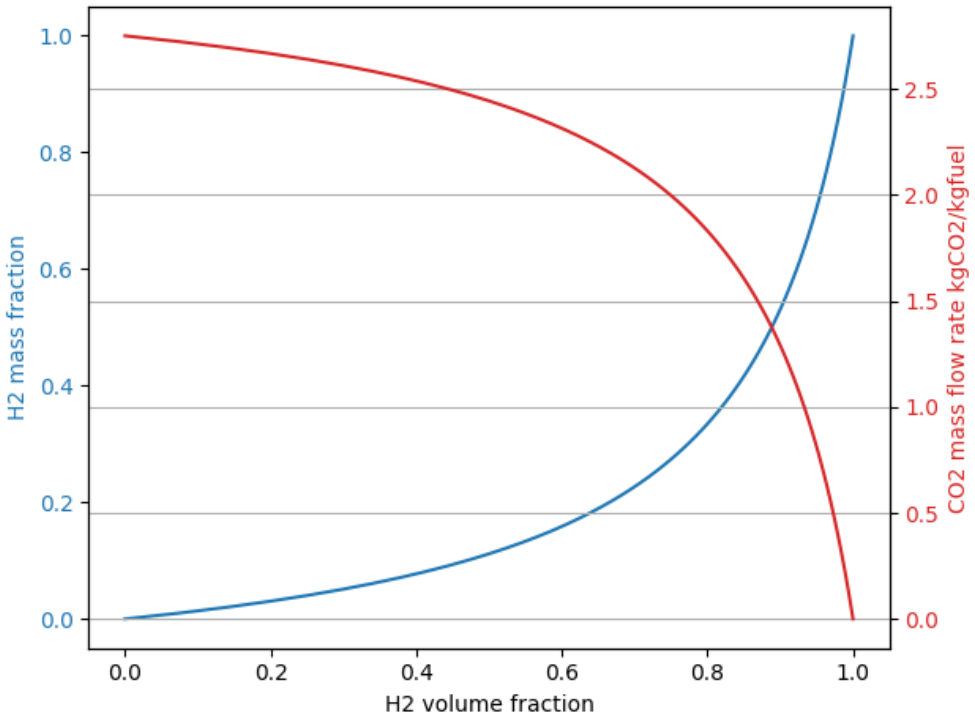

Figure 5.4: H_2 Volume fraction vs kg of CO_2 per kg of fuel employed

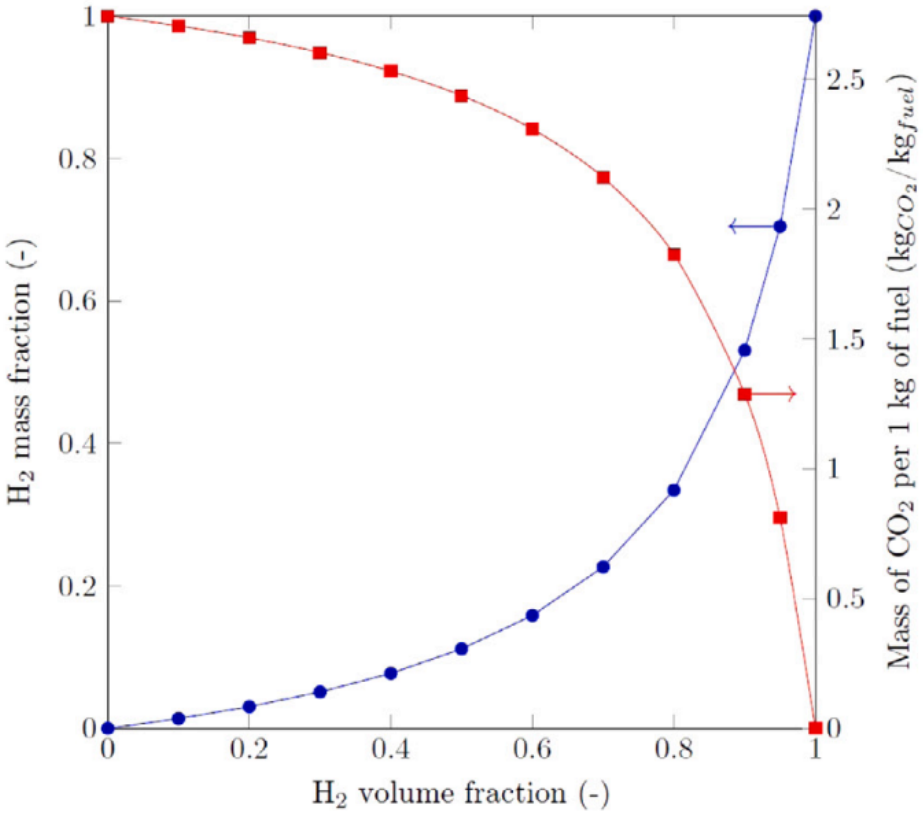

Figure 5.5: H_2 Volume fraction vs kg of CO_2 per kg of fuel employed as reported in article [52]

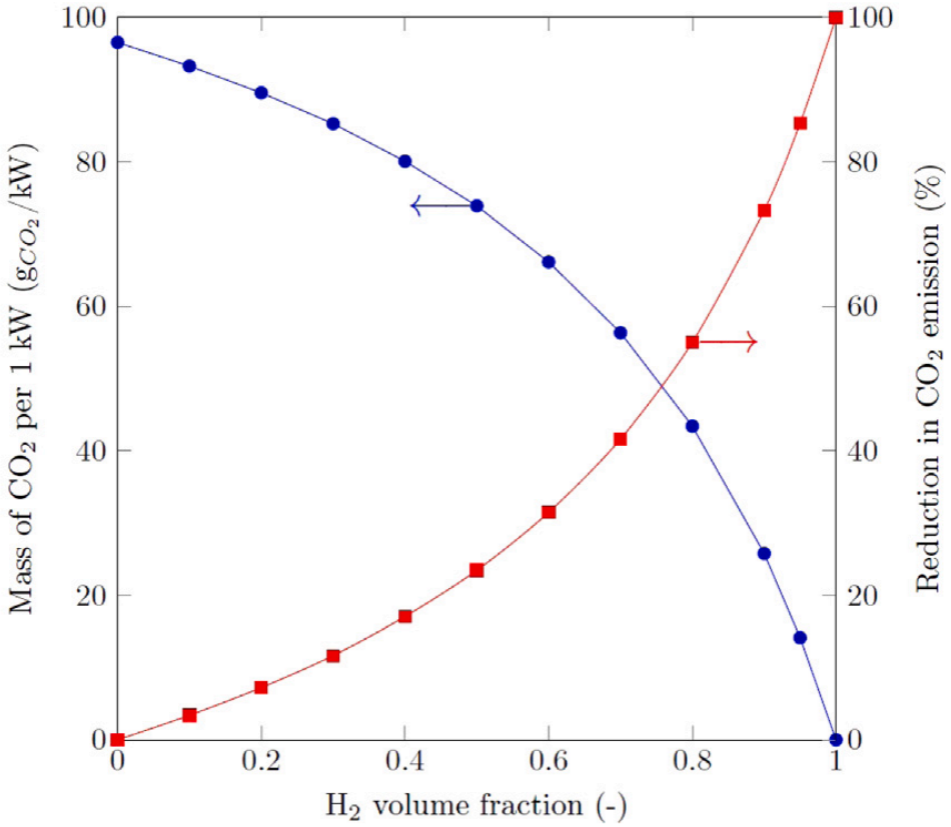

Figure 5.6: H_2 volume fraction vs % of CO_2 decrease [52]

Instead in the article of D. Pashchenko [52] the emissions are plotted for the kg of fuel, that is not dependent on the efficiency, so the graph is the same. The graph related to the percentage decrease of CO_2 with the increase of H_2 mass fraction is also shown.

5.1.3 The real case data and off design conditions

At this point the data from the Rhode power station of the year 2022 (source: Sem-o [11]), as a time series of the mean MW value in intervals of half an hour, was imported in Python thanks to the Pandas library. The choice of year 2022 is related to the quality of the data, in 2022 indeed the peaker plant worked for 415 equivalent hours while in 2023 only for 35 equivalent hours, so for a significant simulation the 2022 was the only possibility. Then for each value of the power, the system calculates the mass flow rates or air and fuel necessary for the operation; keeping into account that the efficiency of the components varies with the off design conditions.
To identify the variation of the efficiency components were used, for both compressor and turbine. These maps are used by manifactures to express the performance of a machine in function of the pressure ratio and mass flow rate employed. In the following graph is reported a summary of the isentropic efficiency in different operating condition for both turbine and compressor:

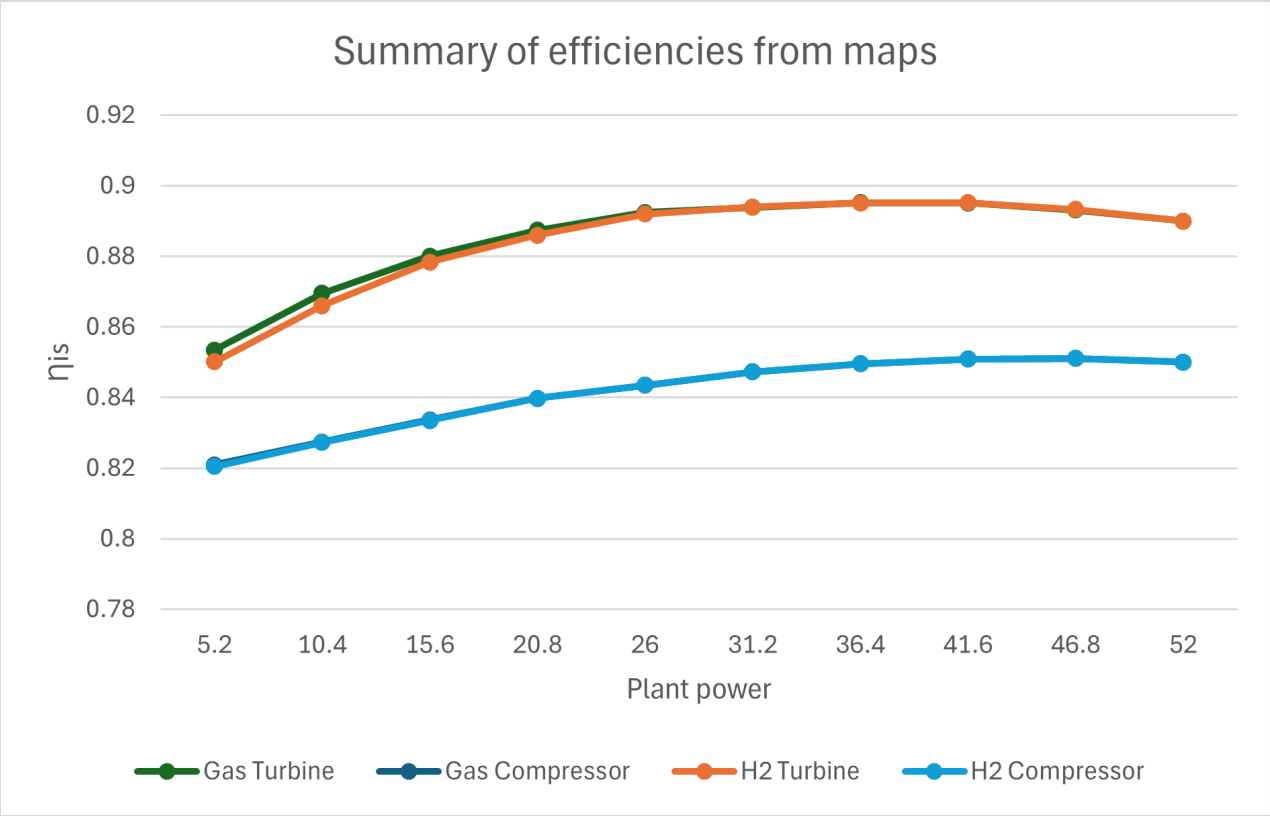

Figure 5.7: Isentropic efficiency of the components in gas and H_2 operation for different loads

In particular the maps used were scaled with the software GasTurb [53]:

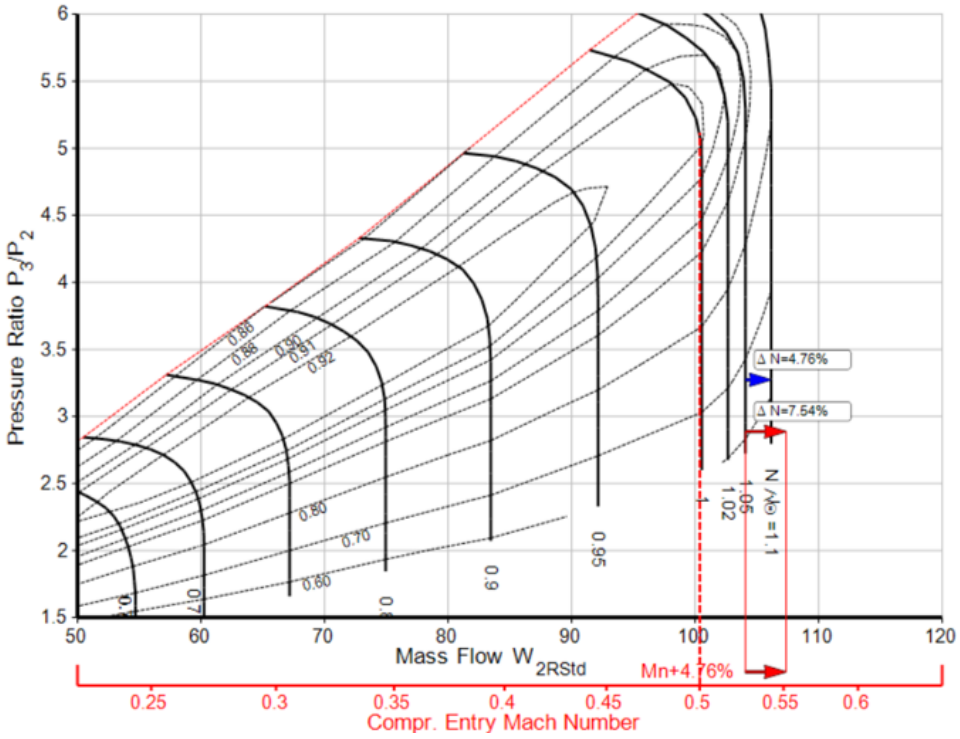

Figure 5.8: Compressor map [54]

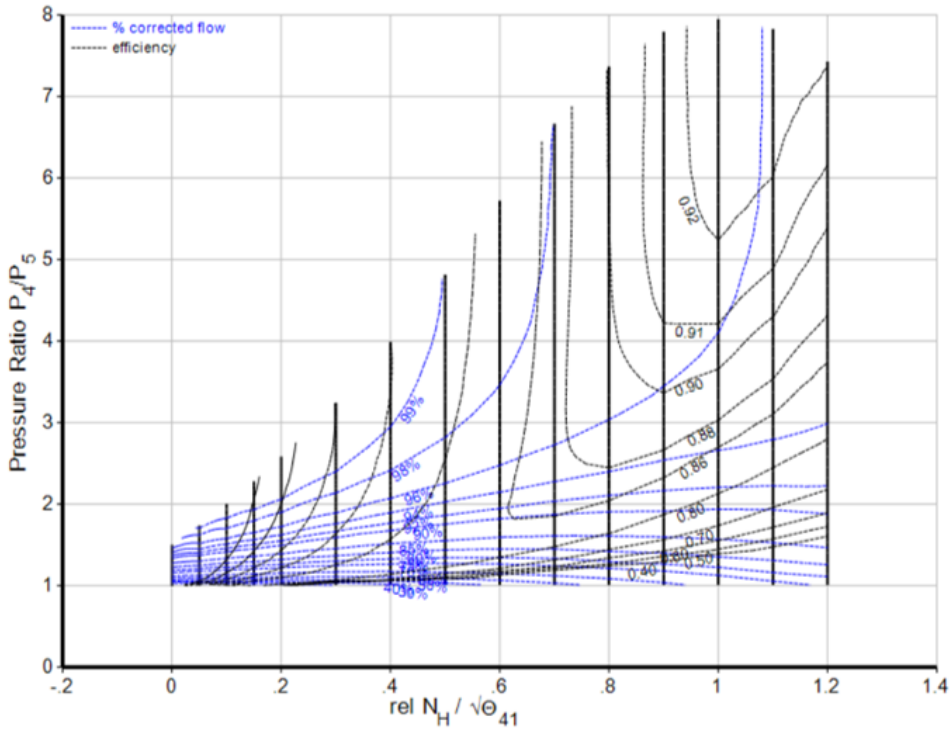

Figure 5.9: Turbine map [55]

Now that the flow rate of fuel required is calculated, the quantity of H_2 needed each 30 minutes is known. This quantity obviously has the same trend as the turbine power output because the fuel is obtained from this preliminary data. For the second unit of Rhode power station the H_2 requirement is show in Fig. 5.10:

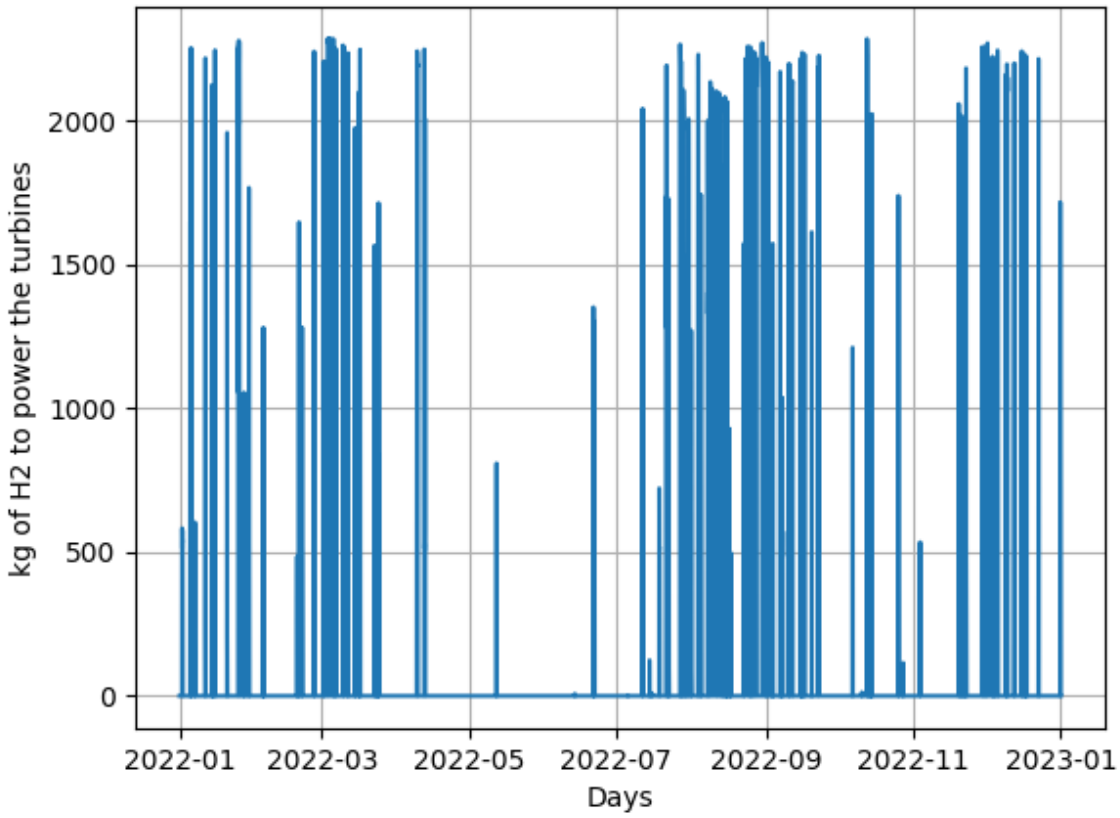

Figure 5.10: H_2 required for the repurposed turbine operation of unit 2, every 30 minutes

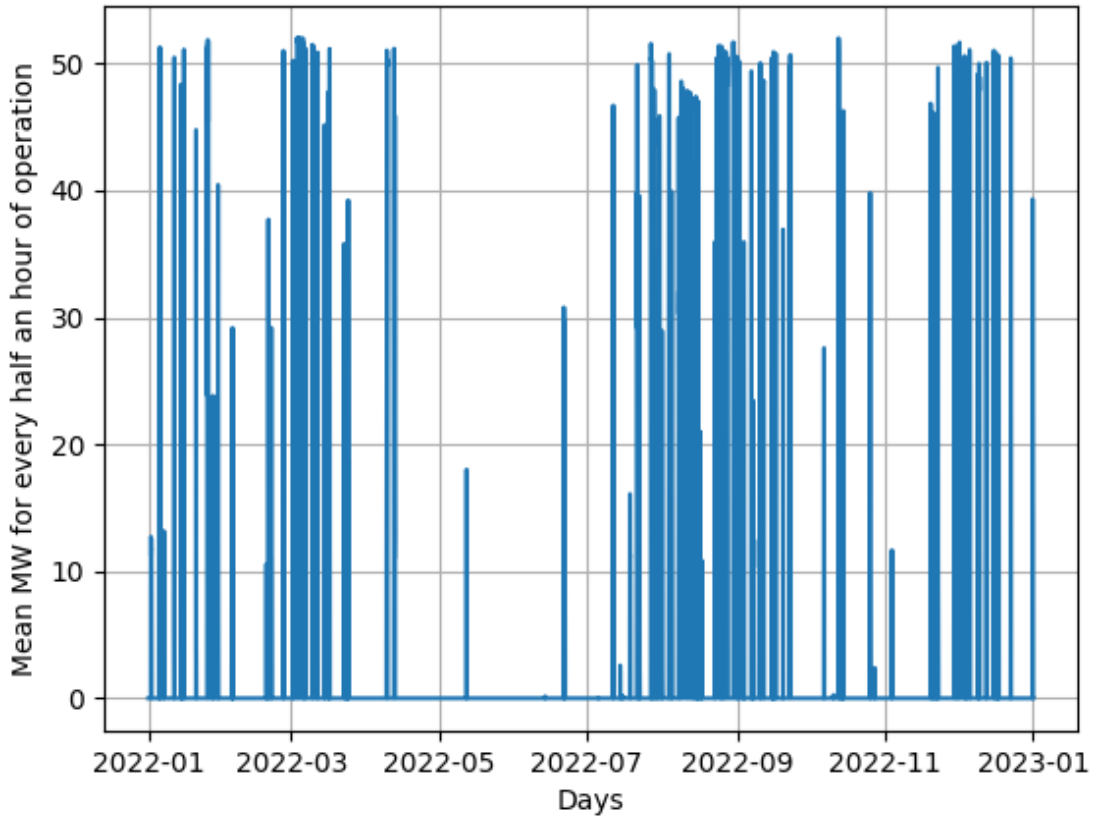

Figure 5.11: MW_e output of the repurposed turbine of unit 2, every 30 minutes

For both units of the Rhode power station (52 MW + 52 MW) is:

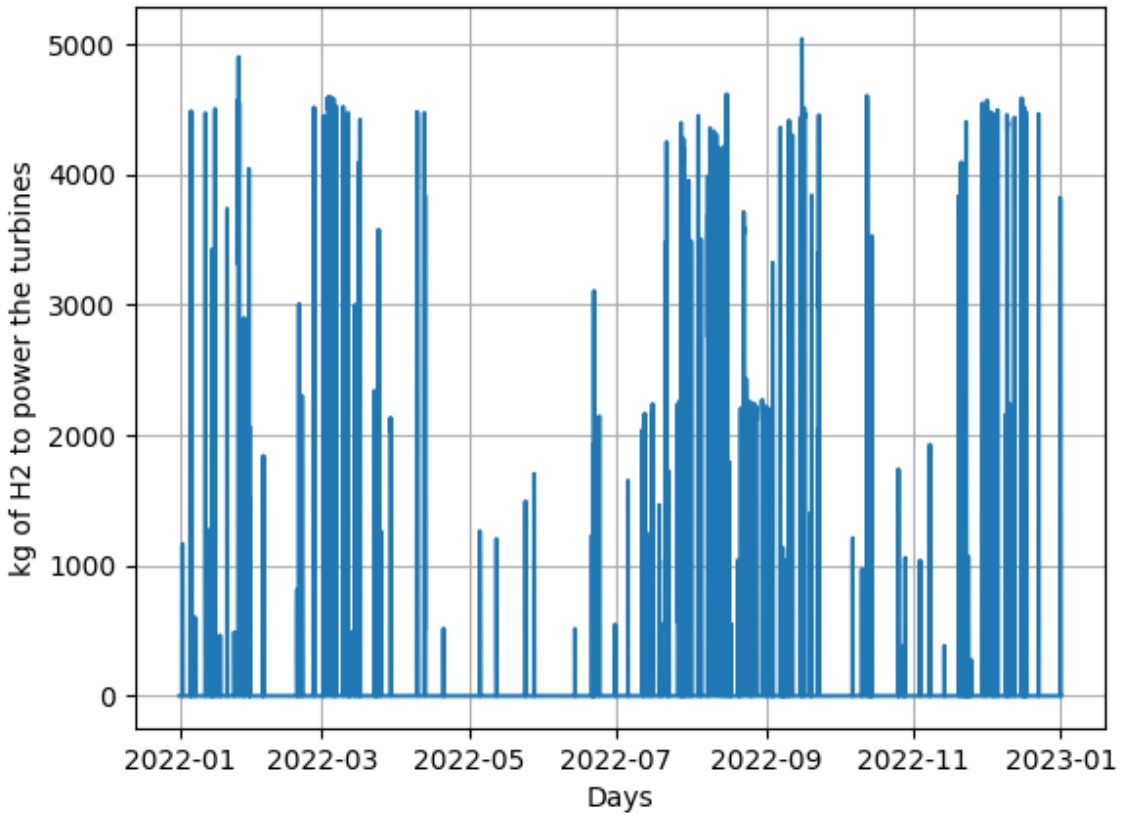

Figure 5.12: H_2 required for the repurposed turbines, every 30 minutes

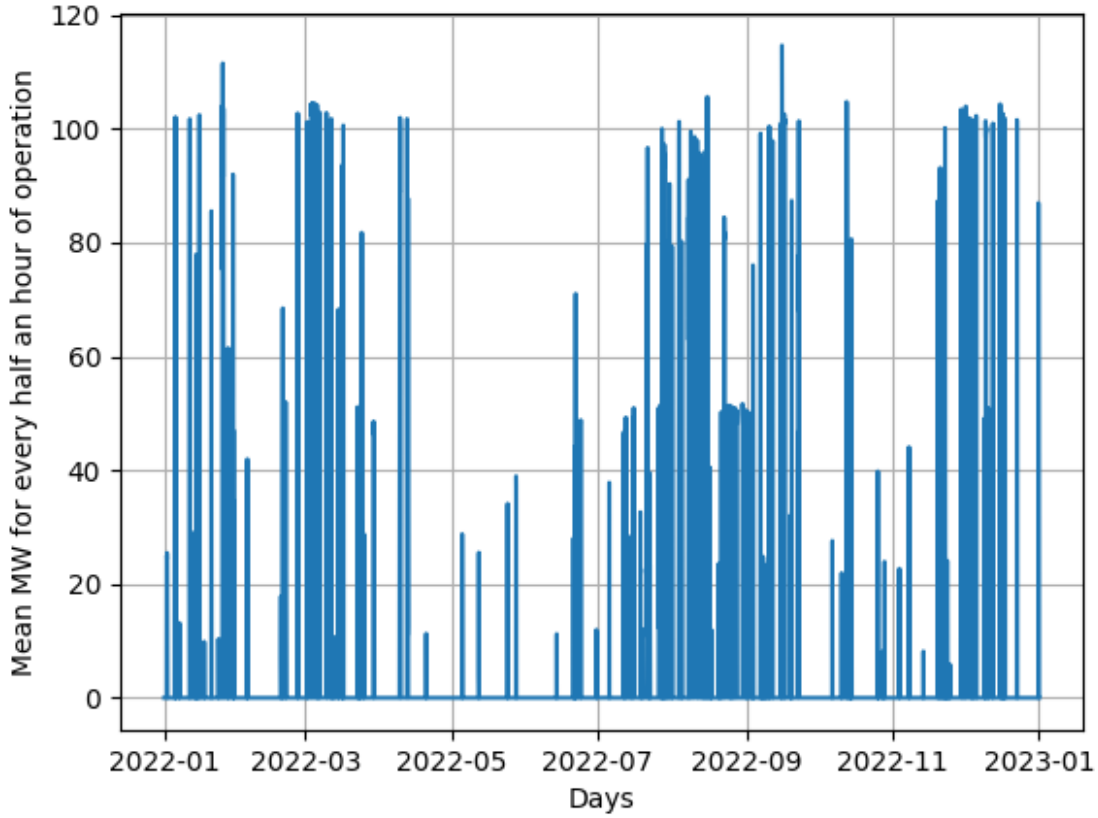

Figure 5.13: MW_e required for the repurposed turbines, every 30 minutes

So the time of employment and the quantity of H_2 needed for unit 2 are **(1902 ton/year)**, the same plots can be shown for unit 1 that has a requirement of **(1878 ton/year)**; these details make it possible to manage the system with a storage.
The model will focus on the powering of unit 2, as it is the one that worked more, and secondly on the possibility to power both of them **(3780 ton/year)**.

5.2 The wind farm

The Mountlucas wind farm [9] has a nominal power of 84 MW, comprised of 28 Siemens 3.0DD-101 turbines, which is used to supply the electricity necessary to produce the hydrogen. In particular below it is possible to see the trend of the wind power generation that was obtained importing the data from an excel file thanks to the Pandas library.
As it can be seen in Figure 5.14 the wind farm mainly operates at nominal capacity in February, October and November while the nominal operating hours at maximum power amount to **2400 h/year.**

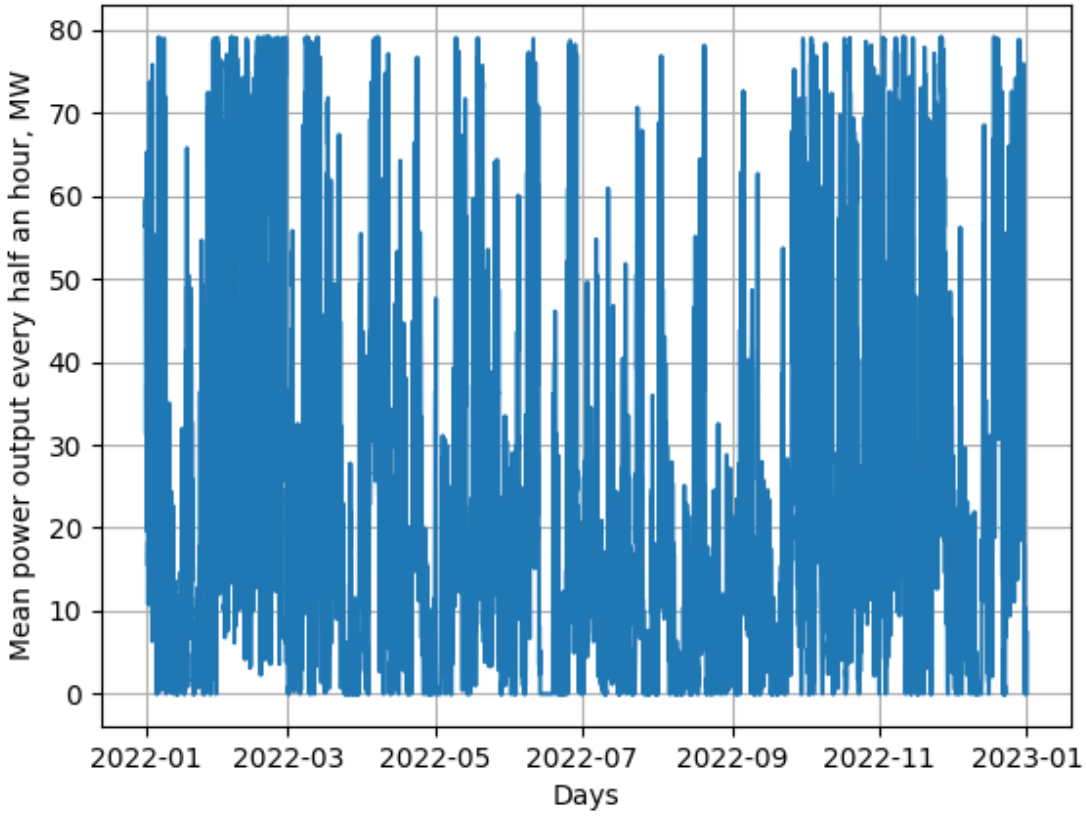

Figure 5.14: Mean MW_e produced from the Mountlucas wind farm each half an hour

5.3 Electrolyser modeling

At this point the analysis of the hydrogen production starts; an electrolyser is powered with the electricity of the wind farm and it is necessary to choose which technology to adopt, with a clear size. This work focused on a performance comparison between PEM and SOEC technologies, as they are still emerging but with more potential than the already mature alkaline technology {3.2.4}.

5.3.1 PEM electrolyser

Electrochemical model

The PEM electrolyser was modeled following the method of Pfennig [19] that gives a clear understanding of the mechanism operating in the cell, such as the voltage and the overpotentials, and then analyses through the model the performance of a real PEM electrolyser from Siemens [20]. The script starts from the model of a single cell and then scales up multiplying by the number of units; in particular as the first thing it calculates the reversible voltage with this empirical formula:

$$E_{rev} = 1.229 - 0.85 \cdot 10^{-3} \cdot (T - 298) = 1.1991V \tag{5.19}$$

With T equal to 333 K as the cell operates at $60°C$.
Then the Nerst potential is calculated:

$$E_{\text{Nerst}} = E_{rev} - \frac{RT}{nF} \ln Q = 1.1992V \tag{5.20}$$

They are basically the same as the only influence is a slightly different temperature. Then assuming that there are 25 cells for each stack, the total number of stacks is 24 (6 in series and 4 in parallel), the area of a cell is 0.6 m^2 and the hydrogen flow rate is 330 m^3/h [20]:

$$j = (\dot{m}_{H_2}/3600 \cdot n \cdot F)/(M_{H_2} \cdot A \cdot 24 \cdot 25) = 2.44A/cm^2 \tag{5.21}$$

With:

- $\dot{m}_{H_2}/3600$ flow rate of H_2 in kg/s
- n = 2, number of charges involved in the reaction
- F, Faraday constant
- M_{H_2} molar mass of hydrogen in kg/mol

The current density at which the system operates is calculated. At this point both the activation and ohmic overpotentials can be obtained while the concentration overpotential is assumed to be negligible because it is an undesired effect that can be avoided limiting the current density. To compute the activation overpotential the Butler Volmer equation is recalled:

$$j = j_0 \left(e^{\frac{\alpha F E_{act}}{RT}} - e^{-\frac{(1-\alpha) F E_{act}}{RT}} \right) \tag{5.22}$$

Where:

- α is the charge transfer coefficient (0.5 for both anode and cathode, the reaction is balanced)

- R is the gas constant (8.314 J / mol K)
- T is temperature
- F is Faraday constant
- E_{act} is the activation overpotential

From the equation it is possible to obtain the overpotential for each electrode, considering the exchange current density of each one.

$$E_{act_{cat}} = \frac{R \cdot T}{\alpha_{cat} \cdot n \cdot F} \cdot ln\left(\frac{j}{j0_{cat}}\right) \tag{5.23}$$

$$E_{act_{an}} = \frac{R \cdot T}{\alpha_{an} \cdot n \cdot F} \cdot ln\left(\frac{j}{j0_{an}}\right) \tag{5.24}$$

Given $j0_{cat} = 0.278\ A/cm^2$ and $j0_{an} = 10^{-5}\ A/cm^2$ with the anode as limiting semi reaction:

$$E_{act} = E_{act_{cat}} + E_{act_{an}} = 0.3523\ V \tag{5.25}$$

To calculate the ohmic overpotential the following expression is used:

$$E_{ohm} = (R_{cc} + R_{bp} + R_{me}) \cdot j \cdot A = 0.2905\ V \tag{5.26}$$

The resistence of the current collector can be computed as:

$$R_{cc} = \frac{\delta_{cc}}{A_{cc} \cdot \sigma_{cc}} = 0.0030\ \Omega \tag{5.27}$$

with δ as the thickness and σ as the conductivity. The resistance of the bipolar plate can be calculated as:

$$R_{bp} = \frac{\delta_{bp}}{A_{bp} \cdot \sigma_{bp}} = 0.0168\ \Omega \tag{5.28}$$

The formula for the resistance of the membrane is the same but the conductivity depends on the temperature of the stack:

$$R_{me} = \frac{\delta_{me}}{A_{me} \cdot \sigma_{me}} = 0.2705\ \Omega \tag{5.29}$$

$$\sigma_{me} = (0.005139 \cdot Y - 0.00326) \cdot e^{(1268 \cdot (1/303 - 1/T))} \tag{5.30}$$

With Y fixed at 22 for liquid water following the source [56].
From this values it is clear that the electrical losses are negligible in comparison to the ionic ones, that is why in some works they are neglected.
So the total voltage $E_{cell} = 1.842V$ and the cell efficiency $\eta_{cell} = \frac{E_{Nernst}}{E_{cell}} =$ **65.1% .**
From this is possible to calculate the stack power and the system real power:

$$P_{stack} = E_{cell} \cdot j \cdot A \cdot 25 = 673.5\ kW \tag{5.31}$$

$$P_{system} = P_{stack} \cdot 24 = 16.16\ MW \tag{5.32}$$

The difference in power ($P_{system_{nom}} = 17.5MW$) is to be attributed to the BoS (balance of system) losses due to the connections of the stacks, which are equivalent to the 7.63% of the power employed. Taking the latter into account the total efficiency of the electrolyser is equal to **60.14%.**

It is also possible to employ a broad range of current densities to find the polarization curve of the cell:

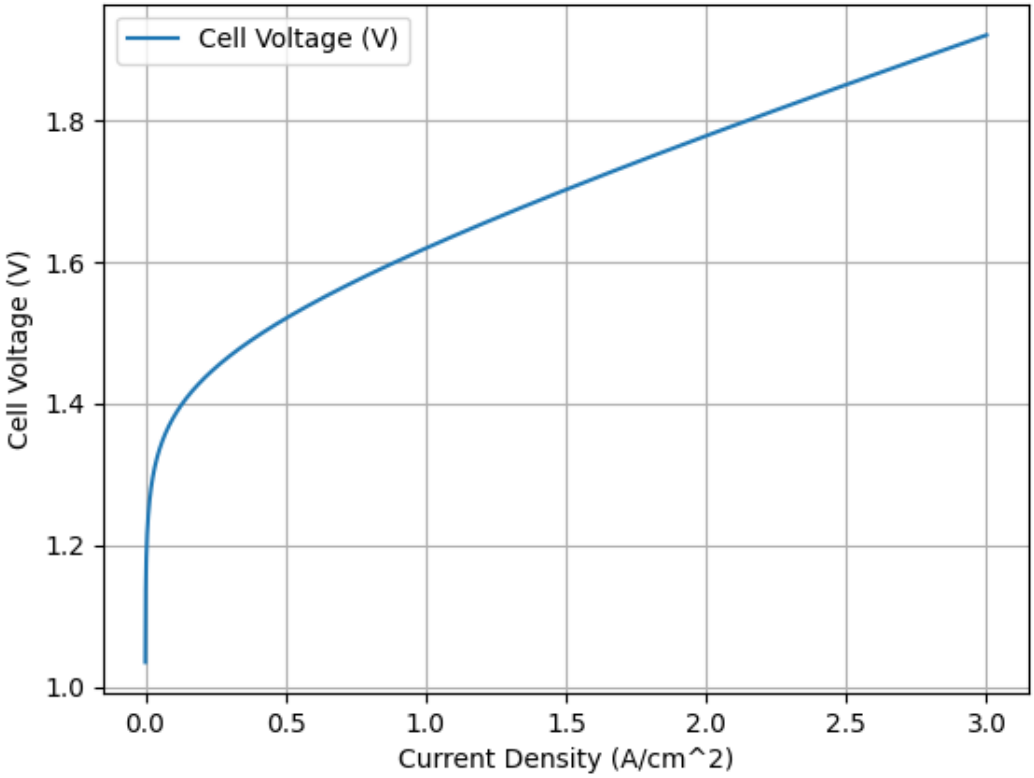

Figure 5.15: Cell Voltage vs Current Density, polarization curve of the PEM cell

Thermal management

As the cell voltage is higher than the thermoneutral condition, in which the system does not require nor dissipate heat, it is necessary to cool the stacks by means of a fan.

$$E_{cell} = 1.842V > E_{th} = 1.48\ V \tag{5.33}$$

To quantify how much heat needs to be dissipated the equation is:

$$\dot{Q}_{cooling} = \dot{W}_{el} - \dot{Q}_{loss} + \sum \dot{m}_{out}\dot{h}_{out} - \sum \dot{m}_{in}\dot{h}_{in} = 7.18\ kW \tag{5.34}$$

There are 3 terms in this equation: the electrical work, the heat losses and the enthalpy change of the species.

$$\dot{W}_{el} = n_{cell} \cdot (E_{cell} - E_{th}) \cdot j \cdot A = 5.28\ kW_t \tag{5.35}$$

$$\dot{Q}_{loss} = h_c \cdot A_0 \cdot (T_{stack} - T_{atm}) = \phi \cdot (T_{stack} - T_{atm}) = 2.35\ kW \tag{5.36}$$

$$\dot{m}_{O_2,out}\dot{h}_{O_2,out}(T_{stack}, p_{an}) + \dot{m}_{H_2,out}\dot{h}_{H_2,out}(T_{stack}, p_{cat}) - \dot{m}_{H_2O,in}\dot{h}_{H_2O,in}(T_{PreHeatedWater}, p_{an}) = \tag{5.37}$$

$$= \sum \dot{m}_{out}\dot{h}_{out} - \sum \dot{m}_{in}\dot{h}_{in} = 4.25\ kW \tag{5.38}$$

Then it is necessary to take into account the water heated for the electrolyser from $25°C$ to $80°C$:

$$P_{sensible} = \dot{m}_{water} \cdot c_{p_{mean}} \cdot (T_2 - T_1) = 84.33\ kW \tag{5.39}$$

Coupling with the wind farm

Now the different powers of the electrolyser are analysed to see which is the best one. Given that the nominal size of the electrolyser is 17.5 MW and is supposed to be made out of 24 stack with 6 units in series and then 4 modules in parallel. To supply the hydrogen for the 52 MW turbines the powers analysed are 17.5/21.875/26.25 MW; one module of 6 units is added successively.
It is also assumed that the efficiency of the system is the same for every operating condition due to the PEM modularity, 4.375 MW per module. In the end the feasibility of a system with nominal power of 87.5 MW (5 electrolysers of 17.5 MW) will be studied to enable the powering for both 52 MW units of the Rhode power station.

PEM electrolyser system of 17.5 MW

The hydrogen produced is 1854.6 ton/year that is lower than the overall requirement of 1902 ton/year therefore a bigger system is needed. However, time needs to be taken into account as every half an hour we have a requirement when the turbine is working and a surplus when it is not, so a storage is needed to operate the system. It is possible to see that the overall hydrogen for a year is not enough but there are important peaks and troughs due to the discontinuity of the wind energy from which hydrogen is produced. Regarding the storage we have that an overall of 1776.7 ton of hydrogen are stored for later usage while only 77.9 ton can be directly used as they are produced when the turbine is also in operation. To store the hydrogen a series of compressors is assumed to increase the pressure up to 700 bar, to do so the necessary power is 500 kW (calculated with $P = \dot{m}_{H_2} \cdot c_p \cdot \Delta T$) with the mass flow that consists of the positive values between the difference of hydrogen produced and consumed every half an hour; instead the outlet temperature of the hydrogen will be set at $60°C$ [19].

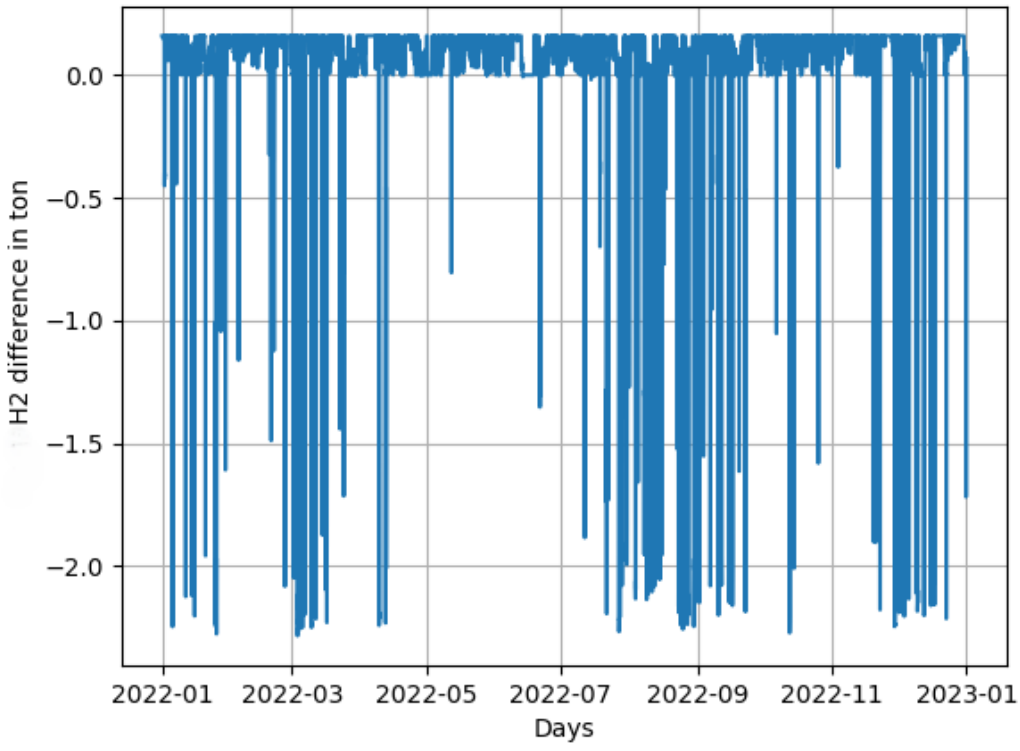

Figure 5.16: Difference between production and consumption of H_2 every half an hour

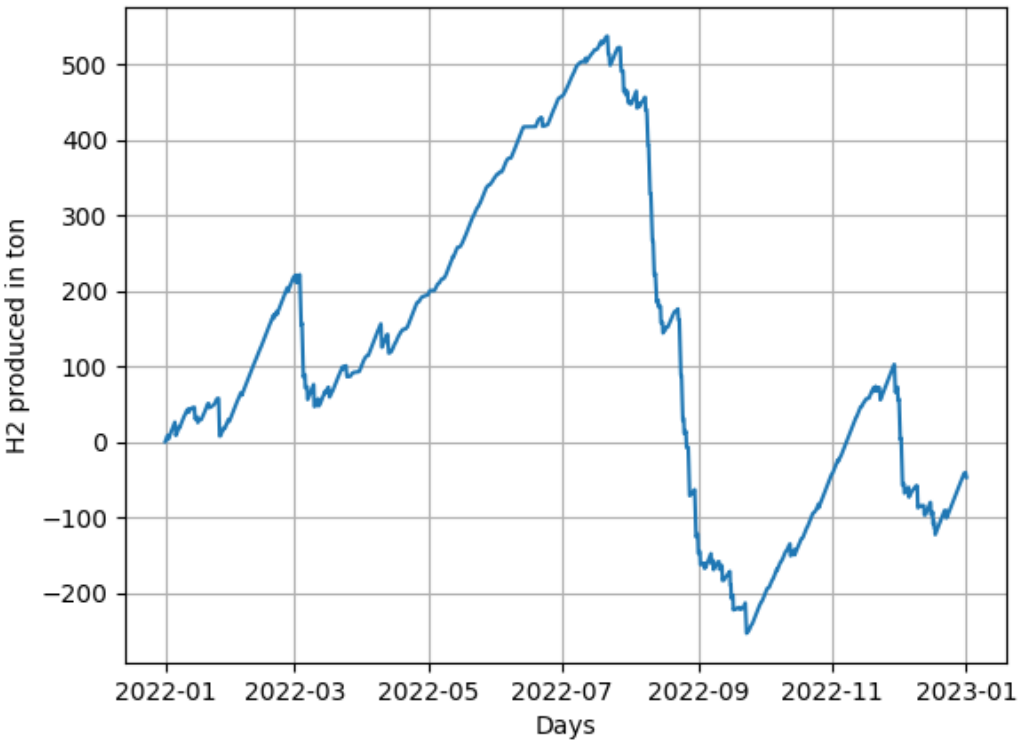

Figure 5.17: Cumulative difference of H_2 production and consumption

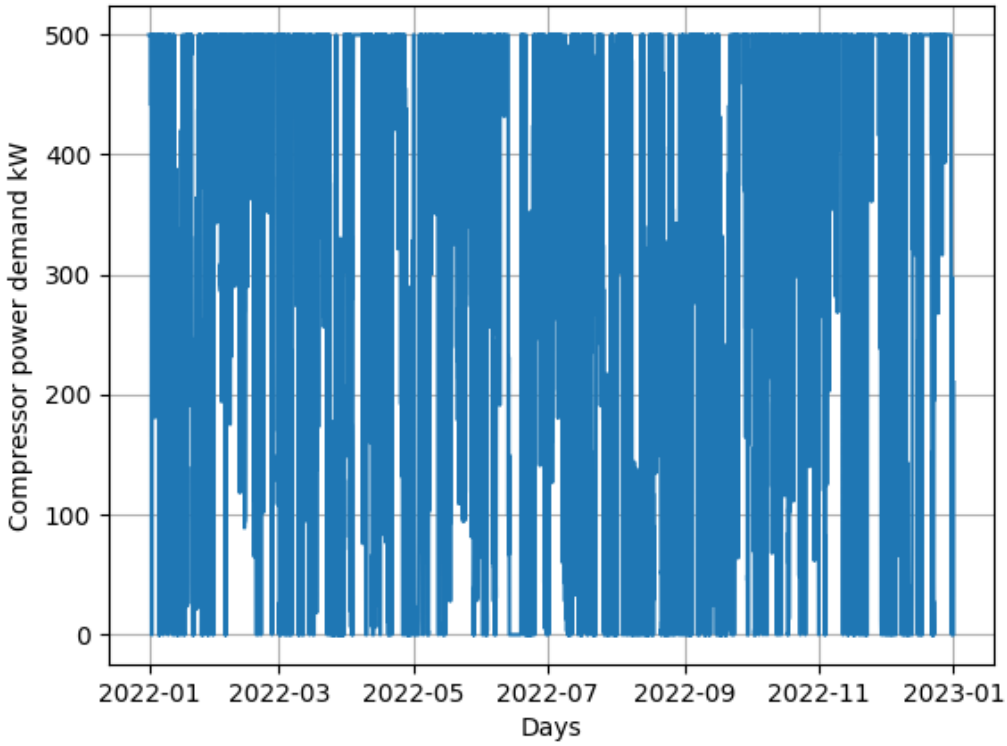

Figure 5.18: Operation power of H_2 compressor every half an hour

In this case we reach peaks of 500 ton of surplus and -200 ton of deficit so the system should be bigger to function properly as a "stand-alone" installation.

PEM electrolyser system of 21.875 MW

The hydrogen produced is 2164.6 ton/year while the demand is 1902 ton/year.
The quantity of H_2 compressed is 2080.7 ton while only 83.9 ton can be directly used in the turbine.

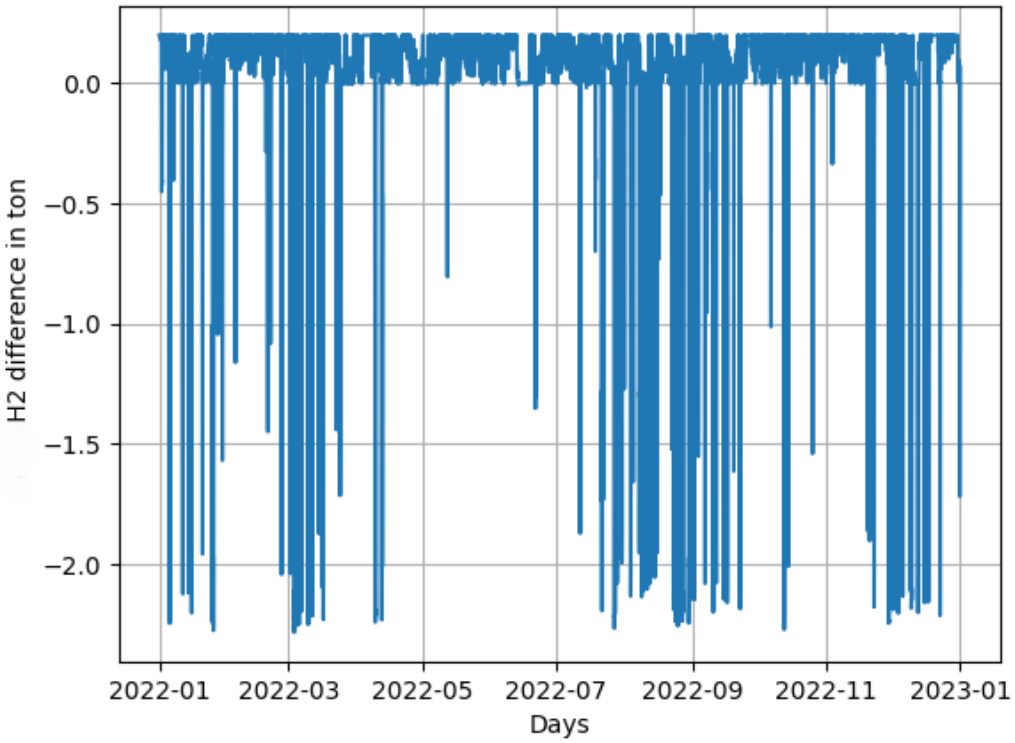

Figure 5.19: Difference between production and consumption of H_2 every half an hour

Figure 5.20: Cumulative difference of H_2 production and consumption

The compressor power to store the hydrogen is equal to 625 kW at the design flow rate:

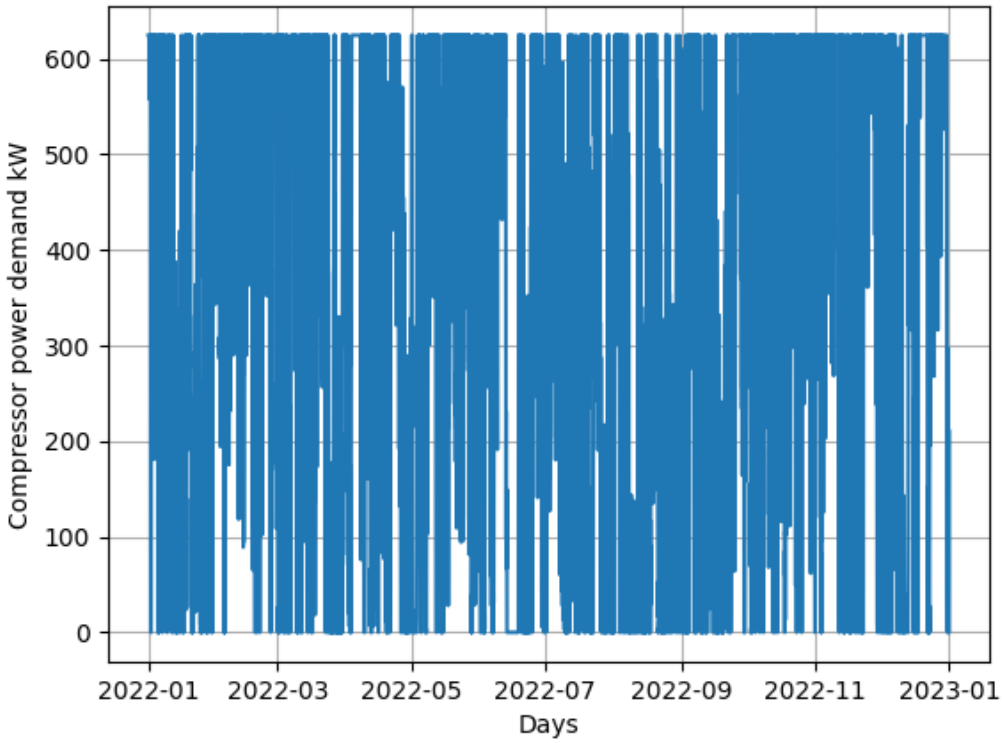

Figure 5.21: Operation power of H_2 compressor every half an hour

This solution seems the most feasible one as the trend for the storage is almost always positive, it is necessary to buy hydrogen only for a handful of days of the year and the quantity is small enough. The power required to operate a compressor is increased only by 125 kW.
Aside from these considerations the cost for the storage tank, that in this case would be for 700 ton instead of 500 ton, is a variable that needs to be taken into account as it could be cheaper to buy more hydrogen than to basically increase by 1.5x the storage size.

PEM electrolyser system of 26.25 MW

In this case the H_2 production increases even more to 2431.2 ton/year which exceeds the demand of 1906 ton/year. Regarding the storage we have that 2343.4 ton of hydrogen are stored for future usage while only 87.8 ton can be directly used as the turbine is in operation at the same time.
The system is clearly oversized for the application as the storage size would need to be 850 ton, on the other hand it is sure that this solution can supply the hydrogen needed at every given time without external sources; plus it is possible to consider this solution if an objective is sell the excess H_2 to the market.
The compressor power to store the hydrogen is equal to 750 kW at the design flow rate, so it is evident that roughly 125 kW of compressor power can cover the 4.375 MW of a module each time it is added; obviously it could differ a bit as the production depends on the wind availability.

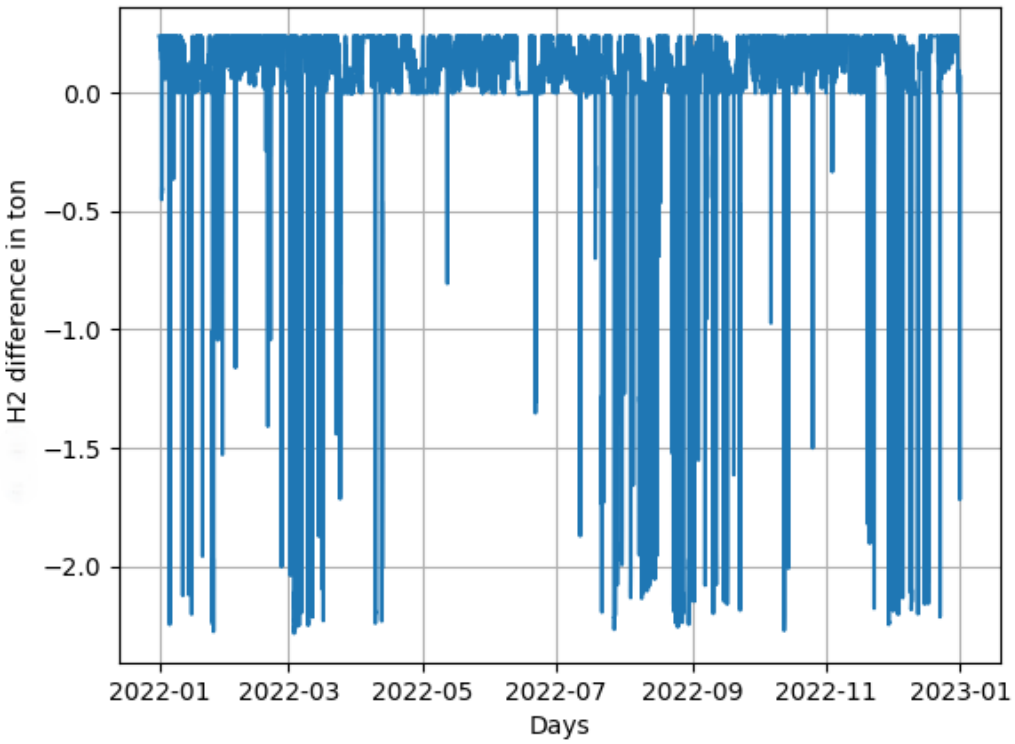

Figure 5.22: Difference between production and consumption of H_2 every half an hour

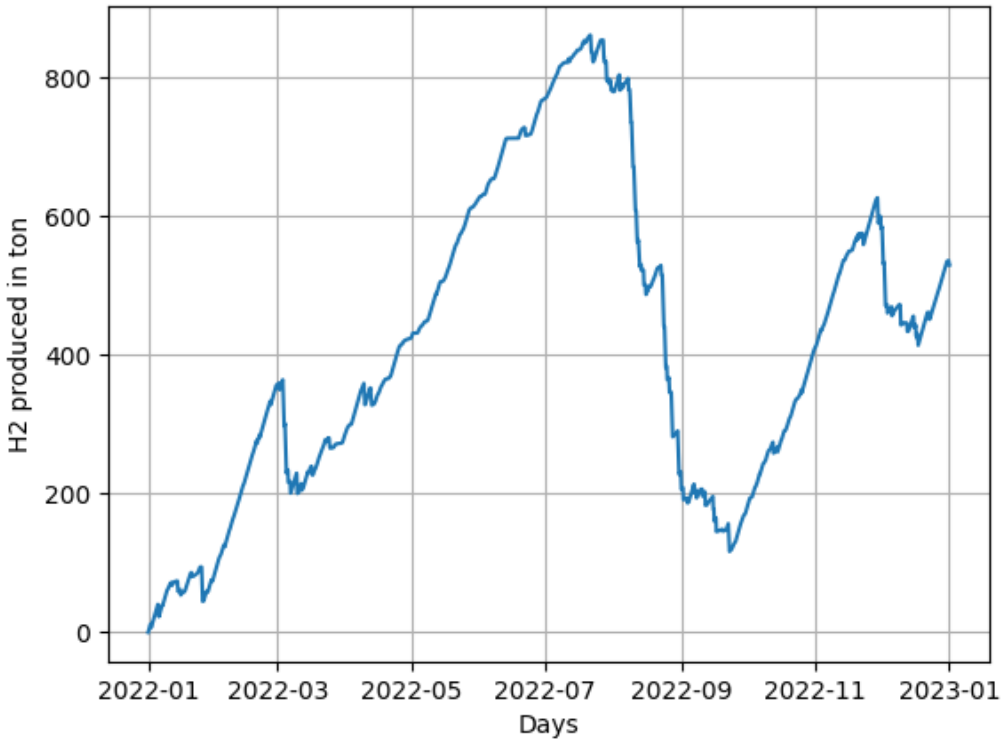

Figure 5.23: Cumulative difference of H_2 production and consumption

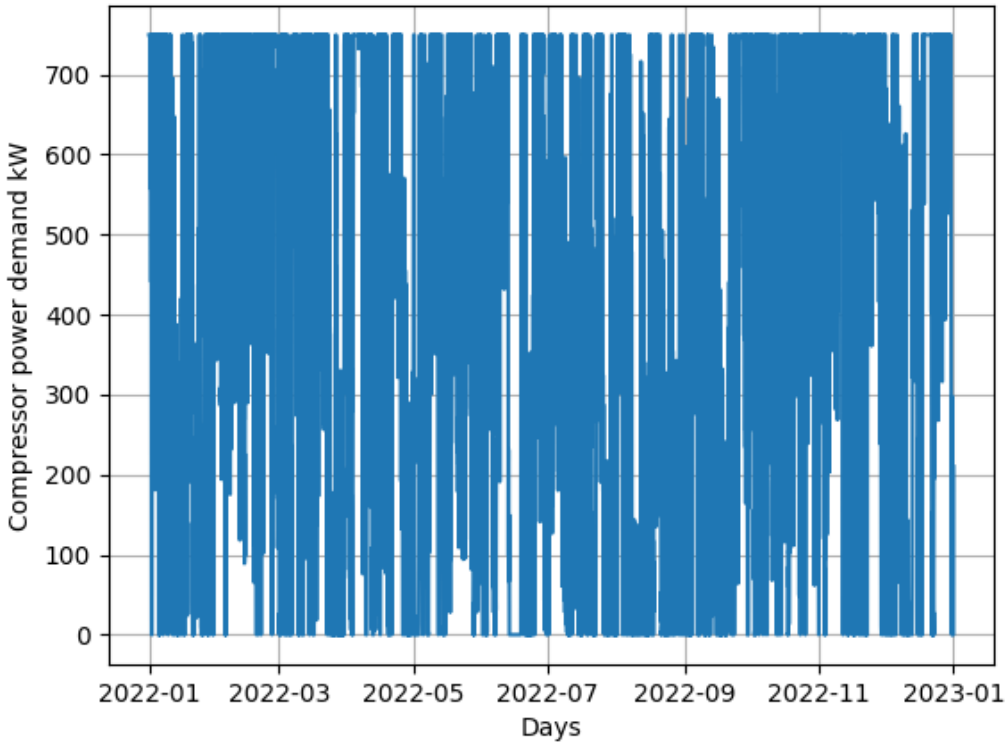

Figure 5.24: Operation power of H_2 compressor every half an hour

PEM electrolyser system of 87.5 MW

The hydrogen produced is 3672.6 ton/year that is lower than the overall requirement of 3780.3 ton/year so it is not possible to fully power both turbines with the capacity of the wind farm. Regarding the storage we have that 3536.5 ton of hydrogen are stored for future usage while only 136.1 ton can be directly used as the turbine is in operation at the same time.

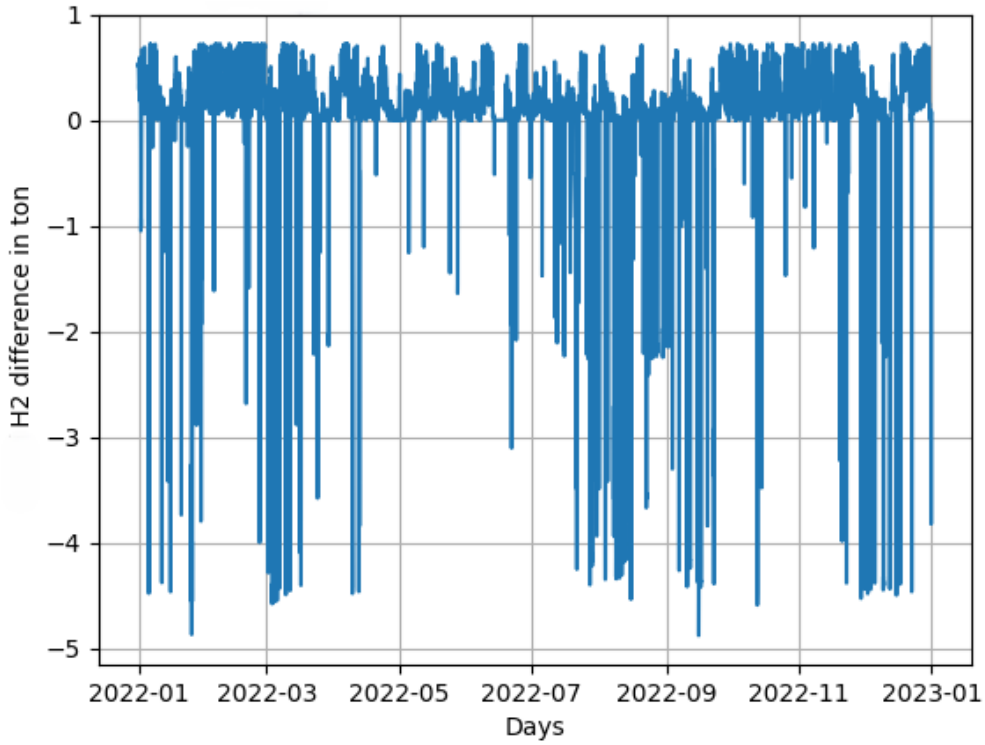

Figure 5.25: Difference between production and consumption of H_2 every half an hour

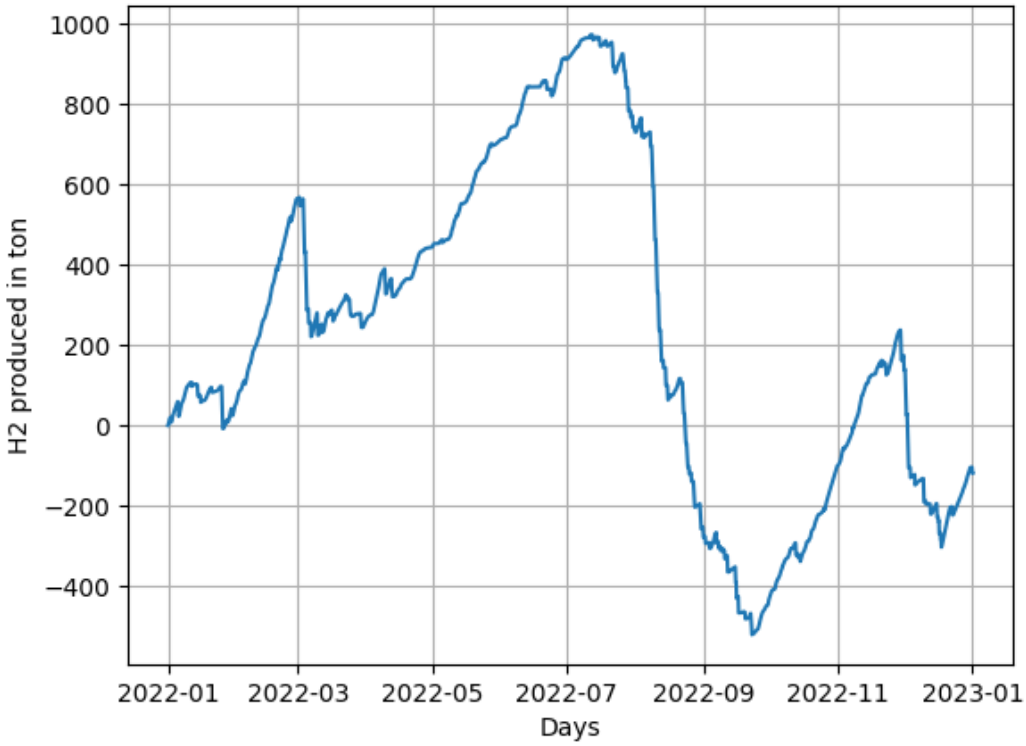

Figure 5.26: Cumulative difference of H_2 production and consumption

The storage size would be massive and the quantity of H_2 would not be enought so it is not worth it. The compressor power is equal to 2250 kW at the design flow rate:

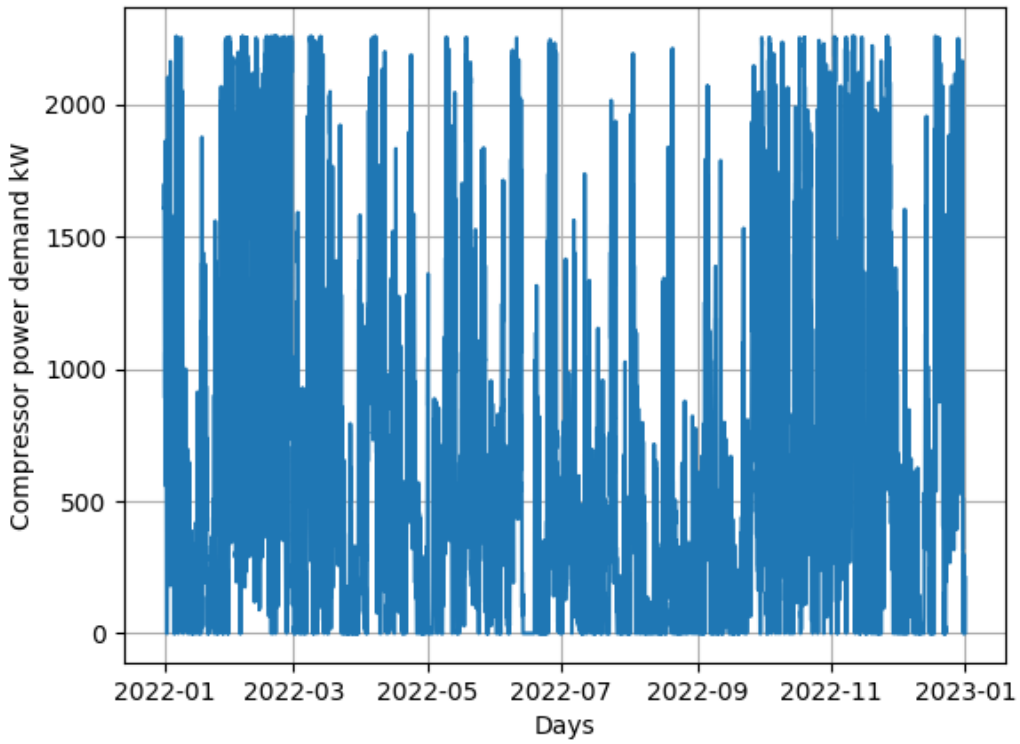

Figure 5.27: Operation power of H_2 compressor every half an hour

It is more than triple the size of the second solution and as seen from the picture it works at full power for less than half time so it is not as cost effective as the other solutions.

5.3.2 SOC electrolyser

Electrochemical model

The SOC electrolyser was modeled following the articles of P. Mottaghizadeh [21], C. Wang [29], P. Kazempoor [28] and P. Wang [57] that give a clear understanding of the mechanism operating in the cell, such as the voltage and the overpotentials. The script starts from the model of a single cell and then scales up multiplying by the number of units; in particular the first thing it calculates the reversible voltage with this empirical formulae [57]:

$$E_{rev} = 1.2535 - 2.45 \cdot 10^{-4} \cdot T = 1.0027\ V \tag{5.40}$$

With T equal to 1023 K as the cell operates at $750°C$ [21].
Then the Nerst potential is calculated:

$$E_{\text{Nerst}} = E_{rev} - \frac{RT}{nF} \ln Q = 0.9284\ V \tag{5.41}$$

This time it is quite different from the reversible voltage due to the temperature that is higher than the standard value and the effect of the partial pressures.
In order to calculate the current density the current is divided by the area:

$$j = \frac{I}{A} \tag{5.42}$$

In this case the current density will vary depending on the operating condition, thus on the current, but at the design condition the value is 0.4715 A/cm^2. At this point the activation, the ohmic and the concentration overpotentials can be obtained; below will be shown the values for the design condition. The activation overpotential formula is the same of the PEM model, as such it can be derived from the Butler Volmer equation:

$$j = j_0 \left(e^{\frac{\alpha F E_{act}}{RT}} - e^{-\frac{(1-\alpha) F E_{act}}{RT}} \right) \tag{5.43}$$

Where:

- α is the charge transfer coefficient (0.5 for both anode and cathode, the reaction is balanced)
- R is the gas constant (8.314 J / mol K)
- T is temperature
- F is Faraday constant
- E_{act} is the activation overpotential

Considering the exchange current density for each electrode:

$$E_{act_{cat}} = \frac{R \cdot T}{\alpha_{cat} \cdot n \cdot F} \cdot ln \left(\frac{j}{j_{0_{cat}}} \right) = 0.107\ V \tag{5.44}$$

$$E_{act_{an}} = \frac{R \cdot T}{\alpha_{an} \cdot n \cdot F} \cdot ln \left(\frac{j}{j_{0_{an}}} \right) = 0.002\ V \tag{5.45}$$

Given $j_{0_{cat}} = 10.542 A/cm^2$ and $j_{0_{an}} = 0.1532\ A/cm^2$ with the anode as limiting semi reaction it is interesting to see how the improved kinetics due to the high temperature can reduce the activation overpotential in comparison to the PEM:

$$E_{act} = E_{act_{cat}} + E_{act_{an}} = 0.109\ V \tag{5.46}$$

Ohmic losses are caused by the resistance to the flow of ions through the electrolyte and the flow of electrons through electrodes, interconnects, and contacts so the losses can be calculated as:

$$E_{ohm} = E_{A_{eld}} + E_{F_{eld}} + E_{el} + E_{IC} + E_{contact} = 0.0571\ V \tag{5.47}$$

The resistance of the anode can be computed as:

$$E_{A_{eld}} = \frac{\delta_{A_{eld}}}{\frac{42 \cdot 10^6}{T} \cdot e^{(\frac{-1200}{T})}} \cdot j = 3.9 \cdot 10^{-9}\ V \tag{5.48}$$

The resistance of the cathode can be computed as:

$$E_{C_{eld}} = \frac{\delta_{C_{eld}}}{\frac{95 \cdot 10^6}{T} \cdot e^{(\frac{-1150}{T})}} \cdot j = 5.0 \cdot 10^{-8}\ V \tag{5.49}$$

with δ as the thickness of the electrode. The resistance of the electrolyte can be calculated as:

$$E_{A_{eld}} = \frac{\delta_{el}}{3.34 \cdot 10^4 \cdot e^{(\frac{-10300}{T})}} \cdot j = 3.5 \cdot 10^{-7}\ V \tag{5.50}$$

The resistance of the interconnect can be calculated as:

$$E_{A_{eld}} = \frac{\delta_{IC}}{\frac{9.3 \cdot 10^6}{T} \cdot e^{(\frac{-1100}{T})}} \cdot j = 7.0 \cdot 10^{-6}\ V \tag{5.51}$$

$$E_{contact} = ASR_{contact} \cdot j = 0.0571\ V \tag{5.52}$$

From this values it is clear that the electrical and ionic losses are negligible in comparison to the contact ones. To quantify the concentration gradient across the electrodes a series of equation is employed as there is not only one mechanism involved. Fick's model is adopted for simulating gas diffusion:

$$E_{diff_A} = \frac{R \cdot T}{(4 \cdot F)} \cdot ln\left(\frac{j_L}{j_L - j}\right) = 9.8 \cdot 10^{-4}\ V \tag{5.53}$$

$$E_{diff_C} = \frac{R \cdot T}{(2 \cdot F)} \cdot ln\left(\frac{j_L}{j_L - j}\right) = 1.8 \cdot 10^{-3}\ V \tag{5.54}$$

$$E_{diff} = E_{diff_A} + E_{diff_C} = 2.8 \cdot 10^{-3}\ V \tag{5.55}$$

This value is negligible at design point operation as the species successfully reach the reaction sites. To specify the terms j_L is the limiting current density that depends on the species affluence through the catalyst layer. In electrolysis processes the anode is the limiting electrode so it will be calculated for that case:

$$j_L = \frac{n \cdot F \cdot D_{eff_{H_2O}} \cdot C_{0_{H_2O}}}{\delta_{A_{eld}}} = 11.386\ A/cm^2 \tag{5.56}$$

Where $D_{eff_{H_2O}}$ is the effective diffusion coefficient for the water and $C_{0_{H_2O}}$ is the water concentration

in bulk flow. As the concentration in bulk condition is 1, the only other variable to calculate is the effective diffusion coefficient; to compute it both the molecular and Knudsen diffusion are taken into account. In particular employing the Bosanquet formula:

$$\frac{1}{D_{eff_{H_2O}}} = \frac{\tau}{\epsilon} \cdot \left(\frac{1}{D_{i_k}} + \frac{1}{D_{i_j}} \right) \tag{5.57}$$

Where:

- $\frac{\tau}{\epsilon}$ is the ratio of tortuosity to porosity of electrode
- D_{i_k} is the Knudsen diffusion
- D_{i_j} is the molecular binary diffusion coefficient

$$D_{H_2O_k} = \frac{2}{3} \cdot r_p \cdot \sqrt{\frac{8 \cdot R \cdot T}{\pi \cdot M_{H_2O}}} \tag{5.58}$$

$$D_{H_2O,H_2} = \frac{10^{-3} \cdot T^{1.75} \cdot \sqrt{\frac{1}{M_{H_2O}} + \frac{1}{M_{H_2}}}}{p \cdot \left(V_{H_2O}^{\frac{1}{3}} + V_{H_2}^{\frac{1}{3}} \right)^2} \tag{5.59}$$

So the total voltage $E_{cell} = 1.0975V$ and the cell efficiency $\eta_{cell} = \frac{E_{Nernst}}{E_{cell}} = \mathbf{84.6\%}$.
From this is possible to calculate the stack power and the system power:

$$P_{stack} = E_{cell} \cdot j \cdot A \cdot 125 \cdot 50 = 268 \ kW \tag{5.60}$$

$$P_{system} = P_{stack} \cdot 10 = 2.68 \ MW \tag{5.61}$$

It was assumed to have 140 cells in series and 35 parallels of them organized in 10 stacks, so that the power is equal to the Multiphly project [58] electrolyser built by Sunfire [58].
As for what regards the flow rates of reagents and products they are equal to those of [58]:

$$\dot{m}_{H_2} = 750 \ \frac{Nm^3}{h} \cdot 0.0899 \ \frac{kg}{Nm^3} = 67.425 \ kg/h \tag{5.62}$$

$$\dot{m}_{H_2O} = 860 \ kg/h \tag{5.63}$$

As the model was adapted to resemble the Sunfire electrolyser it was checked that the flow rate was compliant with the technical scheet:

$$\dot{m}_{H_2} = \frac{P_{system} \cdot 1h \cdot \eta_{cell}}{LHV_{H_2}} = 68.7 \ kg/h \tag{5.64}$$

Which is very close and therefore reliable. For the water instead the results are not similar so it was decided to adapt the data from the manifacturer. For the electrolyser sizing it was chosen to test 4-5 and 6 units to see which was the best fit.
Employing a broad range of current densities the polarization curve of the cell is obtained:

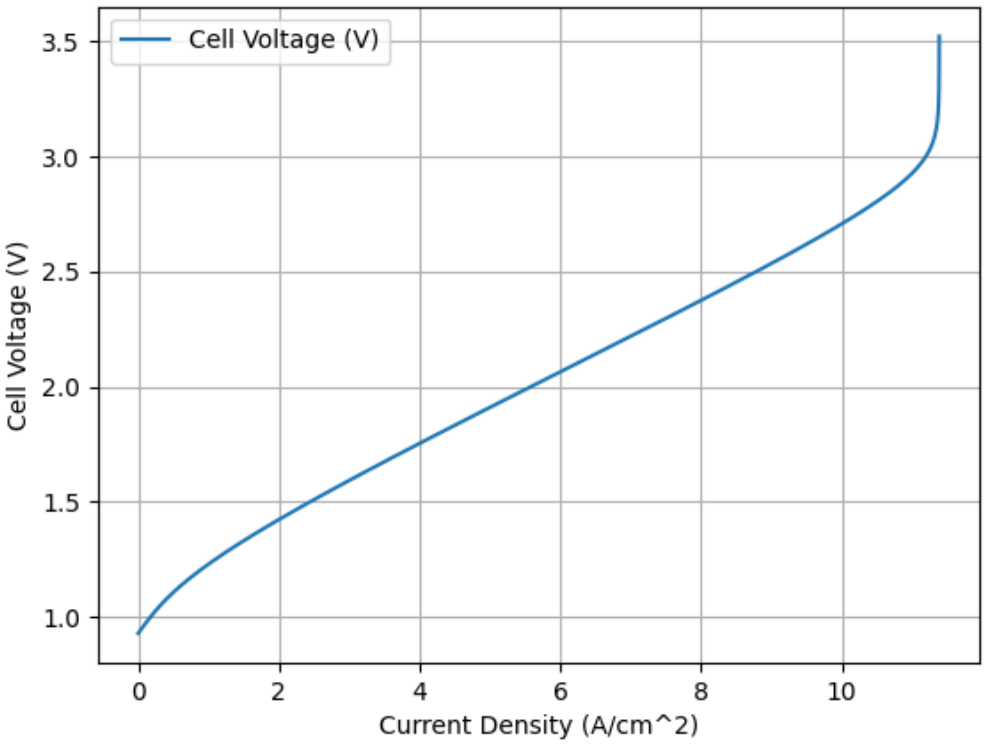

Figure 5.28: Cell Voltage vs Current Density, polarization curve of the SOC cell

Thermal management

The voltage at which our system works is below the thermoneutral one, so a heat supply should be included in the system.

$$E_{cell} = 1.105V < E_{th} = 1.285V -> 750°C \tag{5.65}$$

A wise idea would be to employ the waste heat from the gas turbine to run the electrolyser.
To do so a thermal model has to be built but there are only an handful of papers that employ a simplified approach to the thermal management, without the use of pre-built softwares, and the most complete ones written by C. Wang [57], A. Banerjee [59] are still difficult to interpret, however the very straightforward approach of Y. Zhao [22] works and will be employed.
Then it was chosen to use the parameters stated in the technical sheet [58] which unfortunatelly does not specify the thermal demand of the system. It could be due that the system has an internal heating system or that it always works on par or above the thermoneutral voltage, however the latter is unlikely. Moving forward it is possible to analyse the heat required to form the necessary steam input. The electrolyser requires steam at $150°C$ so the necessary heat starting from water at $25°C$ is:

$$P_{sensible} = \dot{m}_{water} \cdot c_{p_{mean}} \cdot (T_2 - T_1) + \dot{m}_{water} \cdot c_{p_{mean}} \cdot (T_3 - T_2) = 58.6\ kW \tag{5.66}$$

$$P_{latent} = \dot{m}_{water} \cdot r = 539\ kW \tag{5.67}$$

With:

- m_{water} mass flow rate for a module of 2.68 MW (860 / 3600 = 0.239 kg/s)
- $c_{p_{mean}}$ mean specific heat between $25°C$ - $100°C$ and $100°C$ - $150°C$
- r latent heat of vaporization obtained with the difference of enthalpy between vapor and liquid

To quantify the heat demand the formulae from the work of Y. Zhao [22] that developed a simplified model of a 1 MW SOEC system are used. The ohmic losses and the reaction heat are the terms considered and putting them together is possible to obtain the net heat flux of the stack of 2.68 MW:

$$Q_{joule} = j \cdot A \cdot E_{cell} = 2680.4\ kW \tag{5.68}$$

$$Q_{reaction} = j \cdot A \cdot E_{th} = -3138.4\ kW \tag{5.69}$$

$$Q_{net} = j \cdot A \cdot (E_{cell} - E_{th}) = -458.0\ kW \tag{5.70}$$

The negative sign indicates a requirement while the positive sign is a surplus.

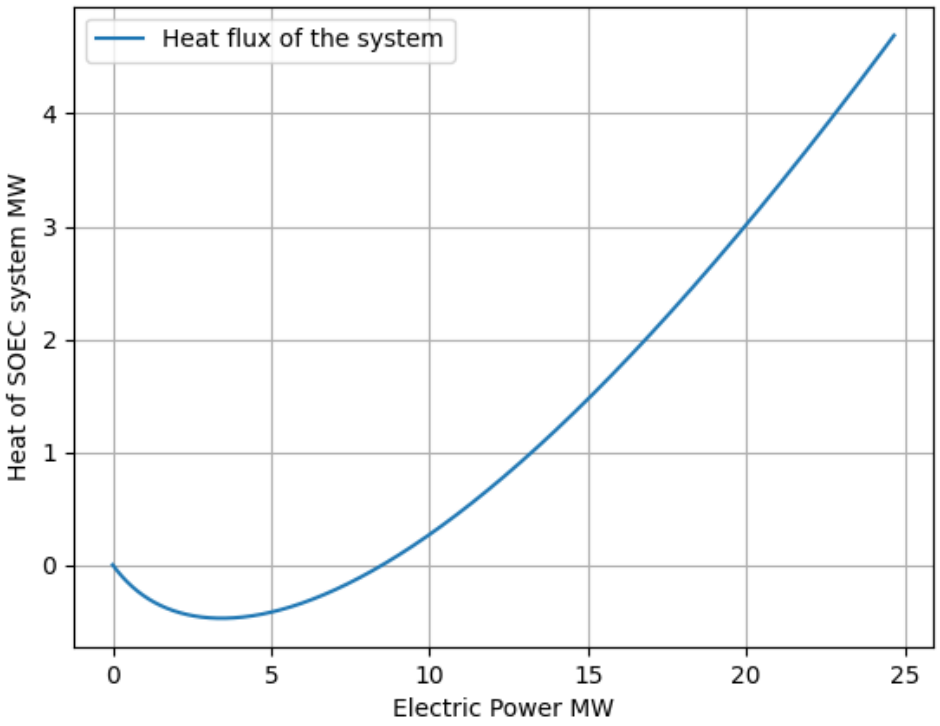

Figure 5.29: Heat requirement for the SOEC system in design condition

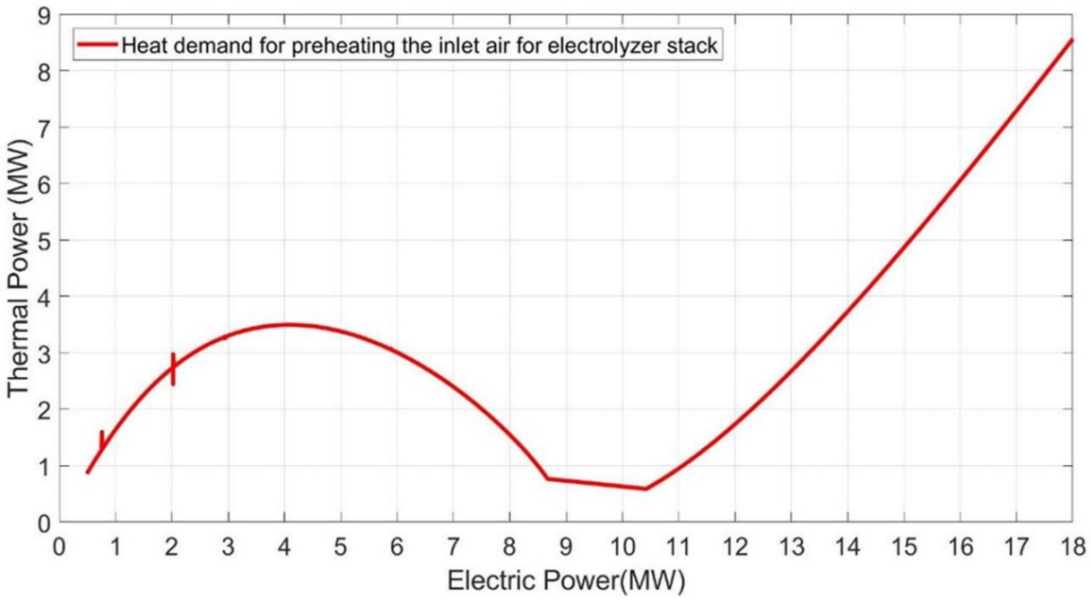

Figure 5.30: Heat requirement for Palm Springs electrolyser

It is possible to validate the heat demand trend of the system thanks to the work of P. Mottaghizadeh [21], as shown in Fig. 5.29 and Fig. 5.30, in which provides the final result of their simulation in form of a graph (the negative terms before 8.5 MW are presented above the axis for convenience). Now zooming in it is clearly visible the thermoneutral point is at the power of 8.5 MW.

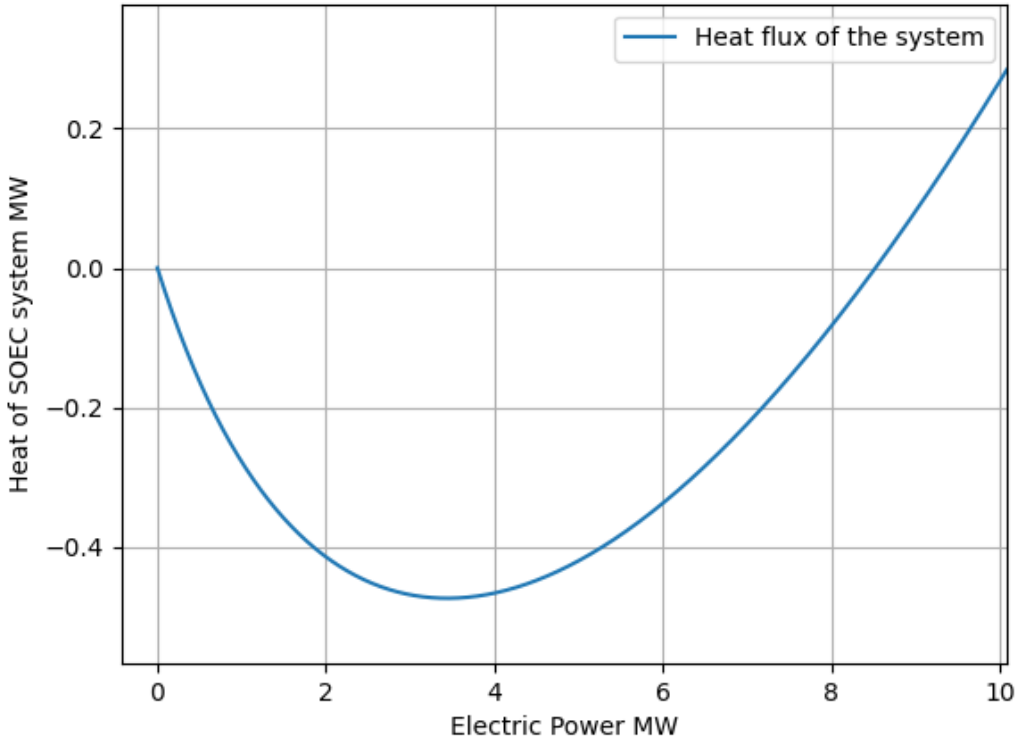

Figure 5.31: Heat requirement for the SOEC system in design condition, zoom

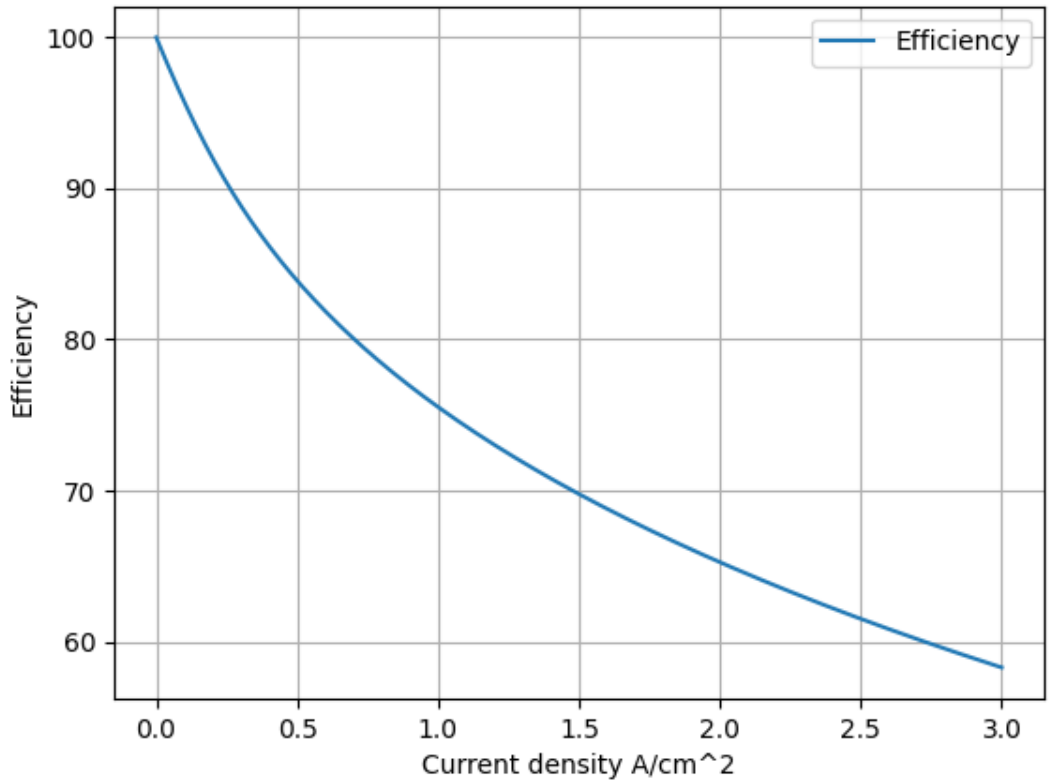

Figure 5.32: Efficiency vs current density plot

The model was designed to have the $E_{th} = 1.285V$ at 8.5 MW system power, following the work of P. Mottaghizadeh [21], with a current density of $\mathbf{1.28A/cm^2}$.
The heat required from the system at the design point of 2.68 MWe is 0.46 MWt; however the system can also operate at the thermoneutral voltage employing an higher current density; this entails a lower efficiency and an higher degradation of the components. As it can be seen from the Fig. 5.32 the thermoneutral point efficiency is 72.2% which is more than 10% lower than the design condition and only 10% higher than the PEM technology.
These results are reasonable enough as the cell voltage and current density comply with the information from A.Hauch [24]:

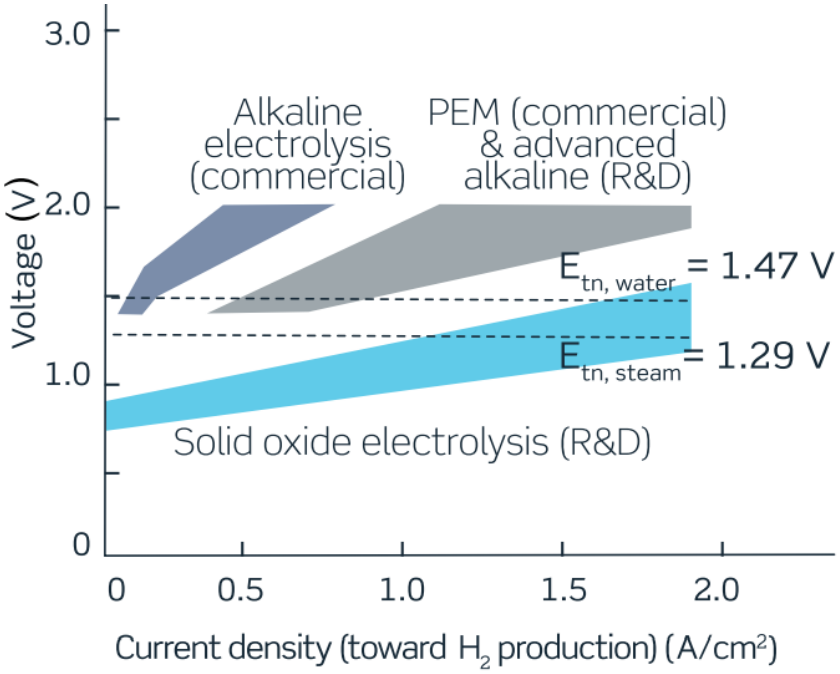

Figure 5.33: Current density vs voltage for different electrolyser models

The thermal demand for a 2.68 MWe module is not limited to the 458 kWt for the operation but it is necessary to produce the steam at $150°C$ from water at $25°C$; thus the total thermal instantaneous demand is equal to:

$$Q_{tot} = Q_{system} + Q_{sensible} + Q_{latent} = 458 + 58.6 + 539 = 1055.6\ kWt \tag{5.71}$$

The analysis will proceed comparing the demand for solutions with different powers to the waste heat available from the turbine/s to see if it is feasible to power the system totally or partially.

Coupling with the wind farm

Now the different power ratings of the electrolyser are analysed to see which is the best one. Given that the nominal size of the electrolyser is 2.68 MW it was chosen to evaluate a system comprised of 4 (10.72 MW), 5 (13.4 MW), 6 (16.08 MW) units to supply the hydrogen for the 52 MW turbine, only the coupling with unit 2 will be studied as it is the one that operated the most. It is also assumed that the efficiency of the system is the same for every operating condition as it is made by more units of electrolysers. In the end the feasibility of a system with nominal power of 26.8 MW (10 electrolysers of 2.68 MW) will be studied to enable the powering for both 52 MW units of the Rhode power station.

	HYLINK SOEC
Hydrogen production	
Net production rate	750 Nm^3/h
Production capacity dynamic range	5 % ... 100 %
Hot idle ramp time	< 10 min
Delivery pressure	0 bar (g)
Hydrogen purity	max. 99,99 %
Power input and electrical efficiency	
System power rating (AC)	2,680 kW
Specific power consumption at stack level (DC)*	3 kWh/Nm3
Specific power consumption at system level (AC)*	3.6 kWh/Nm^3
System electrical efficiency**	84 %
Steam input	
Consumption	860 kg/h
Temperature	150 °C ... 200 °C
Pressure	3.5 bar (g) ... 5.5 bar (g)
Other specs	
Footprint***	~ 300 m^2
Ambient temperature	-20 °C ... 40 °C

Figure 5.34: Sunfire electrolyser datasheet [58]

SOEC electrolyser system of 10.72 MW

The hydrogen produced is 1771.47 ton/year which is lower than the overall required of 1902 ton/year therefore a bigger system is needed. However also the time needs to be taken into account as every half an hour we have a requirement when the turbine is working and a surplus when it is not, so a storage is needed to operate the system. It is possible to see that the overall hydrogen for a year is not enough but there are important peaks and troughs due to the discontinuity of the wind energy from which hydrogen is produced. Regarding the storage we have that 1687.47 ton of hydrogen are stored for future usage while only 84 ton can be directly used as the turbine is in operation at the same time.

To store the hydrogen is assumed to employ a series of compressors that increase the pressure up to 700 bar, to do so the necessary power is 265 kW (calculated with $P = \dot{m}_{H_2} \cdot c_p \cdot \Delta T$) with the mass flow that consists of the positive values between the difference of hydrogen produced and consumed every half an hour, instead the hydrogen outlet temperature is assumed to be 180° C [5].

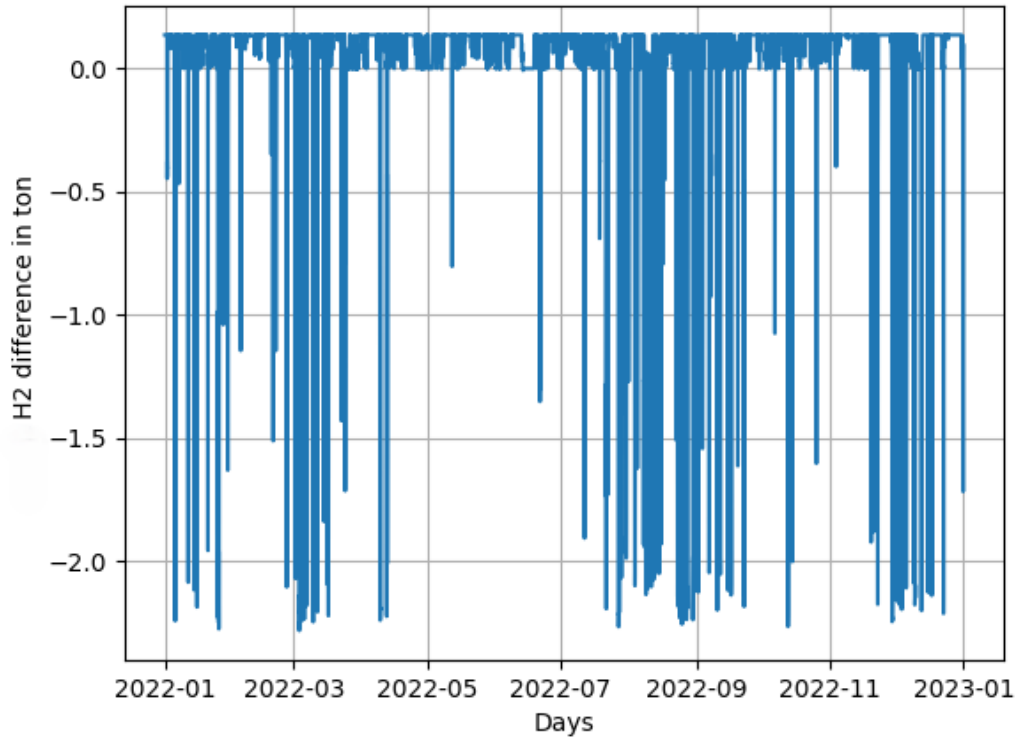

Figure 5.35: Difference between production and consumption of H_2 every half an hour

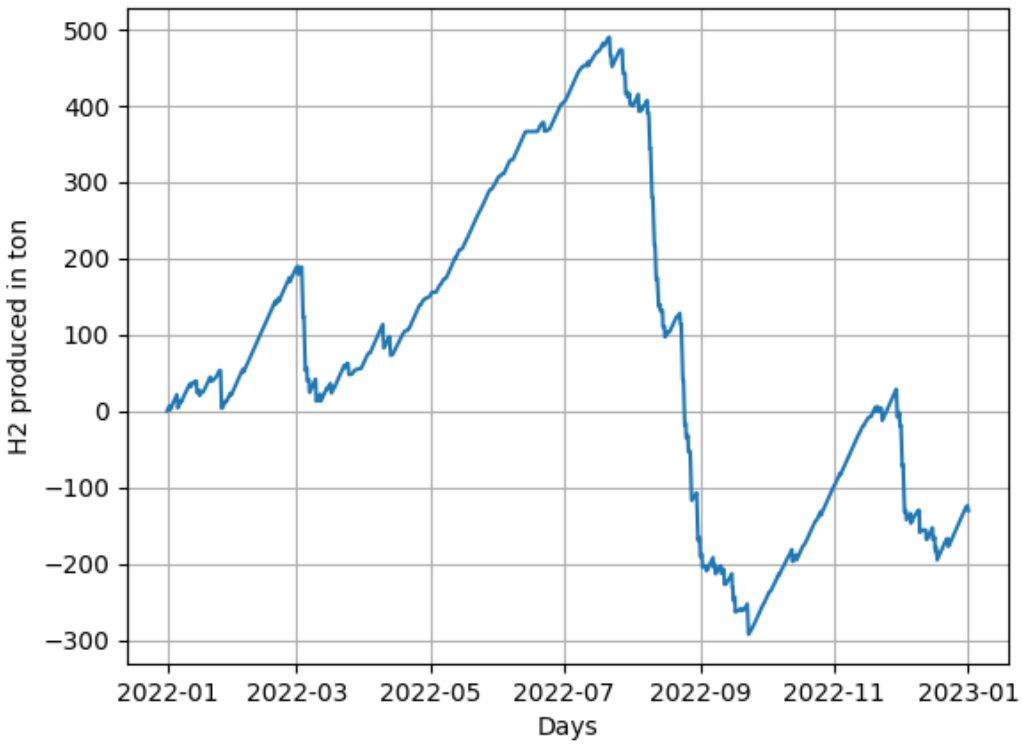

Figure 5.36: Cumulative difference of H_2 production and consumption

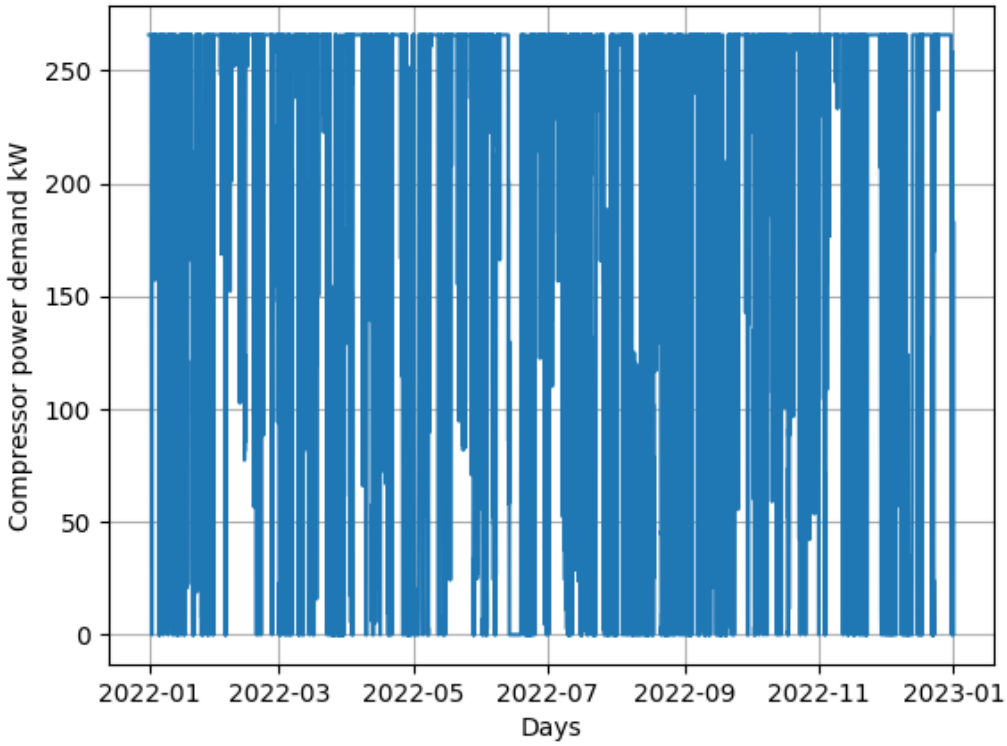

Figure 5.37: Operation power of H_2 compressor every half an hour

Here we reach peaks of 500 ton of surplus and -300 ton of deficit so a larger system is required.

SOEC electrolyser system of 13.4 MW

The hydrogen produced is 2118.79 ton/year while the demand is 1902 ton/year.
The quantity of H_2 compressed is 2023.6 ton while only 95.19 ton can be directly used as the turbine.

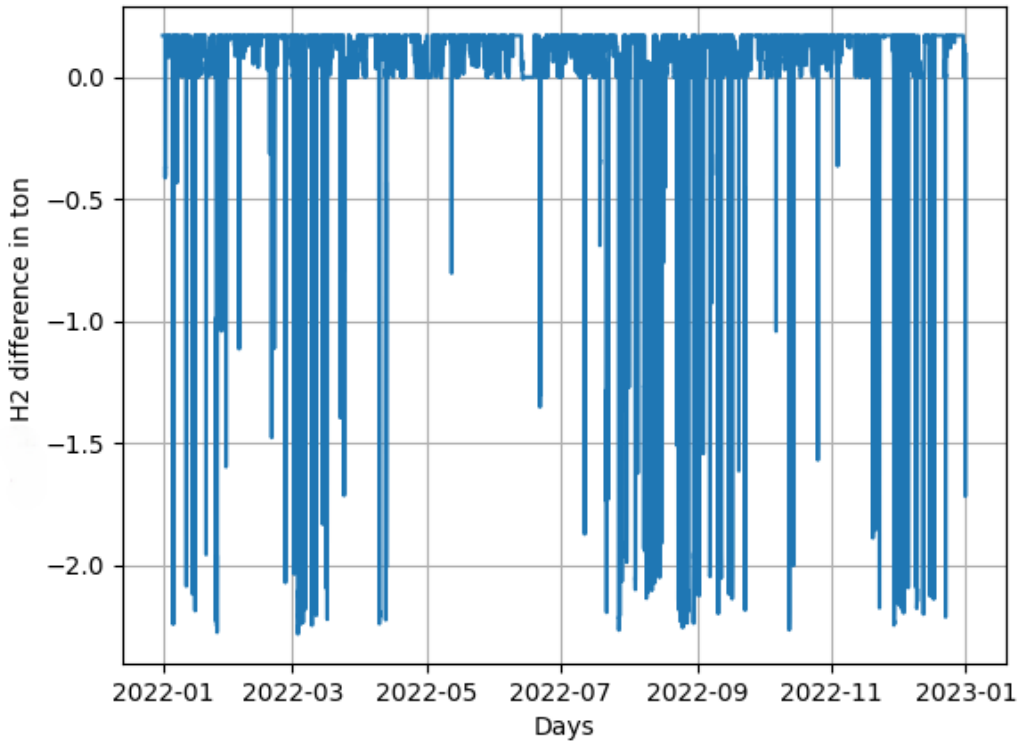

Figure 5.38: Difference between production and consumption of H_2 every half an hour

Figure 5.39: Cumulative difference of H_2 production and consumption

The compressor power to store the hydrogen is equal to 335 kW at the design flow rate:

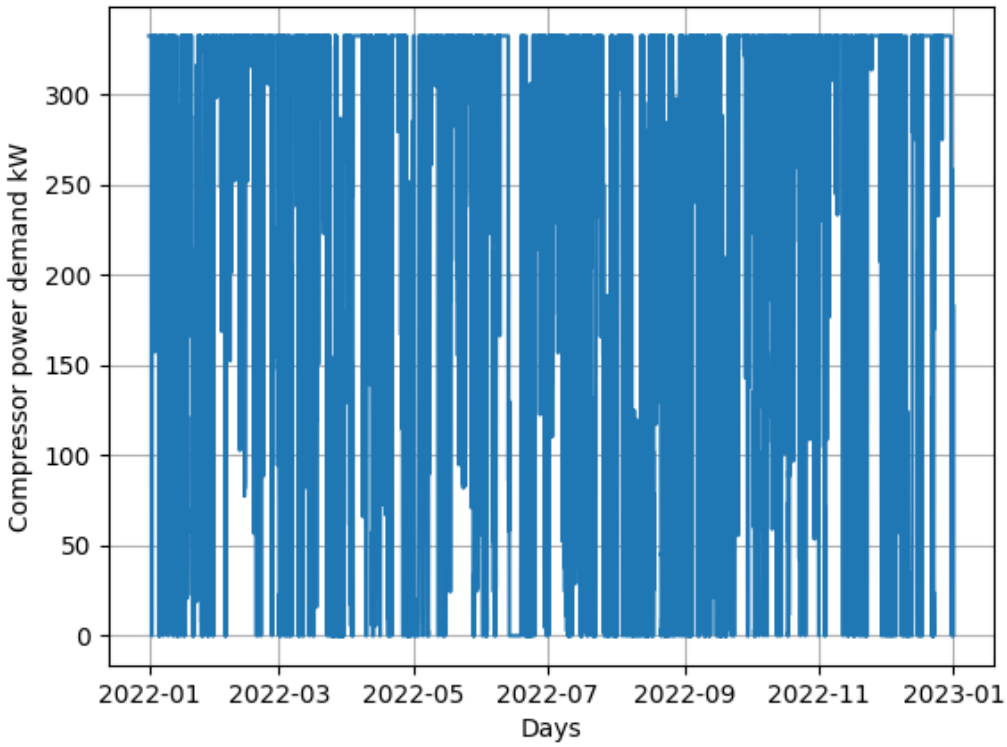

Figure 5.40: Operation power of H_2 compressor every half an hour

This solution seems the most feasible one as the trend for the storage is almost always positive, it is necessary to buy hydrogen only for a handful of days of the year and the quantity is small, and the power required to operate a compressor is increased only by 70 kW.

SOEC electrolyser system of 16.08 MW

Here the H_2 production increases up to 2434.66 ton/year which exceeds the demanded 1906 ton/year; there are 2330.69 ton of hydrogen compressed and stored while only 103.97 ton can be directly used.

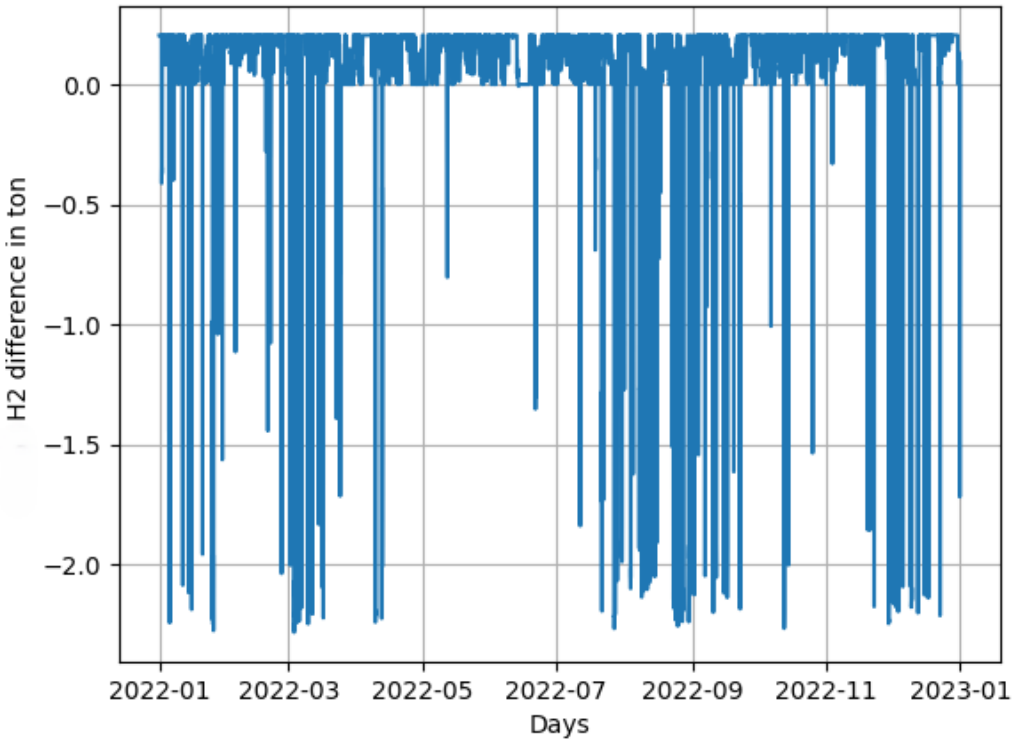

Figure 5.41: Difference between production and consumption of H_2 every half an hour

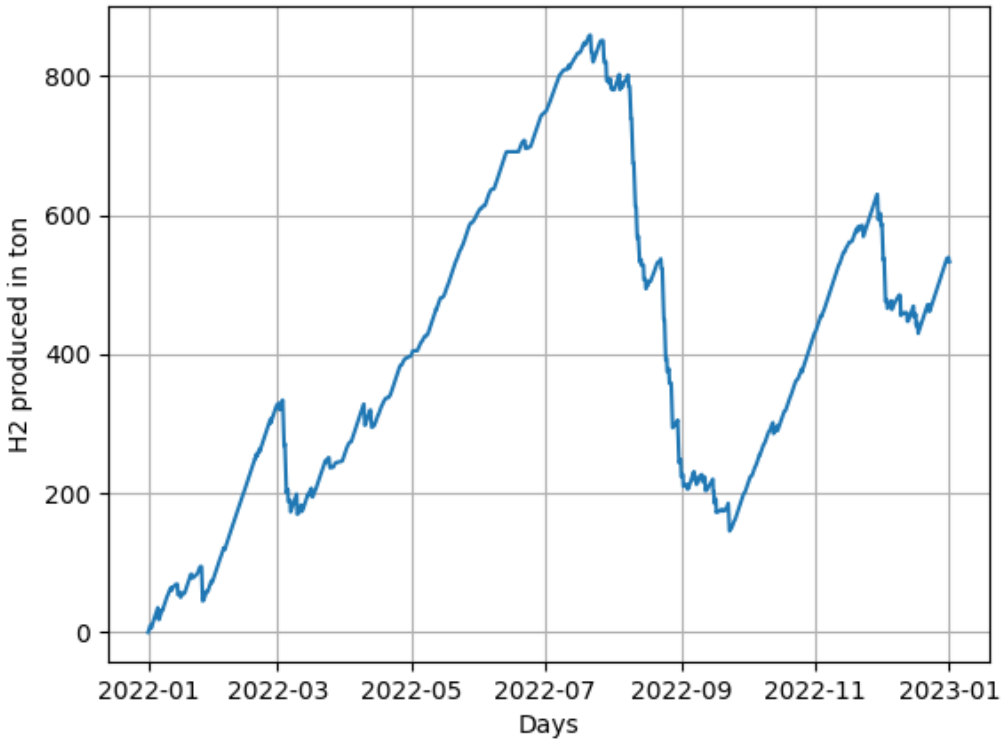

Figure 5.42: Cumulative difference of H_2 production and consumption

The system is clearly oversized for the application as the storage size would need to be 850 ton, on the other hand it is sure that this solution can supply the hydrogen needed at every given time without external sources; plus it is possible to consider this solution if an objective is selling the excess H_2 to the market.

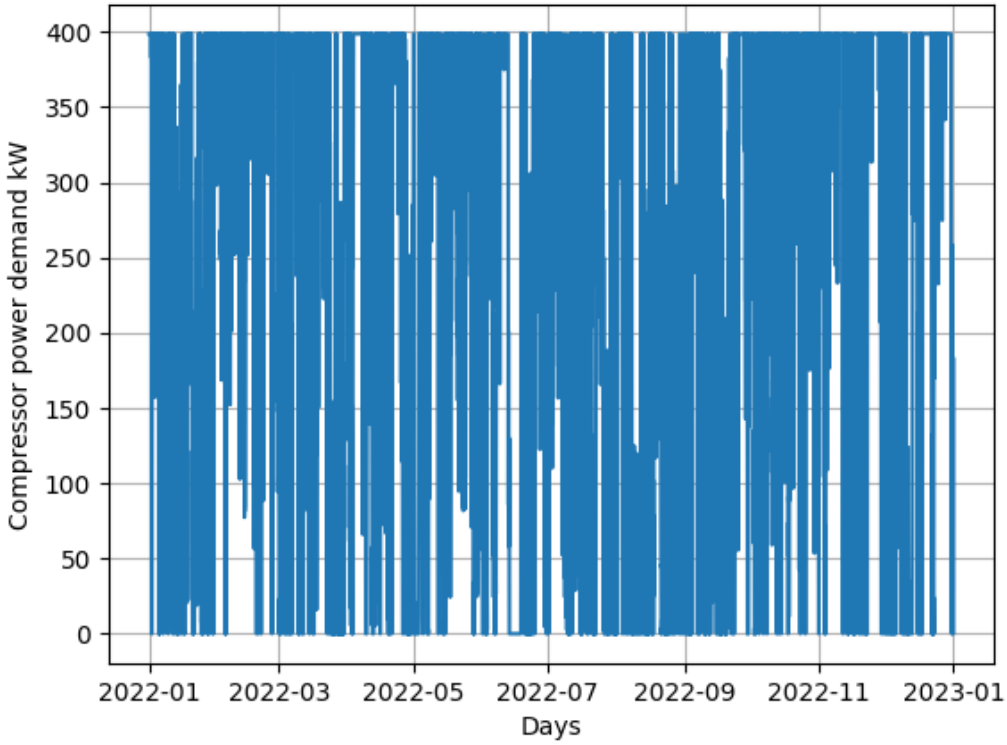

Figure 5.43: Operation power of H_2 compressor every half an hour

The compressor power to store the hydrogen is equal to 400 kW at the design flow rate, so it is evident that roughly 60-70 kW of compressor power can cover 2.68 MW each time it is added; obviously it could differ a bit as the production depends on the wind availability.

SOEC electrolyser system of 32.16 MW

Here the H_2 production is 3811.78 ton/year which is less than the demanded 3791.76 ton/year; there are 3644.19 ton of hydrogen compressed and stored while only 167.59 ton can be directly used.

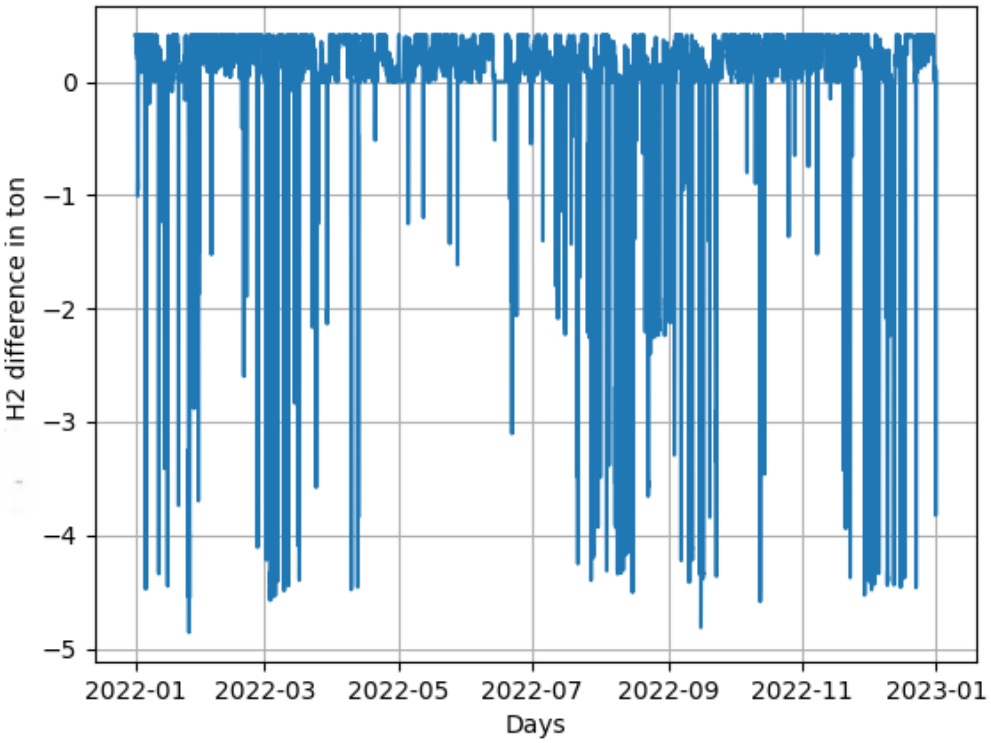

Figure 5.44: Difference between production and consumption of H_2 every half an hour

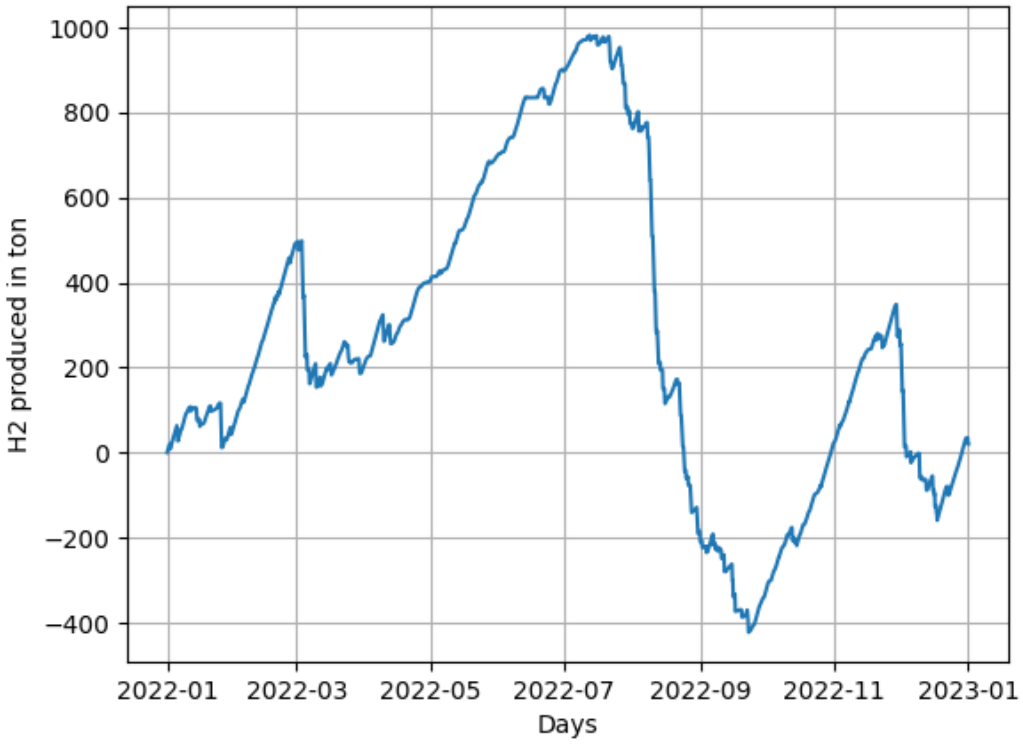

Figure 5.45: Cumulative difference of H_2 production and consumption

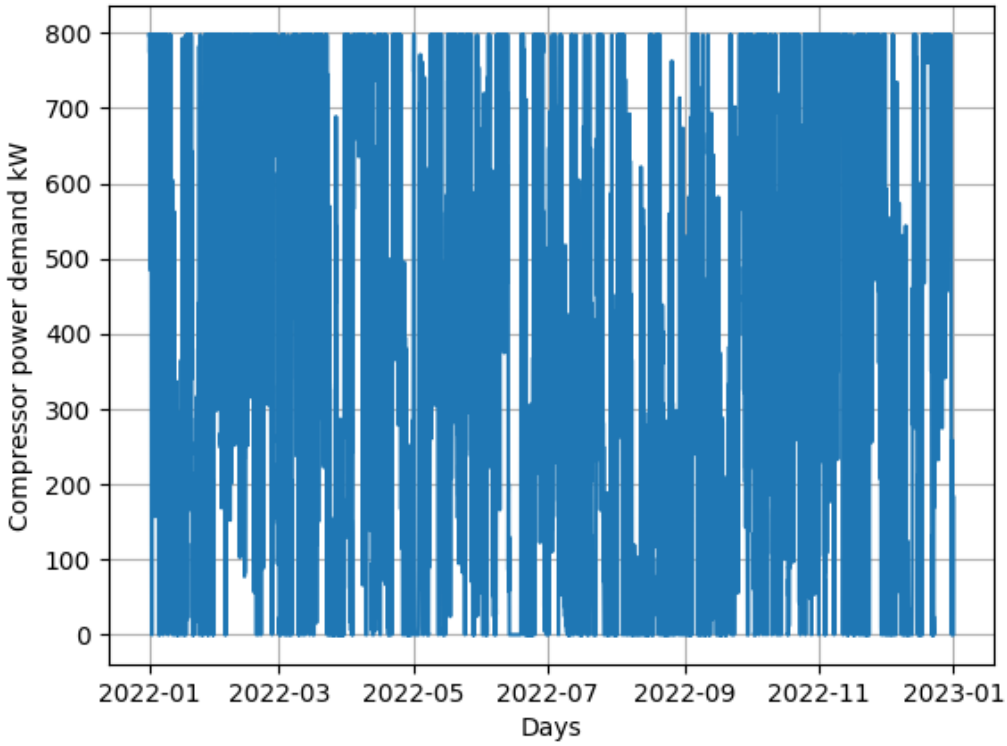

Figure 5.46: Operation power of H_2 compressor every half an hour

In this solution the electrolyser plant works to fuel both units of the Rhode power station (104 MW). Overall the hydrogen produced is enough but due to the discontinuous nature of the production peaks of 1000 ton surplus and 400 ton deficit are reached in August and September so this system is not feasible as a stand alone one. The compressor power to store the hydrogen is equal to 800 kW at the design flow rate showing that it is directly proportional to the flow rate as it is exactly double the value of the 16.08 MW configuration.

Heat requirement for the SOEC electrolyser system of 13.4 MW

The problem of heat management is important when dealing with high temperature electrolysis, here it will be analysed how the coupling of the turbine and electrolyser behaves in terms of heat demand considering the system size scenario of 13.4 MW.
The heat demand for the system operation in design condition is 458 kWt for every 2.68 MWe then to get the total requirement it is necessary to sum the heat to increase the temperature, 58.6 kWt, and change the phase of water to steam, 539 kWt.
So for 13.4 MWe the total heat needed is 5.3 MWt, while the supply can go above 60 MWt but only for small period of times; as the turbine operates only 415 nominal hours in a year.
It will be shown that it is not worth to perform a deep analysis on the system behaviour with a real thermal storage system because the waste heat from the turbine it is not enough to cover all the demand, therefore it is just shown what is the trend of the thermal power. In any case for an application of this type the molten salt storage would be the most suitable. The waste heat obtainable from the gas turbine is calculated for intervals of $100°C$ considering the mean of the specific heat $P = \dot{m}_{gas} \cdot c_{p_{mean}} \cdot \Delta T$:

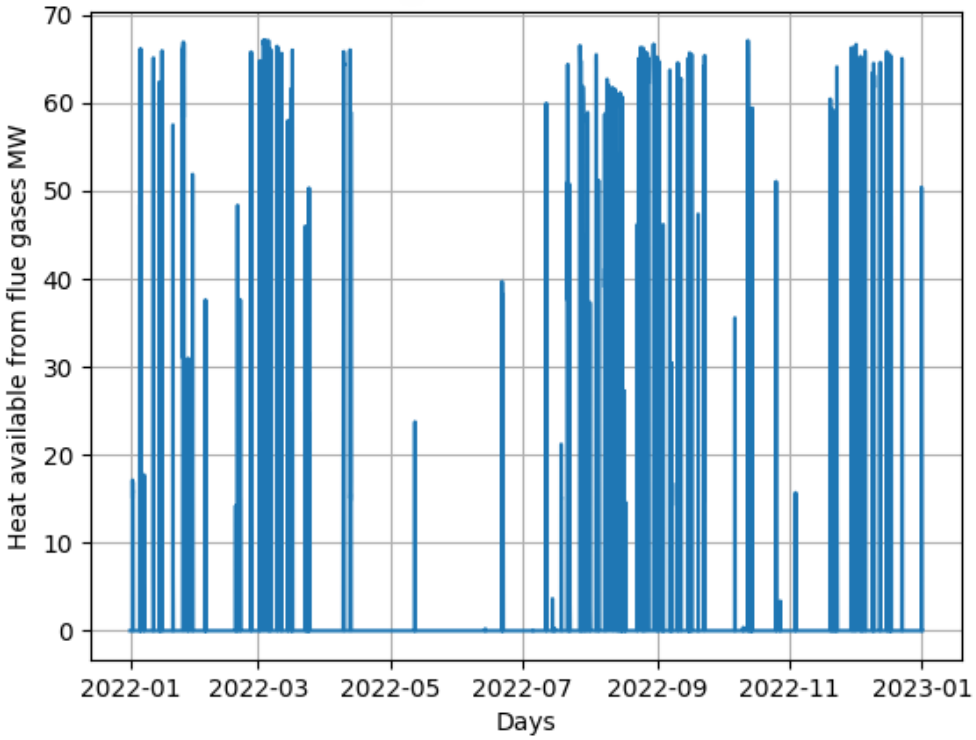

Figure 5.47: Waste heat of the gas in MW ($\Delta T = 750°C - 100°C$)

So also the instantaneous heat difference can be computed as shown in Fig. 5.48:

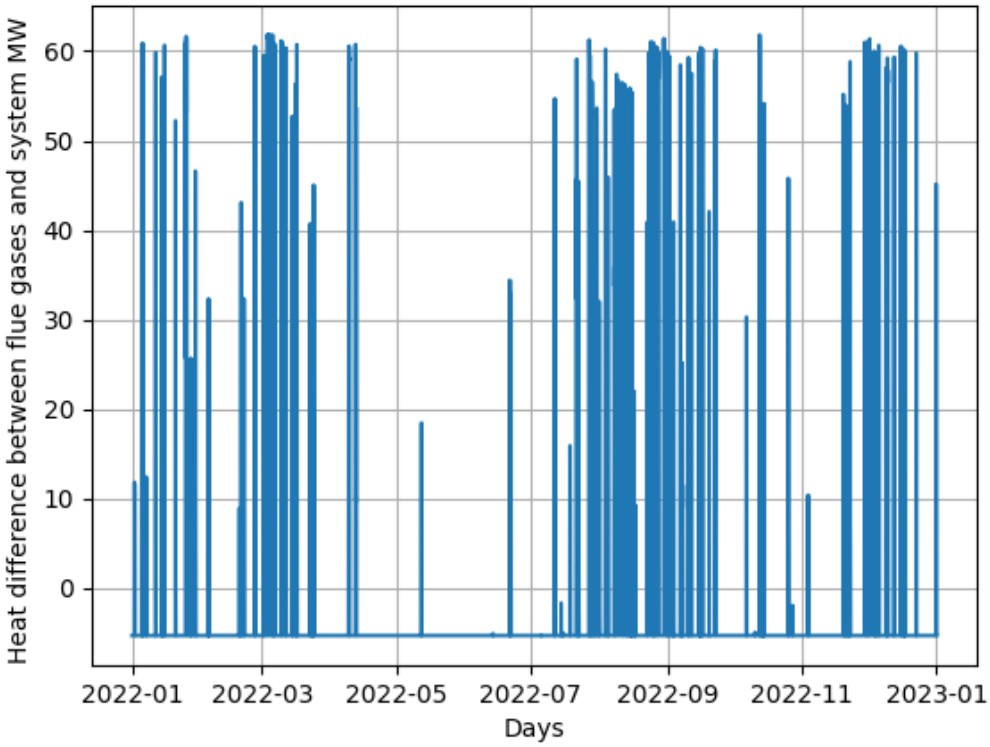

Figure 5.48: Waste heat difference for gas and system in MW

Now the trend is obtained summing all the instantaneous differences:

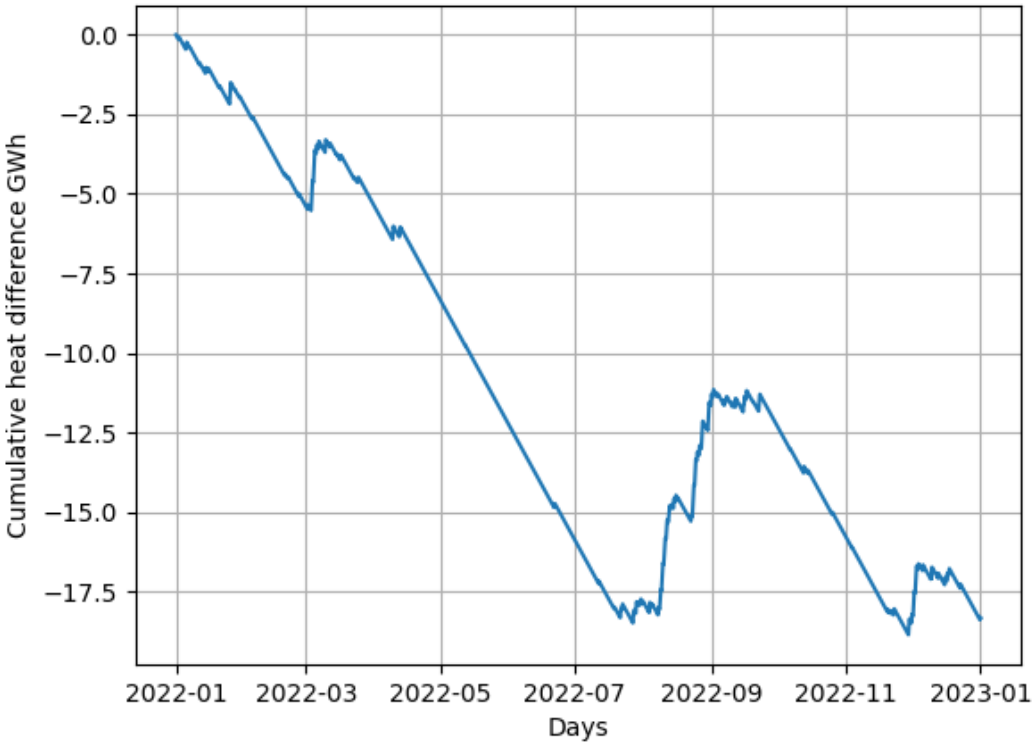

Figure 5.49: Cumulative heat difference for gas and system in GWh

The total heat necessary to operate the system, which is in endothermic mode, is 20.06 GWh_t while to heat and vaporize the water for a whole year 26.18 GWh_t. On the contrary only 27.92 GWh_t are available from the waste heat source. At this point it is possible to compare the waste heat from the flue gases with only the vaporization or the total demand for the water to see if at least this part could be fulfilled properly:

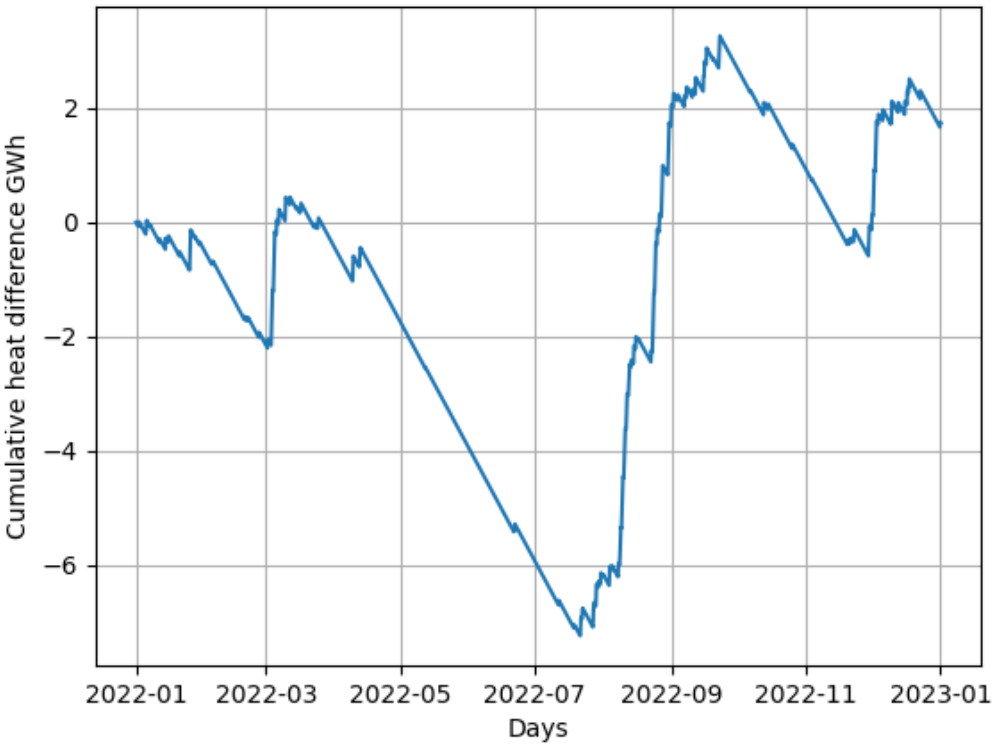

Figure 5.50: Waste heat vs heat required for sensible and latent heat transfer

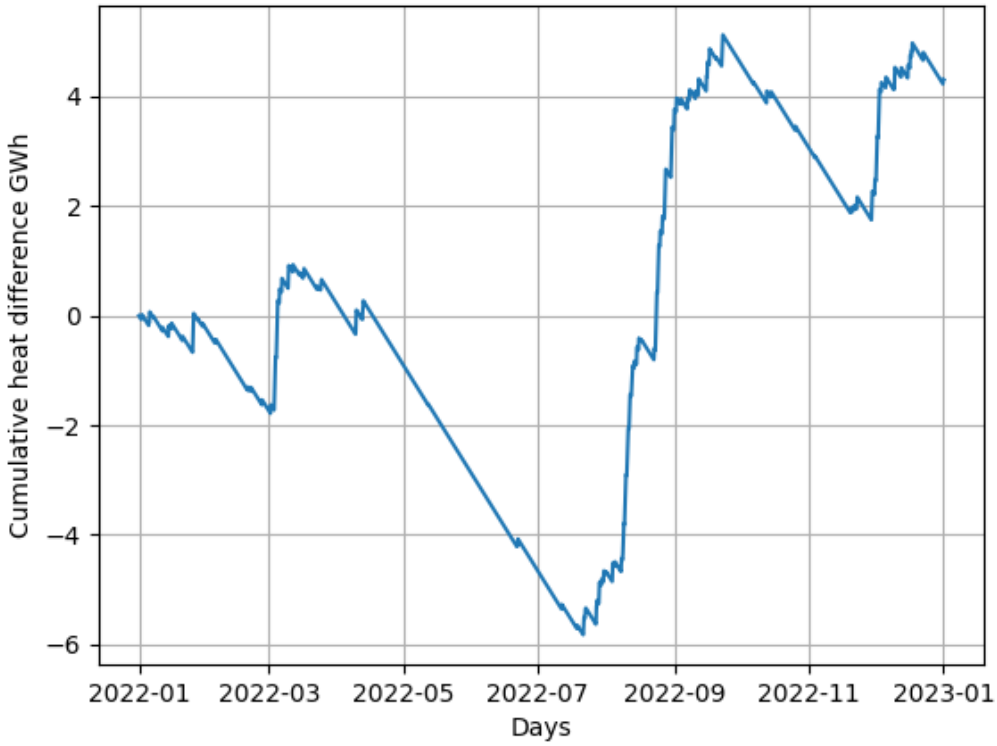

Figure 5.51: Waste heat vs heat required for latent heat transfer

Heat requirement for SOEC system of 32.16 MW

The waste heat obtainable from the gas turbines is calculated for intervals of $100°C$ considering the mean of the specific heat $P = \dot{m}_{gas} \cdot c_{p_{mean}} \cdot \Delta T$:

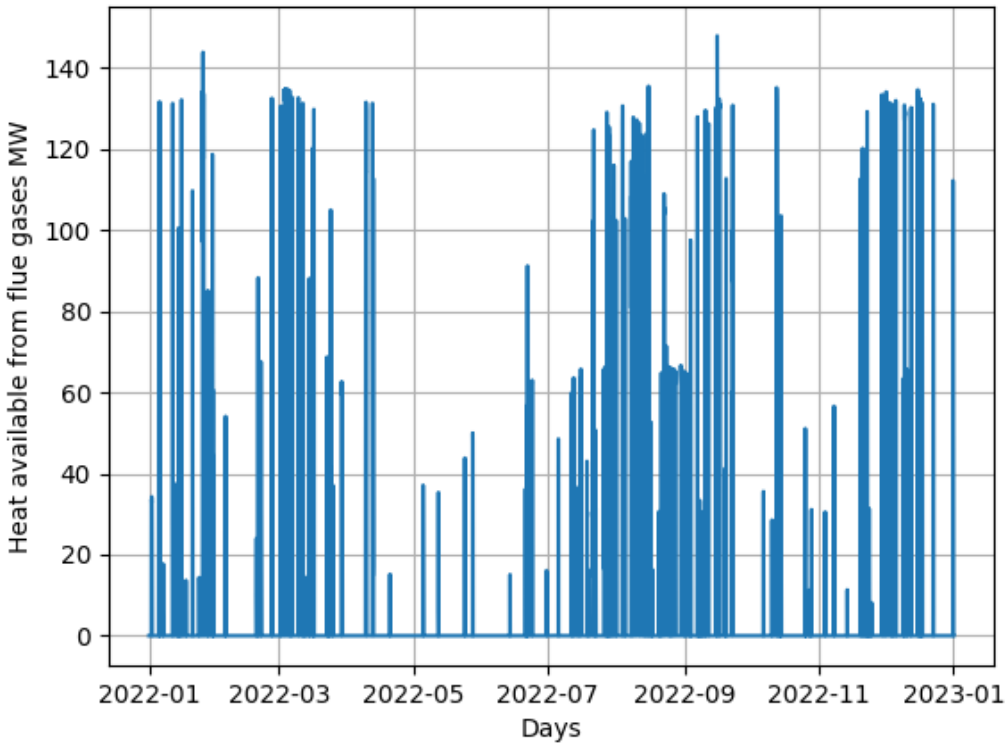

Figure 5.52: Waste heat of the gas in MW ($\Delta T = 750°C - 100°C$)

So also the instantaneous heat difference can be computed as shown in Fig. 5.53:

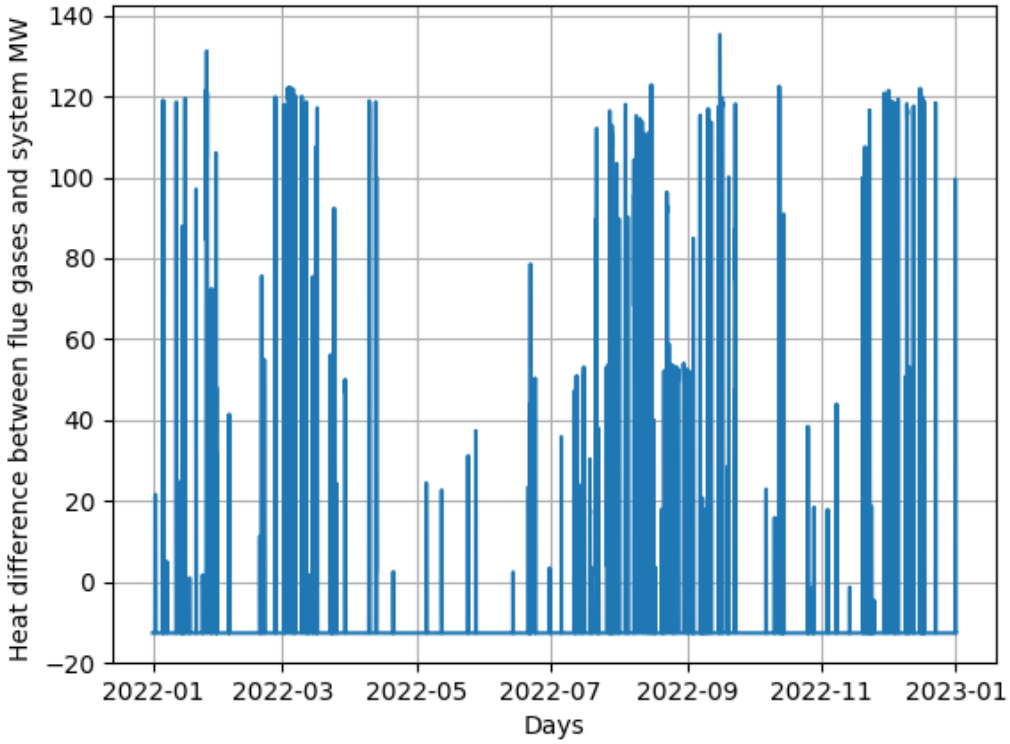

Figure 5.53: Waste heat difference for gas and system in MW

Now the trend is obtained summing all the instantaneous differences:

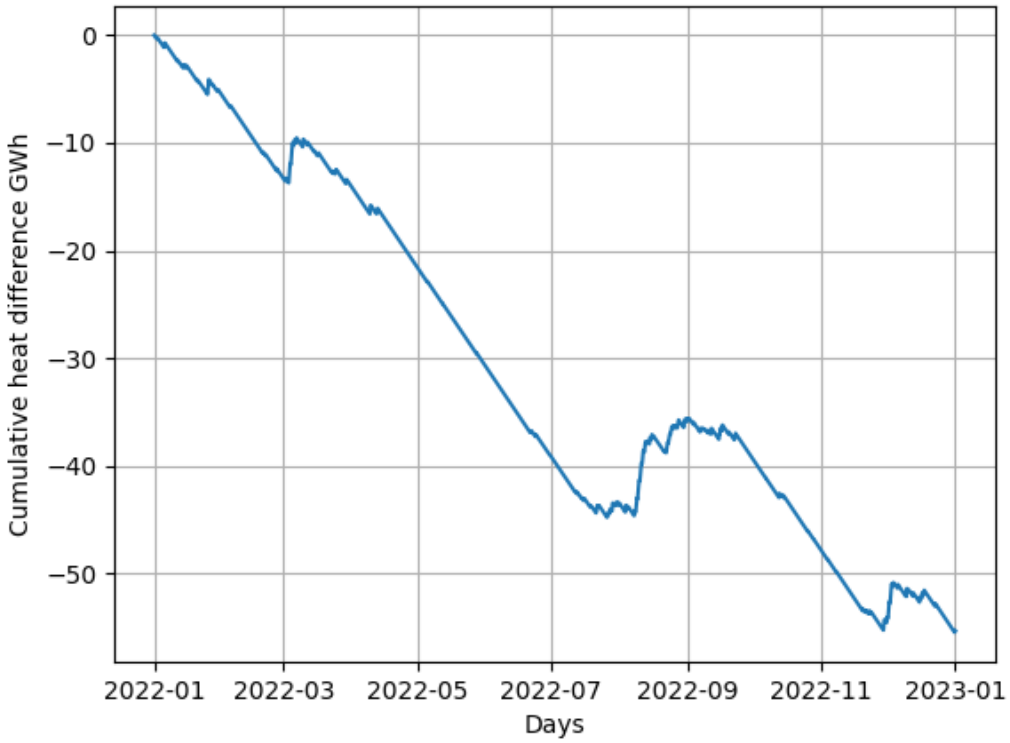

Figure 5.54: Cumulative heat difference for gas and system in GWh

The total heat necessary to operate the system, which is in endothermic mode, is 48.14 GWh_t while to heat and vaporize the water for a whole year 62.82 GWh_t. On the contrary only 55.65 GWh_t are available from the waste heat source.

At this point it is possible to compare the waste heat from the flue gases with only the vaporization or the total demand for the water to see if at least this part could be fulfilled properly:

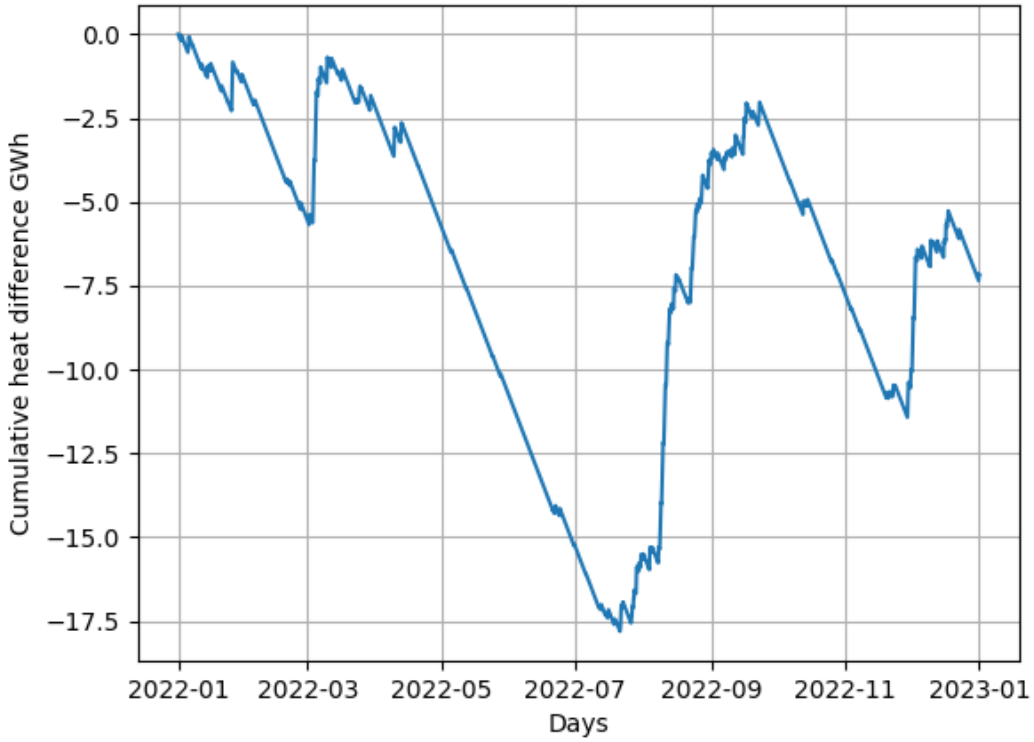

Figure 5.55: Waste heat vs heat required for sensible and latent heat transfer

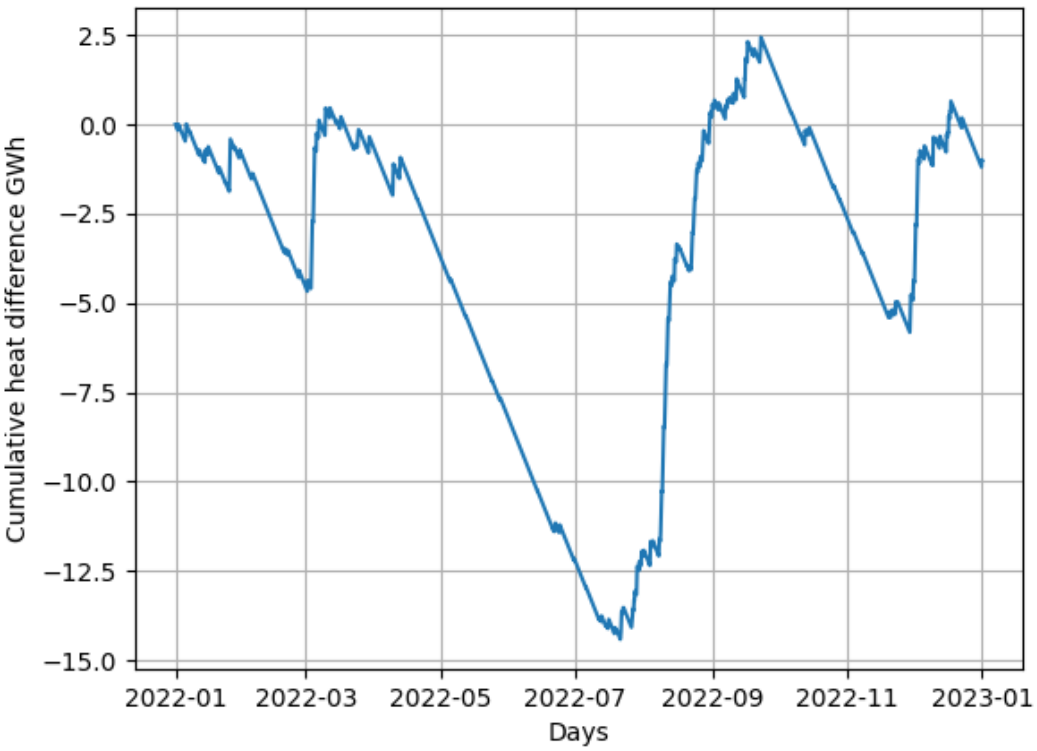

Figure 5.56: Waste heat vs heat required for latent heat transfer

To conclude the system requires 1.055 MWt for every 2.68 MWe to operate. The heat is of course at different temperatures and this must be considered in case of a more detailed analysis with the design of heat exchangers and thermal storage, however just by making a rough estimate it is clear that this quantity is higher than the heat recovered from the flue gases so it is not possible to obtain a self sustained system. Although this process is not attractive from an exergetic point of view, as low temperature heat would be enough, Fig. 5.50, 5.51, 5.55, 5.56 show that it is possible to power partially the water heating and the steam production; however there are problems during June-July because the turbine does not operate for a long time. There could also be a coupling with the system in order to make up the necessary heat for the endothermic operation but the heat available would substantially decrease as only heat above $600°C$ should be considered. It is also plausible that the system works at the thermoneutral voltage, thus with no heat requirement aside from the low temperature heat necessary for the water input, however this solution entails a higher value of the current density and a lower efficiency, according to the literature and the simulation results.

Summary and comparison

To sum up the most convenient configurations to fire a 52 MW turbine are 21.875 MW for the PEM and 13.4 MW for the SOC as they are enough to supply hydrogen at almost all times (in the appendix {7} it is possible to see the trend for unit 1, which is always above zero), even so the heat requirement for the SOC needs to be taken into account.
To operate both units the PEM configuration is not feasible because even using all the wind farm capacity to produce hydrogen, 84 MW, the 87.5 MW electrolyser cannot satisfy the demand both at some times during September and on the overall year; the 32 MW SOC configuration can satisfy the yearly demand but there is an high deficit of hydrogen in September also in this case. It would be possible to increase the size up to 51 MW for example to be sure the H_2 is available at all times but the 32 MW was chosen to compare it with the amount produced with the PEM configuration and to show that even if I double the power for the case 3, which produced more than enough hydrogen for a turbine, it is not enough for two units. The main reason it is difficult or impossible to operate two turbines is because of the wind farm production that not always is at nominal capacity, so increasing the power of the electrolyser does not increase the production of hydrogen by the same amount. The higher the power requested the higher the probability that the wind power available is not enough at some times, leading to lower nominal operating hours of the hydrogen production.
Finally considering the thermal management, the PEM electrolyser just needs some low temperature heat dissipation that can be done with fans; while the SOC system requires high temperature heat to work and this quantity cannot be totally satisfied by the heat recovery of the turbine exhaust gases, so the options are to supply the rest of the heat demand or work at the thermoneutral point, increasing the current density, but with a lower efficiency. Instead the low exergy heat to increase the water temperature and to form the steam could be supplied by other low temperature heat sources.

Table 5.1 presents the summary of all the cases analyzed in the chapter:

	Power	**Unit**	**H_2 produced**	**Peaks**	**Troughs**	**Demand**	**Unit**
PEM-1	17.5	MW	1854.6	537	-254	1902	ton/year
PEM-2	21.875	MW	2164.6	710	-54	1902	ton/year
PEM-3	26.25	MW	2431.2	861	0	1902	ton/year
PEM-4	87.5	MW	3672.6	972	-521	3780.3	ton/year
SOC-1	10.72	MW	1771.5	490	-293	1902	ton/year
SOC-2	13.40	MW	2118.8	683	-62	1902	ton/year
SOC-3	16.08	MW	2434.7	859	0	1902	ton/year
SOC-4	32.16	MW	3811.8	982	-423	3780.3	ton/year

Table 5.1: Levelized cost of hydrogen and compressed hydrogen for SOC scenarios

Chapter 6

Results: Levelized Costs

6.1 Economic parameters

Adding economic analysis to the technical solutions developed in Chapter 5 provides additional contest to the results. Therefore the LCOH (Levelized cost of hydrogen) and the LCOCH (Levelized cost of compressed hydrogen) will be calculated for every configuration and briefly summarised in a table. The hydrogen cost is calculated following the data and formulae reported in the article published in early 2023 by M.Nasser [16].

$$LCOH \ or \ LCOCH = \frac{CAPEX + \sum_{n=1}^{N} OPEX_n + REPEX_n}{\sum_{n=1}^{N} (1 - n \cdot d) \cdot M_{H_2}} \tag{6.1}$$

Where the terms are:

- CAPEX is the project capital expenditure
- OPEX is the operation and maintenance cost
- REPEX is the replacement cost of any component at the end of its lifetime
- i is the real interest rate calculated as: i = $\frac{i_{nom}-f}{1+f}$ with i_{nom} nominal interest rate
- f is the inflation rate
- d is the degradation rate of the components
- M_{H_2} is the annual hydrogen production
- n = 20 is the number of years considered for the calculation, the economic lifetime

The levelized cost of the electricity derived by the combustion of hydrogen in the turbine is then calculated assuming that there is no CAPEX for the gas turbine repurposing even though in reality there will be also this cost to take into account, this choice was due to the lack of sources in the literature, and an OPEX of 4 €/MWh_e as reported by S.Skordoulias [60]:

$$LCOE = \frac{\sum_{n=1}^{N} OPEX_n}{\sum_{n=1}^{N} (1 - n \cdot d) \cdot kWh} + \frac{LCOH \cdot M_{H_2}}{kWh} \tag{6.2}$$

$$LCOE(C) = \frac{\sum_{n=1}^{N} OPEX_n}{\sum_{n=1}^{N}(1 - n \cdot d) \cdot kWh} + \frac{LCOCH \cdot M_{H_2}}{kWh} \tag{6.3}$$

The LCOE is the cost for the electricity assuming that the hydrogen is used in the turbine as soon as it is produced, while LCOE(C) is the cost for the real case scenario with compression and storage.

Component	**Value**	**Unit**	**Component**	**Value**	**Unit**
PEM electrolyser			**Hydrogen tank**		
CAPEX	1337	$/kW	CAPEX	500	$/kg
OPEX	20	$/kW	OPEX	12	$/kg.year
Lifetime	15	years	Lifetime	20	years
SOC electrolyser			**Compressor**		
CAPEX	2000	€/kW	CAPEX	1800	$/kW
OPEX	20	$/kW	OPEX	5.5	$/kW
Lifetime	10	years	Lifetime	20	years
Wind turbine			**Gas turbine**		
CAPEX	1350	$/kW	CAPEX	n.d.	€/kW
OPEX	42	$/kW	OPEX	4	€/MWh_e
Lifetime	20	years	Lifetime	50	years

Table 6.1: Cost and life cycle of the components

The CAPEX of the PEM electrolyser is taken from the NREL report of year 2024 [61] while the CAPEX of a 5 MW system SOC electrolyser is reported according to A. Hauch [24]; Again the CAPEX of the storage tank at 700 bar is obtained from the hydrogen cost analysis of C.Houchins [62] while the replacement cost of the cells is estimated to be 210 €/kW from the IRENA report [63]. All the other data is found in M.Nasser's analysis [16] aside from the cost to reconvert a turbine, which could not be found in the literature and is assumed equal to zero, and the cost to operate it in N.Skordoulias paper [60].

6.1.1 PEM scenario

The LCOH/LCOCH in 20 years is calculated for the four scenarios with the simplification that the turbine works the recorded hours even if there is no hydrogen available at that moment. For example in some scenarios the overall amount may be lower so the total working MWh of the turbine will be weighted on the production; instead even if the overall production is higher than the requirement there could be a lack of fuel during different times of the year, in those cases it will be just mentioned.

PEM system of 17.5 MW rated power

To simplify the economic analysis the wind farm is considered to have the same rated power as the electrolyser (17.5 MW) and the other components are a compressor of 500 kW and an hydrogen tank of 500 tons. The hydrogen production is equal to 1854.6 ton while the demand is 1902 ton, for simplicity it is assumed the turbine continues to work for the assigned hours but the kWh for the calculation of the LCOE will be multiplied by the ratio 1854.6/1902.

Choosing to employ an interest rate of 8.75 %, an inflation rate of 6.55 % and a degradation rate of 0 % the results are (1 $ is 0.92 €):

$$LCOH = \frac{CAPEX_{wind} + CAPEX_{PEM} + \sum_{n=1}^{N} OPEX_{wind} + OPEX_{PEM} + REPEX_{PEM}}{\sum_{n=1}^{N}(1 - n \cdot d) \cdot M_{H_2}} \tag{6.4}$$

$$= \frac{21.74\ M€ + 21.53\ M€ + 10.99\ M€ + 5.23\ M€ + 2.7\ M€}{20 \cdot 1854.6\ ton} = 1.68\ €/kg$$

$$LCOCH = LCOH + \frac{CAPEX_{tank} + CAPEX_{comp} + \sum_{n=1}^{N} OPEX_{tank} + OPEX_{comp}}{\sum_{n=1}^{N}(1 - n \cdot d) \cdot M_{H_2}} = \tag{6.5}$$

$$= 1.68\ €/kg\ + \frac{230\ M€ + 0.8\ M€ + 89.7\ M€ + 0.4\ M€}{20 \cdot 1854.6\ ton} = 10.33\ €/kg$$

Taking into account only the main scenario with i = 8.75 %, f = 6.55%, d = 0% and considering only the configuration with the 52 MW turbine that runs more of the time, (21583 MWh in a year) it is possible to calculate the LCOE assuming that the turbine works all the hours but decreasing the amount of MWh, multiplying for 1854.6/1902 = 0.975, due to the lack of H_2 (Values from Table 6.1):

$$LCOE(C) = \frac{\sum_{n=1}^{N} OPEX_{turbine}}{\sum_{n=1}^{N}(1 - n \cdot d) \cdot kWh} + \frac{LCOCH \cdot M_{H_2}}{kWh} \tag{6.6}$$

$$= \frac{\sum_{n=1}^{N} 4\ €/MWh \cdot 21583 \cdot 0.975\ MWh}{\sum_{n=1}^{N}(1 - n \cdot d) \cdot 21583011 \cdot 0.975\ kWh} + \frac{10.33\ €/kg \cdot 1854600\ kg}{21583011 \cdot 0.975\ kWh} = 0.91\ €/kWh$$

This quantity is very high due to the high volume of storage required; if there would not be any compression and storage, with a direct consumption of the hydrogen the price would be:

$$LCOE = \frac{\sum_{n=1}^{N} OPEX_{turbine}}{\sum_{n=1}^{N}(1 - n \cdot d) \cdot kWh} + \frac{LCOH \cdot M_{H_2}}{kWh} \tag{6.7}$$

$$= \frac{\sum_{n=1}^{N} 4\ €/MWh \cdot 21583 \cdot 0.975\ MWh}{\sum_{n=1}^{N}(1 - n \cdot d) \cdot 21583011 \cdot 0.975\ kWh} + \frac{1.68\ €/kg \cdot 1854600\ kg}{21583011 \cdot 0.975\ kWh} = 0.151\ €/kWh$$

PEM system of 21.875 MW rated power

To simplify the economic analysis the wind farm is considered to have the same rated power as the electrolyser (21.875 MW). Then the other components are a compressor of 625 kW and a hydrogen tank of 700 tons. The hydrogen produced is 2164.6 ton but only 1902 ton are necessary to power the system. Choosing to employ an interest rate of 8.75 %, an inflation rate of 6.55 % and a degradation rate of 0 % the results are as follows (1 $ is 0.92 €):

$$LCOH = \frac{CAPEX_{wind} + CAPEX_{PEM} + \sum_{n=1}^{N} OPEX_{wind} + OPEX_{PEM} + REPEX_{PEM}}{\sum_{n=1}^{N}(1 - n \cdot d) \cdot M_{H_2}} \tag{6.8}$$

$$= \frac{27.17\ M€ + 26.9\ M€ + 13.74\ M€ + 6.54\ M€ + 3.38\ M€}{20 \cdot 2164.6\ ton} = 1.80\ €/kg$$

$$LCOCH = LCOH + \frac{CAPEX_{tank} + CAPEX_{comp} + \sum_{n=1}^{N} OPEX_{tank} + OPEX_{comp}}{\sum_{n=1}^{N}(1 - n \cdot d) \cdot M_{H_2}} = \tag{6.9}$$

$$= 1.80\ €/kg\ + \frac{322\ M€ + 1.04\ M€ + 125.58\ M€ + 0.5\ M€}{20 \cdot 2164.6\ ton} = 12.17\ €/kg$$

Taking into account only the main scenario with i = 8.75 %, f = 6.55%, d = 0% and considering only the configuration with the 52 MW turbine that works more, (21583 MWh in a year with 1902 ton of hydrogen per year) it is possible to calculate the LCOE with only the hydrogen necessary to fire the turbine:

$$LCOE(C) = \frac{\sum_{n=1}^{N} OPEX_{turbine}}{\sum_{n=1}^{N}(1 - n \cdot d) \cdot kWh} + \frac{LCOCH \cdot M_{H_2}}{kWh} \tag{6.10}$$

$$= \frac{\sum_{n=1}^{N} 4\ €/MWh \cdot 21583\ MWh}{\sum_{n=1}^{N}(1 - n \cdot d) \cdot 21583011\ kWh} + \frac{12.18\ €/kg \cdot 2164600\ kg}{21583011\ kWh} = 1.22\ €/kWh$$

This quantity is very high due to the high volume of storage required; if there would not be any compression and storage with a direct consumption of the hydrogen the price would be as follows:

$$LCOE = \frac{\sum_{n=1}^{N} OPEX_{turbine}}{\sum_{n=1}^{N}(1 - n \cdot d) \cdot kWh} + \frac{LCOH \cdot M_{H_2}}{kWh} \tag{6.11}$$

$$= \frac{\sum_{n=1}^{N} 4\ €/MWh \cdot 21583\ MWh}{\sum_{n=1}^{N}(1 - n \cdot d) \cdot 21583011\ kWh} + \frac{1.80\ €/kg \cdot 2164600\ kg}{21583011\ kWh} = 0.183\ €/kWh$$

PEM system of 26.25 MW rated power

To simplify the economic analysis the wind farm is considered to have the same rated power as the electrolyser (26.25 MW). Then the other components are a compressor of 750 kW and a hydrogen tank of 800 tons. The hydrogen produced is 2431.2 ton but only 1902 ton are necessary to power the system. Choosing to employ an interest rate of 8.75 %, an inflation rate of 6.55 % and a degradation rate of 0 % the results are as follows (1 $ is 0.92 €):

$$LCOH = \frac{CAPEX_{wind} + CAPEX_{PEM} + \sum_{n=1}^{N} OPEX_{wind} + OPEX_{PEM} + REPEX_{PEM}}{\sum_{n=1}^{N}(1 - n \cdot d) \cdot M_{H_2}} \tag{6.12}$$

$$= \frac{32.6\ M€ + 32.29\ M€ + 16.48\ M€ + 7.85\ M€ + 4.06\ M€}{20 \cdot 2431.2\ ton} = 1.92\ €/kg$$

$$LCOCH = LCOH + \frac{CAPEX_{tank} + CAPEX_{comp} + \sum_{n=1}^{N} OPEX_{tank} + OPEX_{comp}}{\sum_{n=1}^{N}(1 - n \cdot d) \cdot M_{H_2}} = \tag{6.13}$$

$$= 1.93\ €/kg\ + \frac{368\ M€ + 1.24\ M€ + 143.51\ M€ + 0.6\ M€}{20 \cdot 2431.2\ ton} = 12.48\ €/kg$$

Taking into account only the main scenario with i = 8.75 %, f = 6.55%, d = 0% and considering only the configuration with the 52 MW turbine that works more, (21583 MWh in a year with 1902 ton of hydrogen per year) it is possible to calculate the LCOE with only the hydrogen necessary to fire the turbine:

$$LCOE(C) = \frac{\sum_{n=1}^{N} OPEX_{turbine}}{\sum_{n=1}^{N}(1-n\cdot d)\cdot kWh} + \frac{LCOCH \cdot M_{H_2}}{kWh} \tag{6.14}$$

$$= \frac{\sum_{n=1}^{N} 4\ €/MWh \cdot 21583\ MWh}{\sum_{n=1}^{N}(1-n\cdot d)\cdot 21583011\ kWh} + \frac{12.49\ €/kg \cdot 2431200\ kg}{21583011\ kWh} = 1.41\ €/kWh$$

This quantity is very high due to the high volume of storage required; if there would not be any compression and storage with a direct consumption of the hydrogen the price would be as follows:

$$LCOE = \frac{\sum_{n=1}^{N} OPEX_{turbine}}{\sum_{n=1}^{N}(1-n\cdot d)\cdot kWh} + \frac{LCOH \cdot M_{H_2}}{kWh} \tag{6.15}$$

$$= \frac{\sum_{n=1}^{N} 4\ €/MWh \cdot 21583\ MWh}{\sum_{n=1}^{N}(1-n\cdot d)\cdot 21583011\ kWh} + \frac{1.93\ €/kg \cdot 2431200\ kg}{21583011\ kWh} = 0.219\ €/kWh$$

System of 87.5 MW

In this case all the capacity of the wind farm of 84 MW is employed to power an 87.5 MW electrolyser system. The other components are a compressor of 2250 kW and an hydrogen tank of 900 tons.
The production is 3672.6 ton while the demand is 3780.3 ton, to simplify the economic analysis the turbine is assumed to run as recorded by the national single electricity market operator Sem-o [11].
Choosing to employ an interest rate of 8.75 %, an inflation rate of 6.55 % and a degradation rate of 0 %, the results are as follows (1 $ is 0.92 €):

$$LCOH = \frac{CAPEX_{wind} + CAPEX_{PEM} + \sum_{n=1}^{N} OPEX_{wind} + OPEX_{PEM} + REPEX_{PEM}}{\sum_{n=1}^{N}(1-n\cdot d)\cdot M_{H_2}} \tag{6.16}$$

$$= \frac{104.33\ M€ + 107.63\ M€ + 52.74\ M€ + 26.16\ M€ + 13.52\ M€}{20 \cdot 3672.6\ ton} = 3.99\ €/kg$$

$$LCOCH = LCOH + \frac{CAPEX_{tank} + CAPEX_{comp} + \sum_{n=1}^{N} OPEX_{tank} + OPEX_{comp}}{\sum_{n=1}^{N}(1-n\cdot d)\cdot M_{H_2}} = \tag{6.17}$$

$$= 4.16\ €/kg\ + \frac{414\ M€ + 3.73\ M€ + 161.46\ M€ + 1.8\ M€}{20 \cdot 3672.6\ ton} = 11.61\ €/kg$$

Taking into account only the main scenario with i = 8.75 %, f = 6.55%, d = 0% and considering only the configuration with two 52 MW turbines, (21583 MWh in a year with 1902 ton of hydrogen per year plus 21305 MWh in a year with 1878 ton of hydrogen per year) it is possible to calculate the LCOE, even though there are 8 missing tons, with the hydrogen necessary to fire the turbine:

$$LCOE(C) = \frac{\sum_{n=1}^{N} OPEX_{turbine}}{\sum_{n=1}^{N}(1-n\cdot d)\cdot kWh} + \frac{LCOCH \cdot M_{H_2}}{kWh} \tag{6.18}$$

$$= \frac{\sum_{n=1}^{N} 4\ €/MWh \cdot (21583 + 21305)\ MWh}{\sum_{n=1}^{N}(1-n\cdot d)\cdot (21583011 + 21305357)\ kWh} + \frac{12.07\ €/kg \cdot 3672600\ kg}{(21583011 + 21305357)\ kWh} = 1.04\ €/kWh$$

This quantity is very high due to the high volume of storage required; if there would not be any compression and storage with a direct consumption of the hydrogen the price would be:

$$LCOE = \frac{\sum_{n=1}^{N} OPEX_{turbine}}{\sum_{n=1}^{N}(1-n\cdot d)\cdot kWh} + \frac{LCOH \cdot M_{H_2}}{kWh} \tag{6.19}$$

$$= \frac{\sum_{n=1}^{N} 4\ €/MWh \cdot (21583 + 21305)\ MWh}{\sum_{n=1}^{N}(1-n\cdot d)\cdot (21583011 + 21305357)\ kWh} + \frac{4.16\ €/kg \cdot 3672600\ kg}{(21583011 + 21305357)\ kWh} = 0.358\ €/kWh$$

PEM summary

The prices above are arbitrary values depending on the parameters necessary to quantify the future value of the money so they are subjected to changes for different people with different standards. Now it is possible to see how the multiple prices of every configuration could vary considering different interest rate (i), inflation rate (f) and degradation rate (d):

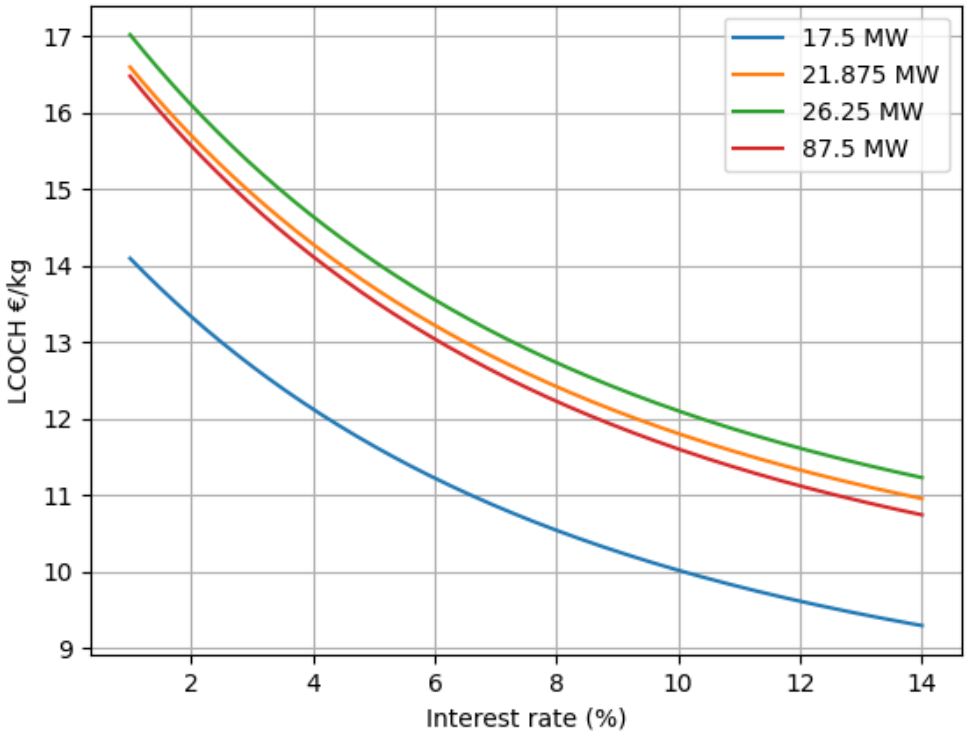

Figure 6.1: Trend of LCOCH varying the interest rate, with inflation rate = 6.55% and degradation rate = 0%

To clarify, the choice of displaying the LCOCH and the range of values for the different parameters on the axis is to make a comparison with configuration 3 and 4 from the article of M.Nasser [16] in which he reports the cost for PEM-Wind and SOC-Wind systems, see more on appendix for further comparison between figures {7}.

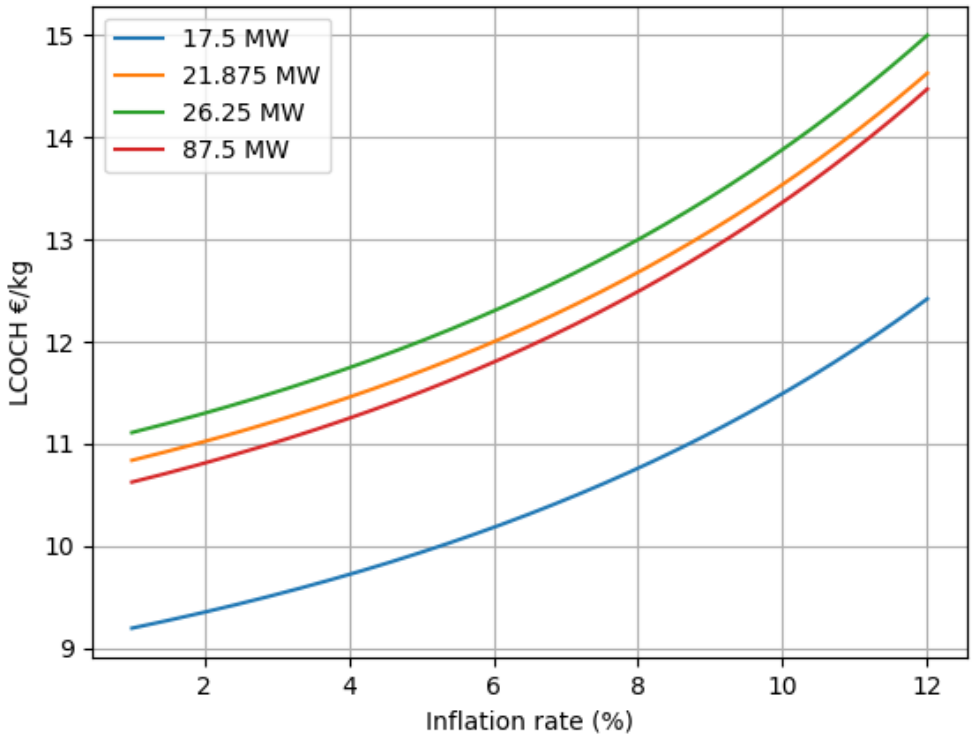

Figure 6.2: Trend of LCOCH varying the inflation rate, with interest rate = 8.75% and degradation rate = 0%

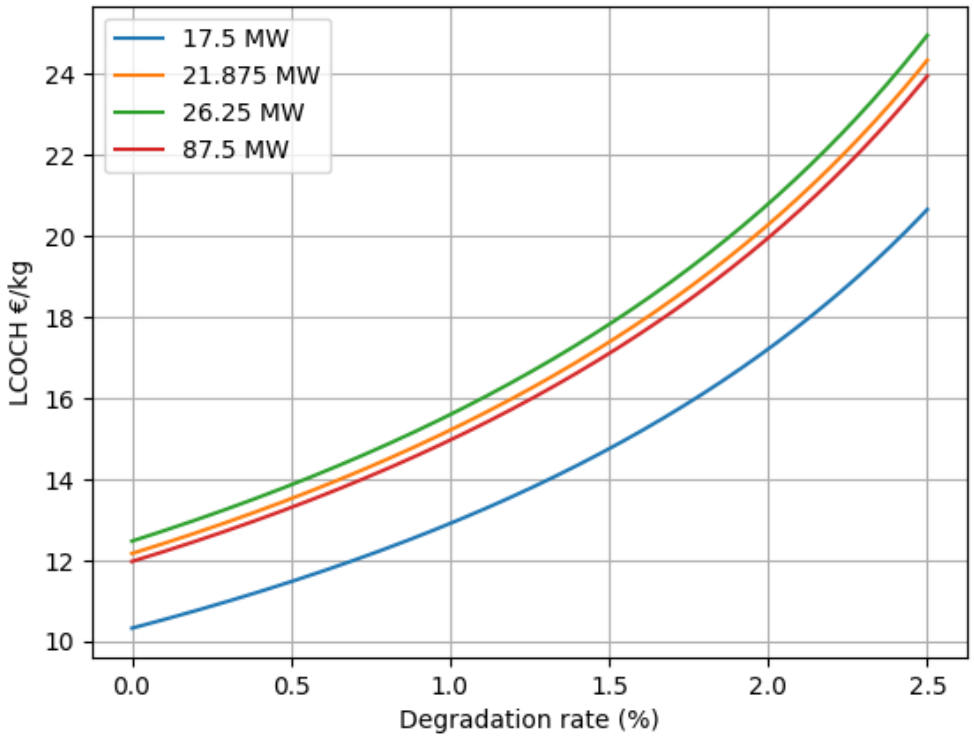

Figure 6.3: Trend of LCOCH varying the degradation rate, with interest rate = 8.75% and inflation rate = 6.55%

The results are around 17.1 $/kg equal to 15.7 €/kg for the PEM and 11.6 $/kg equal to 10.7 €/kg for the SOC. The numbers for our system are very similar but the efficiencies used in the article are a bit different (84% vs 91% for SOC and 60% vs 66% for PEM) so those affect the results.

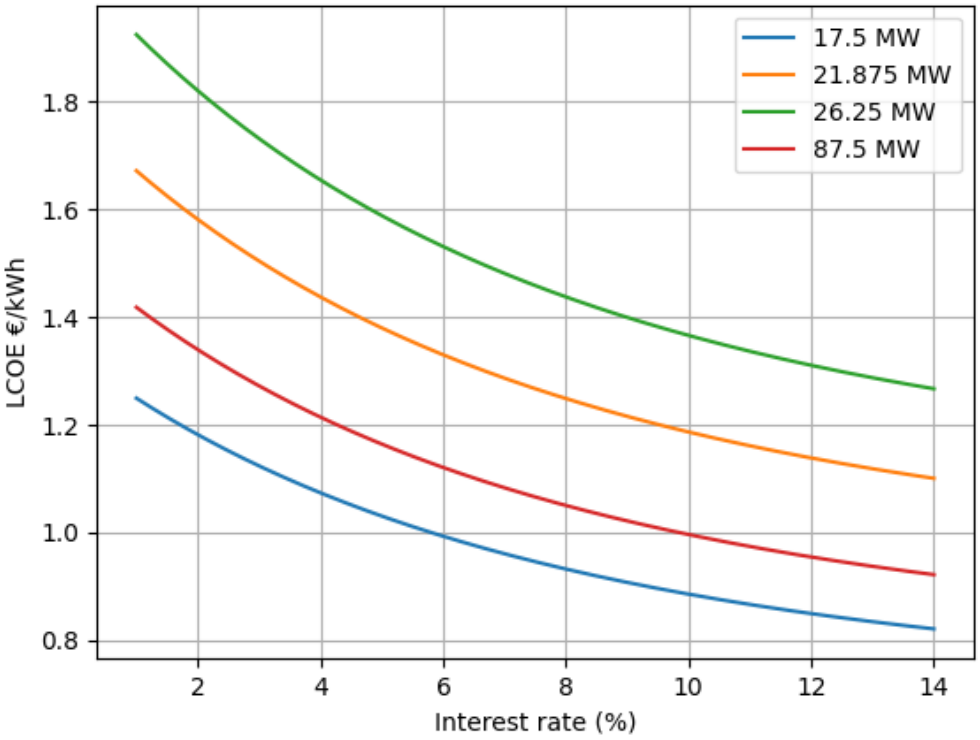

Figure 6.4: Trend of LCOE(C) varying the interest rate, with inflation rate = 6.55% and degradation rate = 0%

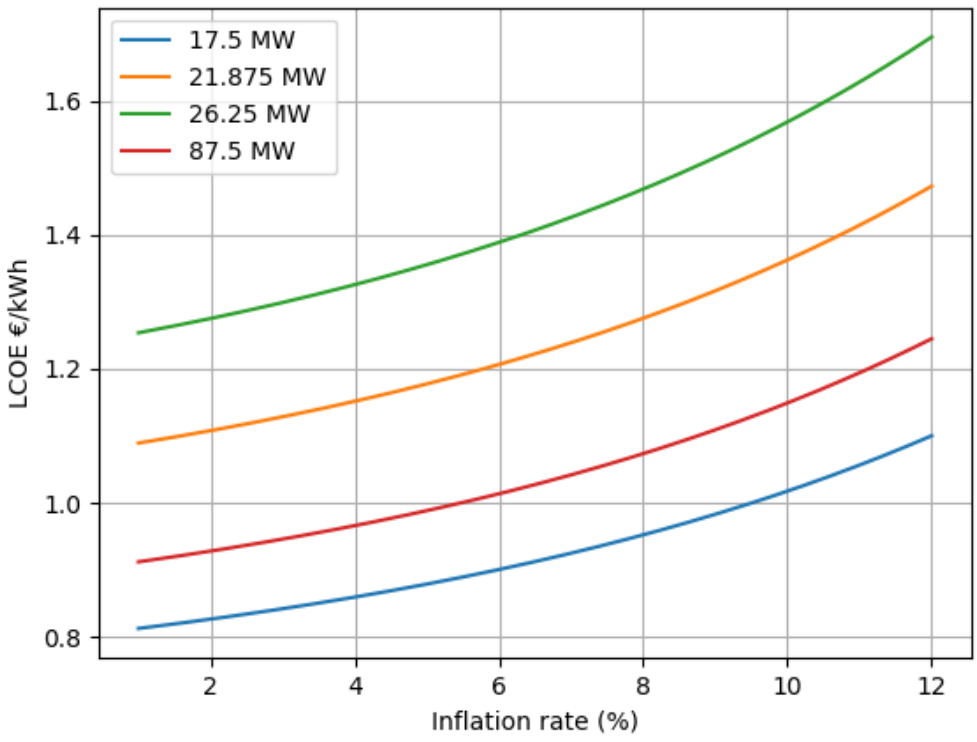

Figure 6.5: Trend of LCOE(C) varying the inflation rate, with interest rate = 8.75% and degradation rate = 0%

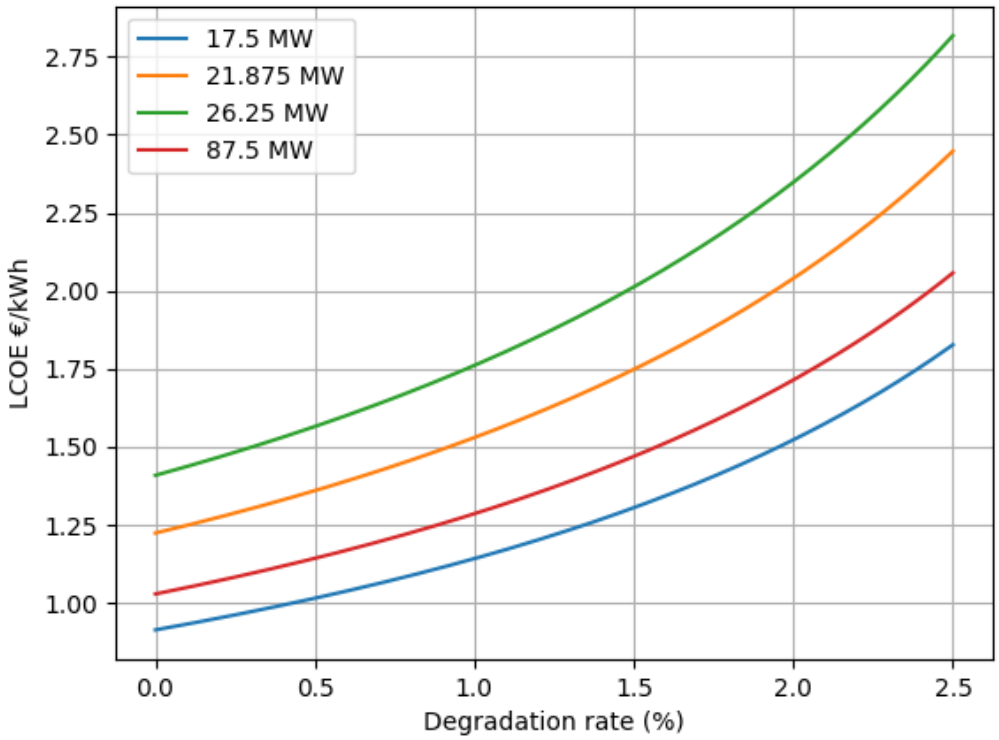

Figure 6.6: Trend of LCOE(C) varying the degradation rate, with interest rate = 8.75% and inflation rate = 6.55%

As the interest rate varies, the sum to invest in order to get a specific amount of money in the future varies; if the interest rate is low the money to invest in order to get a specific amount increases, instead if the interest rate is high less money is needed today to reach some future amount. On the other hand if inflation increases the value of money decreases so more is needed to achieve a future goal, degradation is a simple concept as the higher it is the more money is needed to replace something.

Table 6.2 presents the summary of all prices with the nominal rates together:

Rated Power	Unit	LCOH	LCOCH	Unit	LCOE	LCOE(C)	Unit
17.500	MW	1.68	10.33	€/kg	0.151	0.91	€/kWh
21.875	MW	1.80	12.17	€/kg	0.183	1.22	€/kWh
26.250	MW	1.92	12.48	€/kg	0.219	1.41	€/kWh
87.500	MW	4.06	12.00	€/kg	0.351	1.03	€/kWh

Table 6.2: Levelized cost of hydrogen, compressed hydrogen and electricity from not compressed, compressed hydrogen for PEM scenarios: interest rate (i) = 8.75%, inflation rate (f) = 6.55%, degradation rate (d) = 0%

The LCOCH and the LCOE(C) decrease as the interest rate increase while they increase for the other two cases. It is possible to conclude that the bigger the system size for a one turbine configuration, the higher the cost as the initial investment is the most expensive factor, in particular the hydrogen storage tank. For powering both turbines instead the LCOH is doubled due to the increase of capacity for electrolyser and wind farm while the LCOCH is very similar to the previous ones, even lower than the 2^{nd} and 3^{rd} configurations, as the tank capacity needed does not increase too much. The electricity cost trend follows the LCOCH price but looking at the expense for each kWh it is clear that no solution can be practised unless subsidies are employed to finance it as a zero emission technology.

6.1.2 SOC scenario

The LCOH/LCOCH in 20 years is calculated for the four scenarios with the simplification that the turbine works the recorded hours even if there is no hydrogen available at that moment. For example in some scenarios the overall amount may be lower so the total working MWh of the turbine will be weighted on the production; instead even if the overall production is higher than the requirement there could be a lack of fuel during different times of the year, in those cases it will be just mentioned.

SOC system of 10.72 MW rated power

To simplify the economic analysis the wind farm is considered to have the same rated power as the electrolyser (10.72 MW). The other components are a compressor of 265 kW and an hydrogen tank of 500 tons. The hydrogen produced is 1771.4 ton while the requirement is 1902 ton so there is a lack of fuel, for simplicity it is assumed the turbine continues to work for the assigned hours but the kWh for the calculation of the LCOE will be multiplied by the ratio 1771.4/1902. Choosing to employ an interest rate of 8.75 %, an inflation rate of 6.55 % and a degradation rate of 0 % the results are as follows (1 $ is 0.92 €):

$$LCOH = \frac{CAPEX_{wind} + CAPEX_{SOC} + \sum_{n=1}^{N} OPEX_{wind} + OPEX_{SOC} + REPEX_{SOC}}{\sum_{n=1}^{N}(1 - n \cdot d) \cdot M_{H_2}} \tag{6.20}$$

$$= \frac{13.31\ M€ + 21.44\ M€ + 6.73\ M€ + 3.21\ M€ + 1.84\ M€}{20 \cdot 1771.4\ ton} = 1.31\ €/kg$$

$$LCOCH = LCOH + \frac{CAPEX_{tank} + CAPEX_{comp} + \sum_{n=1}^{N} OPEX_{tank} + OPEX_{comp}}{\sum_{n=1}^{N}(1 - n \cdot d) \cdot M_{H_2}} = \tag{6.21}$$

$$= 1.31\ €/kg\ + \frac{230\ M€ + 0.44\ M€ + 89.7\ M€ + 0.21\ M€}{20 \cdot 1771.4\ ton} = 10.36\ €/kg$$

Taking into account only the main scenario with i = 8.75 %, f = 6.55%, d = 0% and considering only the configuration with the 52 MW turbine that works more, (21583 MWh in a year) it is possible to calculate the LCOE assuming that the turbine works all the hours but decreasing the amount of MWh, multiplying for 1771.4/1902 = 0.931, due to the lack of H_2:

$$LCOE(C) = \frac{\sum_{n=1}^{N} OPEX_{turbine}}{\sum_{n=1}^{N}(1 - n \cdot d) \cdot kWh} + \frac{LCOCH \cdot M_{H_2}}{kWh} \tag{6.22}$$

$$= \frac{\sum_{n=1}^{N} 4\ €/MWh \cdot 21583 \cdot 0.931\ MWh}{\sum_{n=1}^{N}(1 - n \cdot d) \cdot 21583011 \cdot 0.931\ kWh} + \frac{10.36\ €/kg \cdot 1771400\ kg}{21583011 \cdot 0.931\ kWh} = 0.92\ €/kWh$$

This quantity is very high due to the high volume of storage required; if there would not be any compression and storage with a direct consumption of the hydrogen the price would be:

$$LCOE = \frac{\sum_{n=1}^{N} OPEX_{turbine}}{\sum_{n=1}^{N}(1 - n \cdot d) \cdot kWh} + \frac{LCOH \cdot M_{H_2}}{kWh} \tag{6.23}$$

$$= \frac{\sum_{n=1}^{N} 4\ €/MWh \cdot 21583 \cdot 0.931\ MWh}{\sum_{n=1}^{N}(1 - n \cdot d) \cdot 21583011 \cdot 0.931\ kWh} + \frac{1.31\ €/kg \cdot 1771400\ kg}{21583011 \cdot 0.931\ kWh} = 0.119\ €/kWh$$

SOC system of 13.4 MW rated power

To simplify the economic analysis the wind farm is considered to have the same rated power as the electrolyser (13.4 MW). The other components are a compressor of 335 kW and an hydrogen tank of 650 tons. The hydrogen produced is 2118.7 ton but only 1902 ton are necessary to power the system. Choosing to employ an interest rate of 8.75 %, an inflation rate of 6.55 % and a degradation rate of 0 % the results are as follows (1 $ is 0.92 €)

$$LCOH = \frac{CAPEX_{wind} + CAPEX_{SOC} + \sum_{n=1}^{N} OPEX_{wind} + OPEX_{SOC} + REPEX_{SOC}}{\sum_{n=1}^{N}(1 - n \cdot d) \cdot M_{H_2}} \tag{6.24}$$

$$= \frac{16.64\ M€ + 26.8\ M€ + 8.41\ M€ + 4\ M€ + 2.29\ M€}{20 \cdot 2118.7\ ton} = 1.37\ €/kg$$

$$LCOCH = LCOH + \frac{CAPEX_{tank} + CAPEX_{comp} + \sum_{n=1}^{N} OPEX_{tank} + OPEX_{comp}}{\sum_{n=1}^{N}(1 - n \cdot d) \cdot M_{H_2}} = \tag{6.25}$$

$$= 1.37\ €/kg\ + \frac{299\ M€ + 0.55\ M€ + 116.61\ M€ + 0.27\ M€}{20 \cdot 2118.7\ ton} = 11.2\ €/kg$$

Taking into account only the main scenario with i = 8.75 %, f = 6.55%, d = 0% and considering only the configuration with the 52 MW turbine that works more, (21583 MWh in a year) it is possible to calculate the LCOE assuming that the turbine works all the hours even if there is a lack of on-site generated and stored H_2:

$$LCOE(C) = \frac{\sum_{n=1}^{N} OPEX_{turbine}}{\sum_{n=1}^{N}(1 - n \cdot d) \cdot kWh} + \frac{LCOCH \cdot M_{H_2}}{kWh} \tag{6.26}$$

$$= \frac{\sum_{n=1}^{N} 4\ €/MWh \cdot 21583\ MWh}{\sum_{n=1}^{N}(1 - n \cdot d) \cdot 21583011\ kWh} + \frac{11.2\ €/kg \cdot 2118700\ kg}{21583011\ kWh} = 1.10\ €/kWh$$

This quantity is very high due to the high volume of storage required; if there would not be any compression and storage with a direct consumption of the hydrogen the price would be:

$$LCOE = \frac{\sum_{n=1}^{N} OPEX_{turbine}}{\sum_{n=1}^{N}(1 - n \cdot d) \cdot kWh} + \frac{LCOH \cdot M_{H_2}}{kWh} \tag{6.27}$$

$$= \frac{\sum_{n=1}^{N} 4\ €/MWh \cdot 21583\ MWh}{\sum_{n=1}^{N}(1 - n \cdot d) \cdot 21583011\ kWh} + \frac{1.37\ €/kg \cdot 2118700\ kg}{21583011\ kWh} = 0.138\ €/kWh$$

SOC system of 16.08 MW rated power

To simplify the economic analysis the wind farm is considered to have the same rated power as the electrolyser (16.08 MW). The other components are a compressor of 400 kW and an hydrogen tank of 850 tons. The hydrogen produced is 2434.6 ton but only 1902 ton are necessary to power the system. Choosing to employ an interest rate of 8.75 %, an inflation rate of 6.55 % and a degradation rate of 0 % the results are as follows (1 $ is 0.92 €):

$$LCOH = \frac{CAPEX_{wind} + CAPEX_{SOC} + \sum_{n=1}^{N} OPEX_{wind} + OPEX_{SOC} + REPEX_{SOC}}{\sum_{n=1}^{N}(1 - n \cdot d) \cdot M_{H_2}} \quad (6.28)$$

$$= \frac{19.97\ M€ + 32.16\ M€ + 10.10\ M€ + 4.8\ M€ + 2.75\ M€}{20 \cdot 2434.6\ ton} = 1.43\ €/kg$$

$$LCOCH = LCOH + \frac{CAPEX_{tank} + CAPEX_{comp} + \sum_{n=1}^{N} OPEX_{tank} + OPEX_{comp}}{\sum_{n=1}^{N}(1 - n \cdot d) \cdot M_{H_2}} = \quad (6.29)$$

$$= 1.43\ €/kg\ + \frac{391\ M€ + 0.66\ M€ + 152.49\ M€ + 0.32\ M€}{20 \cdot 2434.6\ ton} = 12.62\ €/kg$$

Taking into account only the main scenario with i = 8.75 %, f = 6.55%, d = 0% and considering only the configuration with the 52 MW turbine that works more, (21583 MWh in a year) it is possible to calculate the LCOE:

$$LCOE(C) = \frac{\sum_{n=1}^{N} OPEX_{turbine}}{\sum_{n=1}^{N}(1 - n \cdot d) \cdot kWh} + \frac{LCOCH \cdot M_{H_2}}{kWh} \quad (6.30)$$

$$= \frac{\sum_{n=1}^{N} 4\ €/MWh \cdot 21583\ MWh}{\sum_{n=1}^{N}(1 - n \cdot d) \cdot 21583011\ kWh} + \frac{12.62\ €/kg \cdot 2118700\ kg}{21583011\ kWh} = 1.43\ €/kWh$$

This quantity is very high due to the high volume of storage required; if there would not be any compression and storage with a direct consumption of the hydrogen the price would be:

$$LCOE = \frac{\sum_{n=1}^{N} OPEX_{turbine}}{\sum_{n=1}^{N}(1 - n \cdot d) \cdot kWh} + \frac{LCOH \cdot M_{H_2}}{kWh} \quad (6.31)$$

$$= \frac{\sum_{n=1}^{N} 4\ €/MWh \cdot 21583\ MWh}{\sum_{n=1}^{N}(1 - n \cdot d) \cdot 21583011\ kWh} + \frac{1.43\ €/kg \cdot 2118700\ kg}{21583011\ kWh} = 0.165\ €/kWh$$

System of 32.16 MW

To simplify the economic analysis the wind farm is considered to have the same rated power as the electrolyser (32.16 MW). The other components are a compressor of 800 kW and an hydrogen tank of 950 tons. The hydrogen produced is 3811.78 ton while the requirement is 3780.3 ton so there is enough fuel (without considering the dynamic aspect). Choosing to employ an interest rate of 8.75 %, an inflation rate of 6.55 % and a degradation rate of 0 % the results are as follows (1 $ is 0.92 €):

$$LCOH = \frac{CAPEX_{wind} + CAPEX_{SOC} + \sum_{n=1}^{N} OPEX_{wind} + OPEX_{SOC} + REPEX_{SOC}}{\sum_{n=1}^{N}(1 - n \cdot d) \cdot M_{H_2}} \quad (6.32)$$

$$= \frac{39.94\ M€ + 64.32\ M€ + 20.19\ M€ + 9.62\ M€ + 5.5\ M€}{20 \cdot 3811.78\ ton} = 1.83\ €/kg$$

$$LCOCH = LCOH + \frac{CAPEX_{tank} + CAPEX_{comp} + \sum_{n=1}^{N} OPEX_{tank} + OPEX_{comp}}{\sum_{n=1}^{N}(1 - n \cdot d) \cdot M_{H_2}} = \tag{6.33}$$

$$= 1.83\ €/kg\ + \frac{437\ M€ + 1.32\ M€ + 170.43\ M€ + 0.65\ M€}{20 \cdot 3811.78\ ton} = 9.82\ €/kg$$

Taking into account only the main scenario with i = 8.75 %, f = 6.55%, d = 0% and considering only the configuration with the 52 MW turbine that works more, (21583 MWh in a year) it is possible to calculate the LCOE assuming that the turbine works all the hours even if there is lack of H_2:

$$LCOE(C) = \frac{\sum_{n=1}^{N} OPEX_{turbine}}{\sum_{n=1}^{N}(1 - n \cdot d) \cdot kWh} + \frac{LCOCH \cdot M_{H_2}}{kWh} \tag{6.34}$$

$$= \frac{\sum_{n=1}^{N} 4\ €/MWh \cdot (21583 + 21305)\ MWh}{\sum_{n=1}^{N}(1 - n \cdot d) \cdot (21583011 + 21305357)\ kWh} + \frac{9.82\ €/kg \cdot 2118700\ kg}{(21583011 + 21305357)\ kWh} = 0.88\ €/kWh$$

This quantity is very high due to the high volume of storage required; if there would not be any compression and storage with a direct consumption of the hydrogen the price would be:

$$LCOE = \frac{\sum_{n=1}^{N} OPEX_{turbine}}{\sum_{n=1}^{N}(1 - n \cdot d) \cdot kWh} + \frac{LCOH \cdot M_{H_2}}{kWh} \tag{6.35}$$

$$= \frac{\sum_{n=1}^{N} 4\ €/MWh \cdot (21583 + 21305)\ MWh}{\sum_{n=1}^{N}(1 - n \cdot d) \cdot (21583011 + 21305357)\ kWh} + \frac{1.83\ €/kg \cdot 2118700\ kg}{(21583011 + 21305357)\ kWh} = 0.166\ €/kWh$$

The resume of the results will be shown as in the PEM scenario.

SOC summary

The prices above are arbitrary values depending on the parameters necessary to quantify the future value of the money so they are subjected to changes for different people with different standards.
To clarify, the choice of displaying the LCOCH and the range of values for the different parameters on the axis is to make a comparison with configuration 3 and 4 from the article of M.Nasser [16] in which he reports the cost for PEM-Wind and SOC-Wind systems, see more on appendix for further comparison between figures {7}.
Now it is possible to see how the multiple prices of every configuration could vary considering different interest rate (i), inflation rate (f) and degradation rate (d):

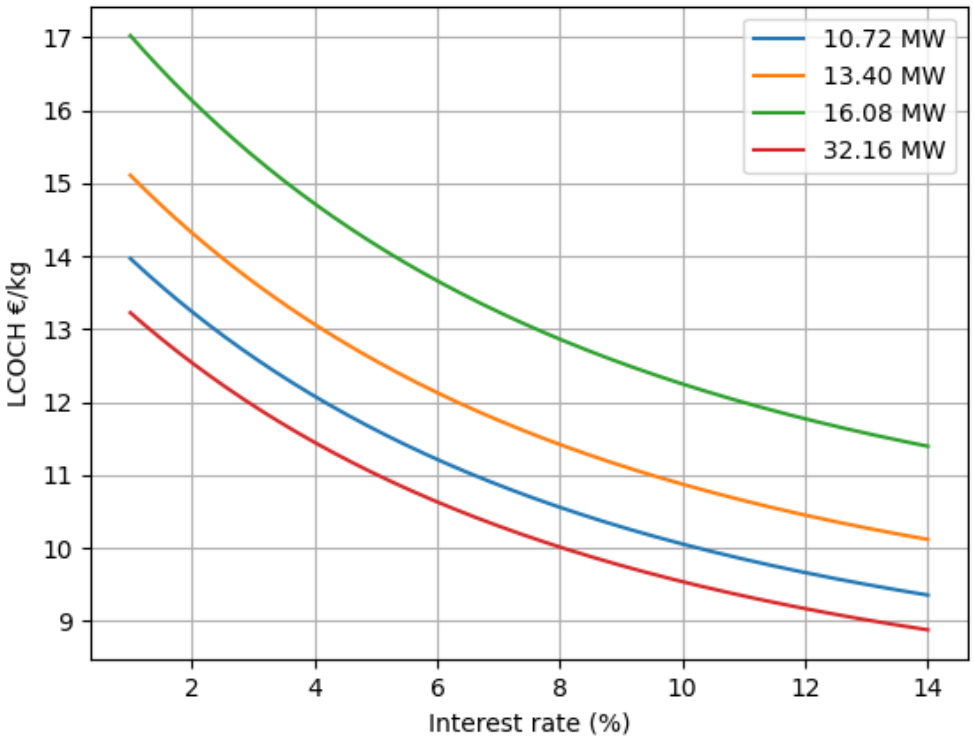

Figure 6.7: Trend of LCOCH varying the interest rate, with inflation rate = 6.55% and degradation rate = 0%

The results are around 17.1 $/kg equal to 15.7 €/kg for the PEM and 11.6 $/kg equal to 10.7 €/kg for the SOC. The numbers for our system are very similar but the efficiencies used in the article are a bit different (84% vs 91% for SOC and 60% vs 66% for PEM) so those affect the results.

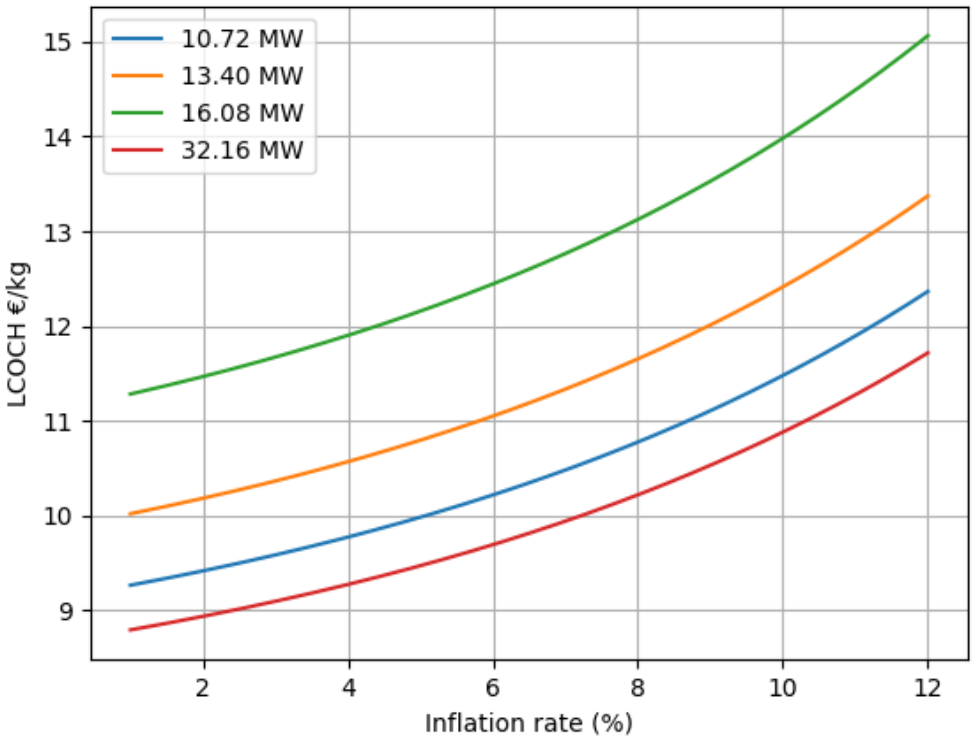

Figure 6.8: Trend of LCOCH varying the inflation rate, with interest rate = 8.75% and degradation rate = 0%

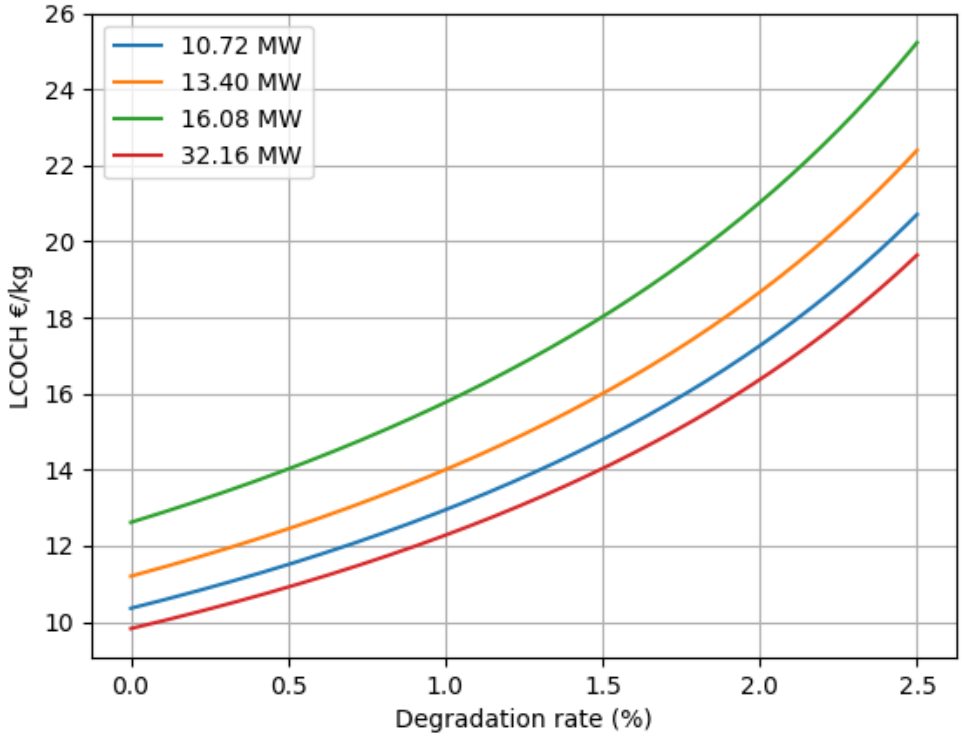

Figure 6.9: Trend of LCOCH varying the degradation rate, with interest rate = 8.75% and inflation rate = 6.55%

As the interest rate varies, the sum to invest in order to get a specific amount of money in the future varies. If the interest rate is low the money to invest increases, instead if the interest rate is high less money is needed today to reach some future amount. On the other hand if inflation increases the value of money decreases so more is needed to achieve a future goal, while degradation is a simple concept as the higher it is the more money is needed to replace something.

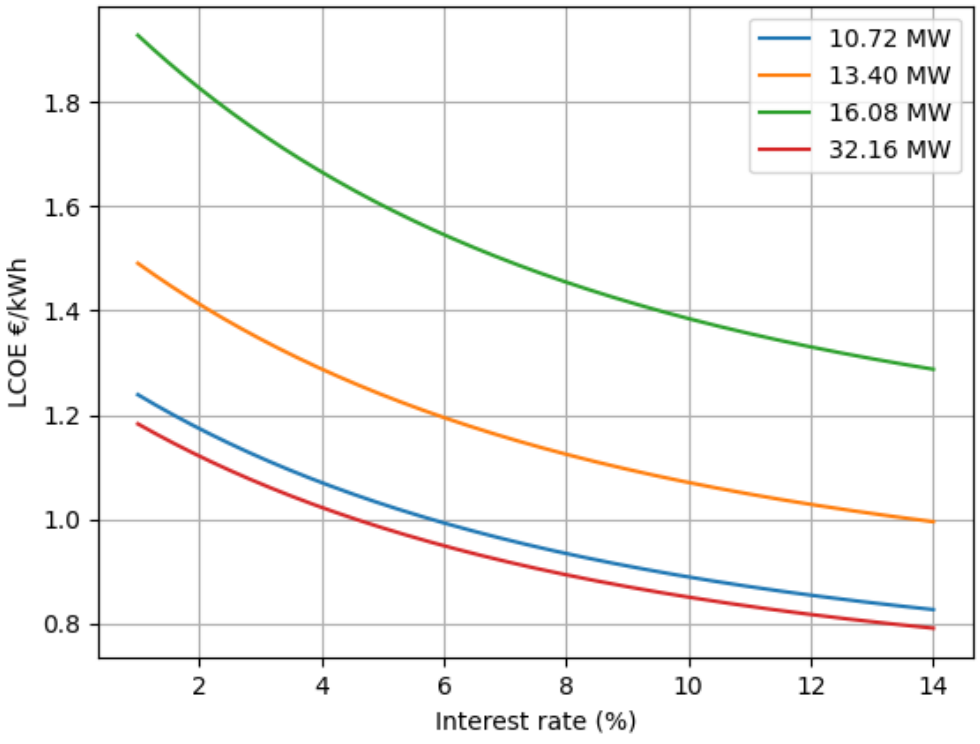

Figure 6.10: Trend of LCOE(C) varying the interest rate, with inflation rate = 6.55% and degradation rate = 0%

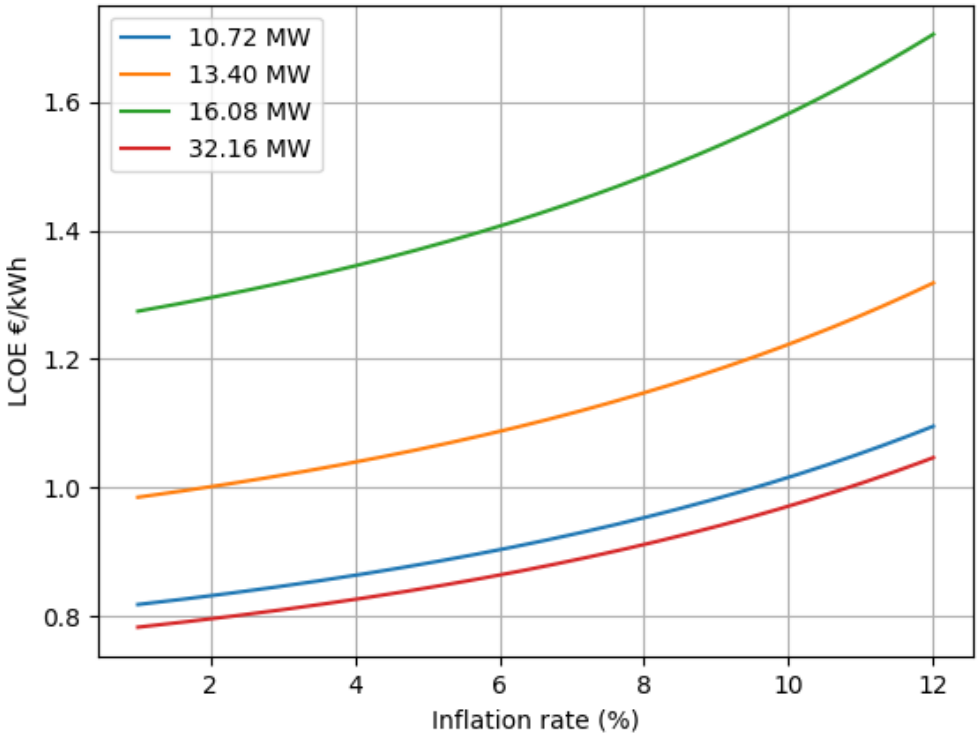

Figure 6.11: Trend of LCOE(C) varying the inflation rate, with interest rate = 8.75% and degradation rate = 0%

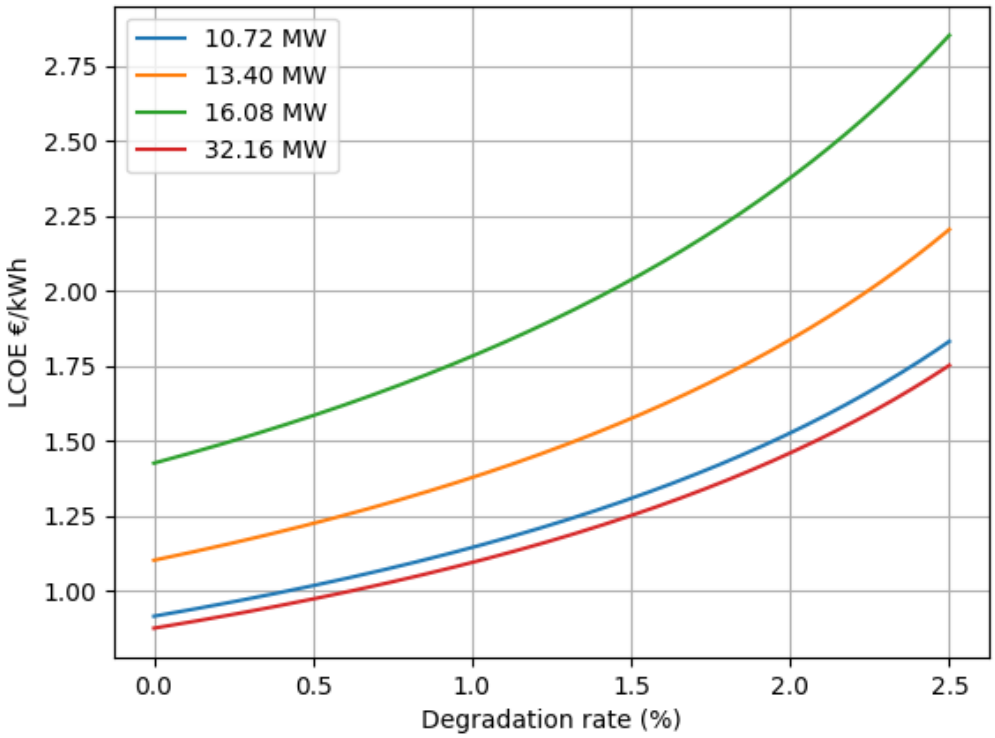

Figure 6.12: Trend of LCOE(C) varying the degradation rate, with interest rate = 8.75% and inflation rate = 6.55%

Table 6.3 presents the summary of all prices with the nominal rates together:

Rated Power	Unit	LCOH	LCOCH	Unit	LCOE	LCOE(C)	Unit
10.72	MW	1.31	10.36	€/kg	0.119	0.92	€/kWh
13.40	MW	1.37	11.20	€/kg	0.138	1.10	€/kWh
16.08	MW	1.43	12.62	€/kg	0.165	1.43	€/kWh
32.16	MW	1.83	9.82	€/kg	0.166	0.88	€/kWh

Table 6.3: Levelized cost of hydrogen, compressed hydrogen and electricity from not compressed, compressed hydrogen for SOC scenarios: interest rate (i) = 8.75%, inflation rate (f) = 6.55%, degradation rate (d) = 0%

The LCOCH and the LCOE decrease as the interest rate increase while they increase for the other two cases. It is possible to conclude that the bigger the system size for a one turbine configuration, the higher the cost as the initial investment is the most expensive factor, in particular of the hydrogen storage tank. However the price is lower and it does not increase, between scenarios, as much as in the PEM solution. For powering both turbines instead the LCOCH slightly increases due to the increase of capacity for electrolyser and wind farm, on the other hand the LCOCH is very similar to the previous ones, in some cases even less, as the tank capacity needed does not increase too much.
The electricity cost trend follows the LCOCH price but looking at the expense for each kWh it is clear that no solution can be practised unless subsidies are employed to finance it as a zero emission technology.

Chapter 7

Conclusion

From the results presented in this thesis, it is evident that the round trip efficiency is low for this type of application but this was already taken into account before the start of the work, the main focus of the study was to simulate the system performance in order to quantify the price for the electricity produced. The final result is deeply affected by the year/s chosen for the case study, indeed the best thing would be to consider a pool of data as abundant as possible to get a clear view on the system dynamics. However the available data covered only the last two years and for the year 2023 the peaker plants in Ireland operated a very low amount of hours, so the only option was to base the study on the data from 2022. The **price** was reported for **each kWh**, the values range from **0.8 €/kWh** to **1.8 €/kWh**. They are way above the peak value for the kWh cost registered in Ireland for both 2022 and 2023; as reported by the **SEAI** [64] in the energy price trends analysis for the last 10 years, the peak of the average value is **28.4 c€** in **2022**.

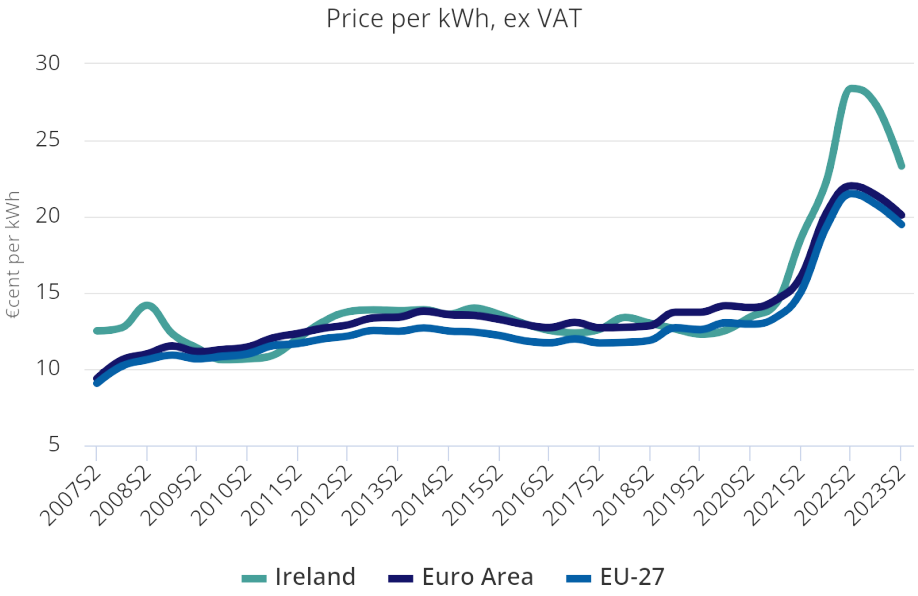

Figure 7.1: Average electricity price to business based on Eurostat data

This is mainly due to the compression and storage of the gas, in particular the tank size, that raised the final price by a factor of five to six. On the other hand if the system could ideally work **without the storage process** we would have a price that varies from **9 c€/kWh** to **18 c€/kWh** showing that with a smaller or null storage required this could really be a feasible solution.

According to the results it is not convenient to run a stand alone P2P system based on a wind farm, an electrolyser and a gas turbine. On the contrary the direct selling of **hydrogen** after the production seems profitable as it is obtained with a price of **1-2 €/kg** for most cases. As matter of fact there is an **ongoing hydrogen project**, called **SH2AMROCK** [65], that includes the Mountlucas wind farm; this project will develop Ireland's first hydrogen valley and a multi-modal hydrogen transport hub in Galway thanks to the production of the Mountlucas wind farm in Rhode.

A brief summary of results for the levelized costs and round trip efficiencies is reported:

1. The round trip efficiency for a PEM-turbine system is 22.5 %, operating under design condition
2. The round trip efficiency for a SOC-turbine system is 30.9 %, operating under design condition
3. The 21.9 MW PEM electrolyser coupled with a 52 MW turbine has:
   - a LCOH of 1.80 €/kg, a LCOCH of 12.17 €/kg
   - an electricity price of 18.3 c€/kWh and 1.22 €/kWh without and with compression-storage.
4. The 13.4 MW SOC electrolyser coupled with a 52 MW turbine has:
   - a LCOH of 1.37 €/kg, a LCOCH of 11.20 €/kg
   - an electricity price of 13.8 c€/kWh and 1.10 €/kWh without and with compression-storage.
5. The 87.5 MW PEM electrolyser coupled with two 52 MW turbine has:
   - a LCOH of 3.99 €/kg, a LCOCH of 11.61 €/kg
   - an electricity price of 35.8 c€/kWh and 1.04 €/kWh without and with compression-storage.
6. The 32.1 MW SOC electrolyser coupled with two 52 MW turbine has:
   - a LCOH of 1.83 €/kg, a LCOCH of 9.82 €/kg
   - an electricity price of 16.6 c€/kWh and 0.88 €/kWh without and with compression-storage.

The issue of the hydrogen storage should be the main focus of research in order to enable the development of a proper hydrogen economy. As a matter of fact solutions such as storage in salt cavern under the sea level are of increasing interest in the literature nowadays; however in this case only the compressed storage option is analysed as the system is not offshore and simplicity is prioritized. Another field to focus on is the gas turbine repurposing; up to now the most promising technology is the Micro-Mixing combustion that allows low NO_x emissions and a good combustion efficiency, however it is a complex technology that needs to be optimized for every fuel-air ratio. The turbine developed by the KAWASAKI Heavy Industries [36] can produce 1.1 MW_e from 2.8 MW_t with a 27% efficiency, which is still not at the level of a conventional gas turbine. Another important topic is the heat management of the SOC systems, the technology is very promising in terms of efficiency but high amount of heat and steam are required for the operation in endothermic condition that maximizes the efficiency. The direction to improve those weak points is for sure the coupling with waste heat sources that could make up the heat requirement and supply steam to the system.
The conclusion for this P2P system is that it is too expensive to make it work without subsidies but taking into account only the green hydrogen production it is possible to sell it at good enough price that makes the electrolyser application feasible.

Appendix

The appendix presents the link to the Github website in which all the code is made available for consultation, a further comparison on the LCOH from M.Nasser publication [16] and other plots.
The following link (`https://github.com/TBrondolin/Thermodynamic-and-economic-assessment-of-an-electrolyser---hydrogen-turbine-system`) leads to a depository in which the Python scripts developed for the thesis are made available divided by argument:

- Script of the PEM electrolyzer for the hydrogen production
- Script of the SOC electrolyzer for the hydrogen production
- Script of the Gas Turbine for electricity production with PEM coupling
- Script of the Gas Turbine for electricity production with SOC coupling
- Script of the Economic Assessment

Now it is possible to have a more detailed comparison with M.Nasser [16] case studies:

- Configuration 1, PV and PEM electrolyser
- Configuration 2, PV and SOC electrolyser
- Configuration 3, Wind farm and PEM electrolyser
- Configuration 4, Wind farm and SOC electrolyser
- Configuration 5, Rankine cycle based on waste heat recovery and PEM electrolyser
- Configuration 6, Rankine cycle based on waste heat recovery and SOC electrolyser
- Configuration 7, Electricity from the national grid and PEM electrolyser
- Configuration 8, Electricity from the national grid and SOC electrolyser

Comparison between variation of interest rates:

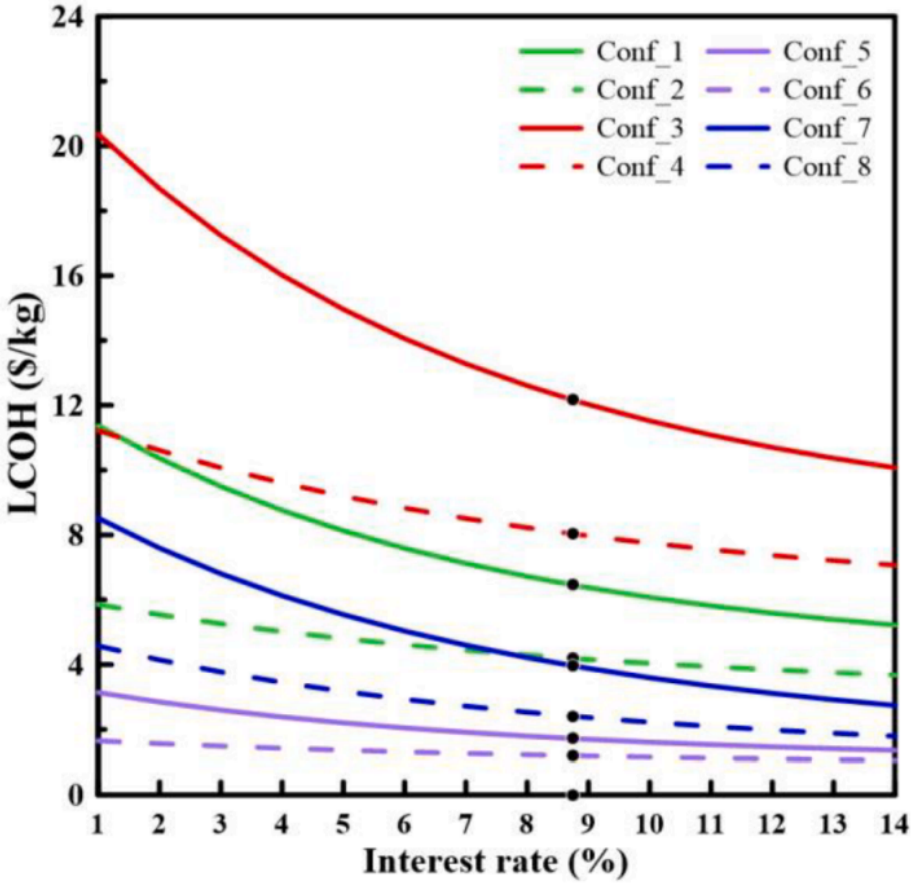

Figure 7.2: Trend of LCOCH for Nasser's work varying the interest rate, with inflation rate = 6.55% and degradation rate = 0%

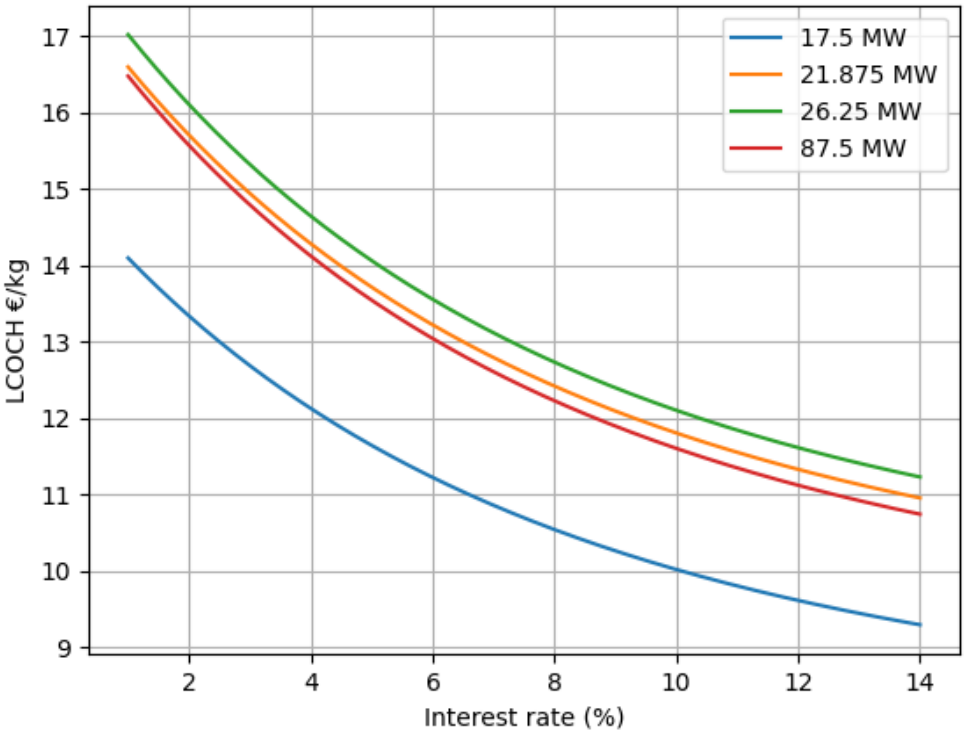

Figure 7.3: Trend of LCOCH varying the interest rate, with inflation rate = 6.55% and degradation rate = 0%

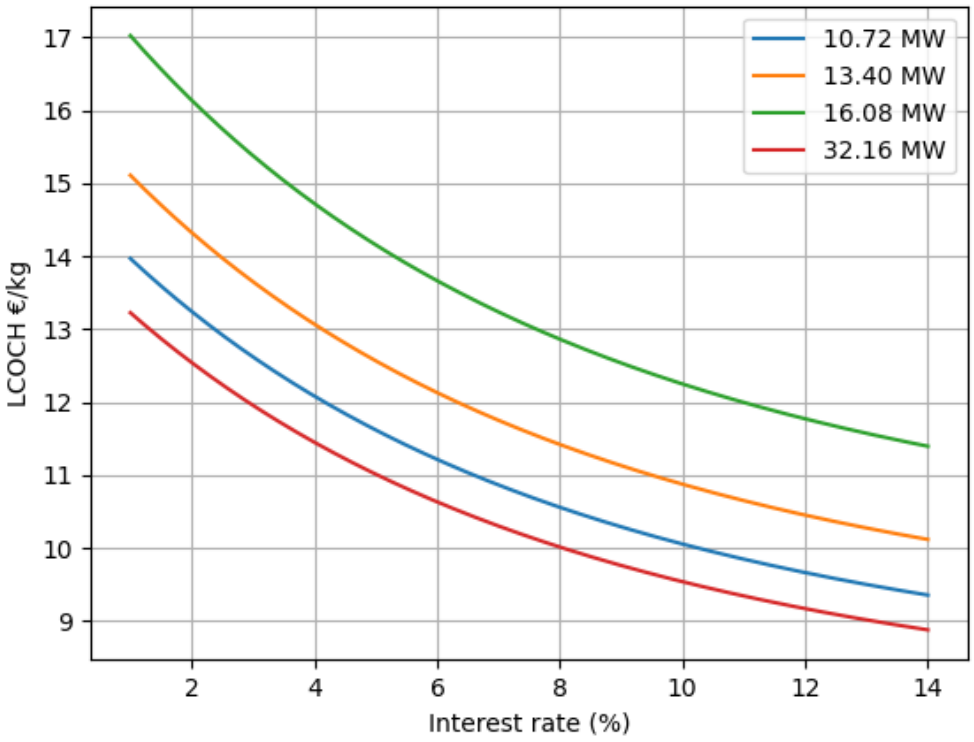

Figure 7.4: Trend of LCOCH varying the interest rate, with inflation rate = 6.55% and degradation rate = 0%

Comparison between variation of inflation rates:

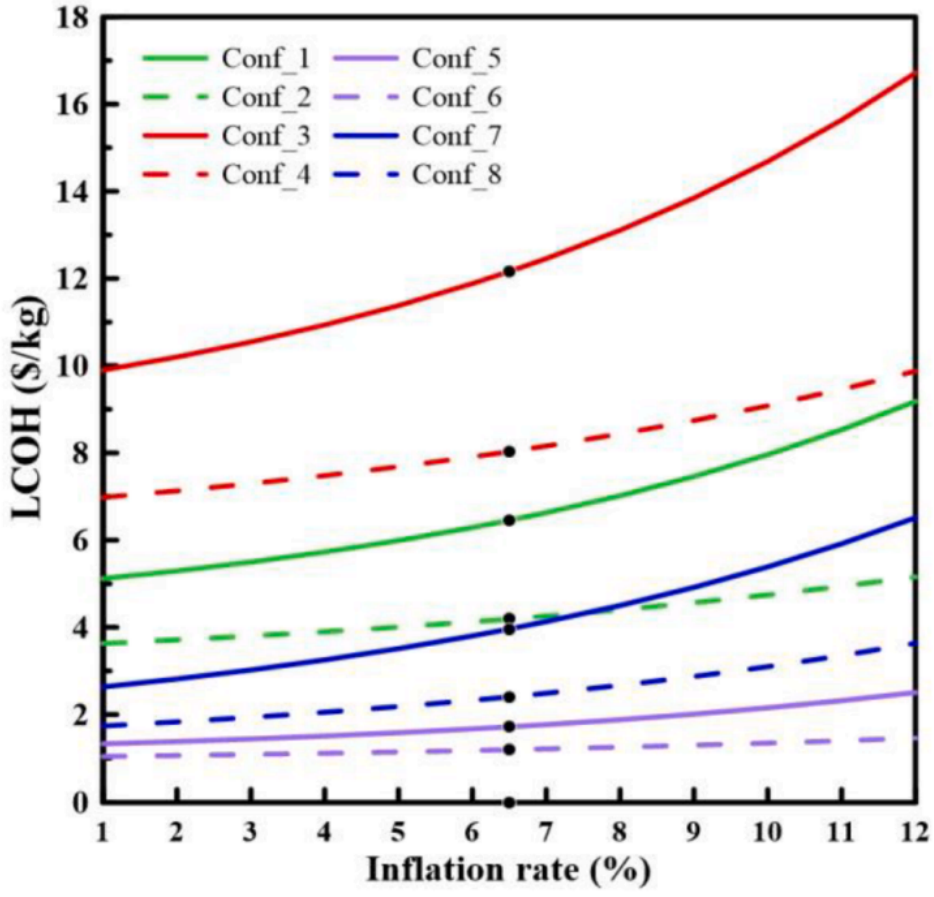

Figure 7.5: Trend of LCOCH for Nasser's work varying the inflation rate, with interest rate = 8.75% and degradation rate = 0%

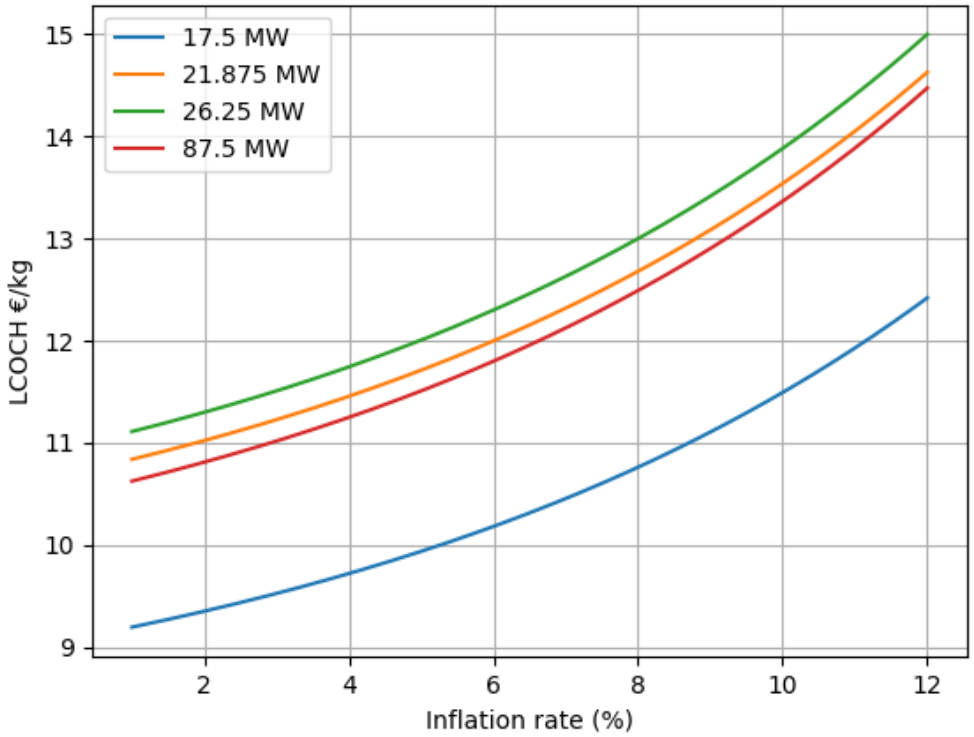

Figure 7.6: Trend of LCOCH varying the inflation rate, with interest rate = 8.75% and degradation rate = 0%

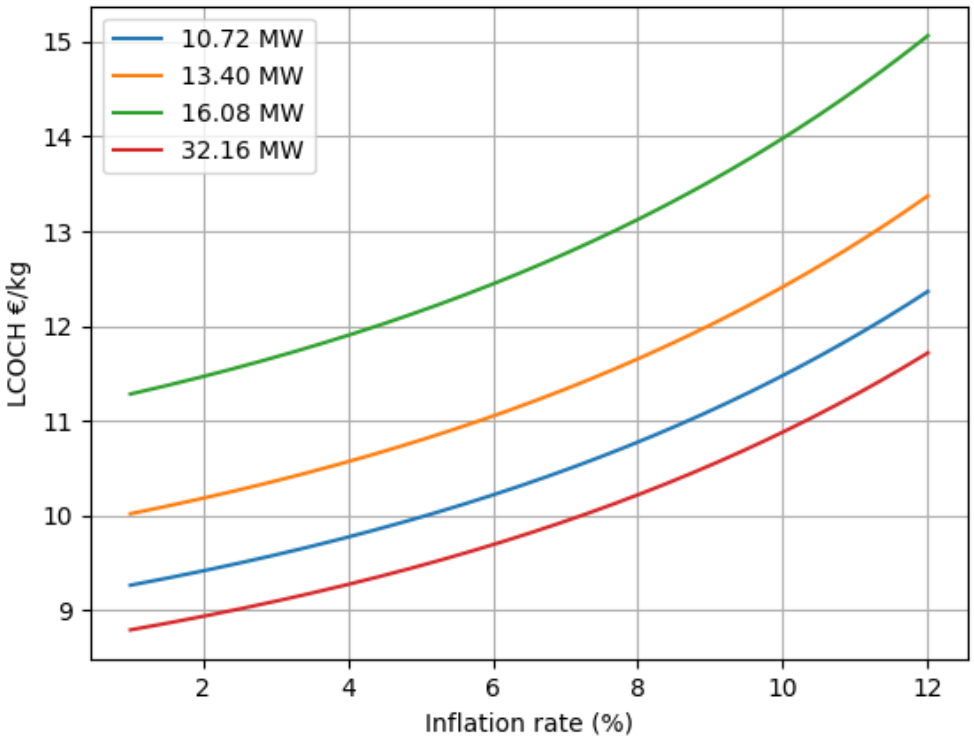

Figure 7.7: Trend of LCOCH varying the inflation rate, with interest rate = 8.75% and degradation rate = 0%

Comparison between variation of degradation rates:

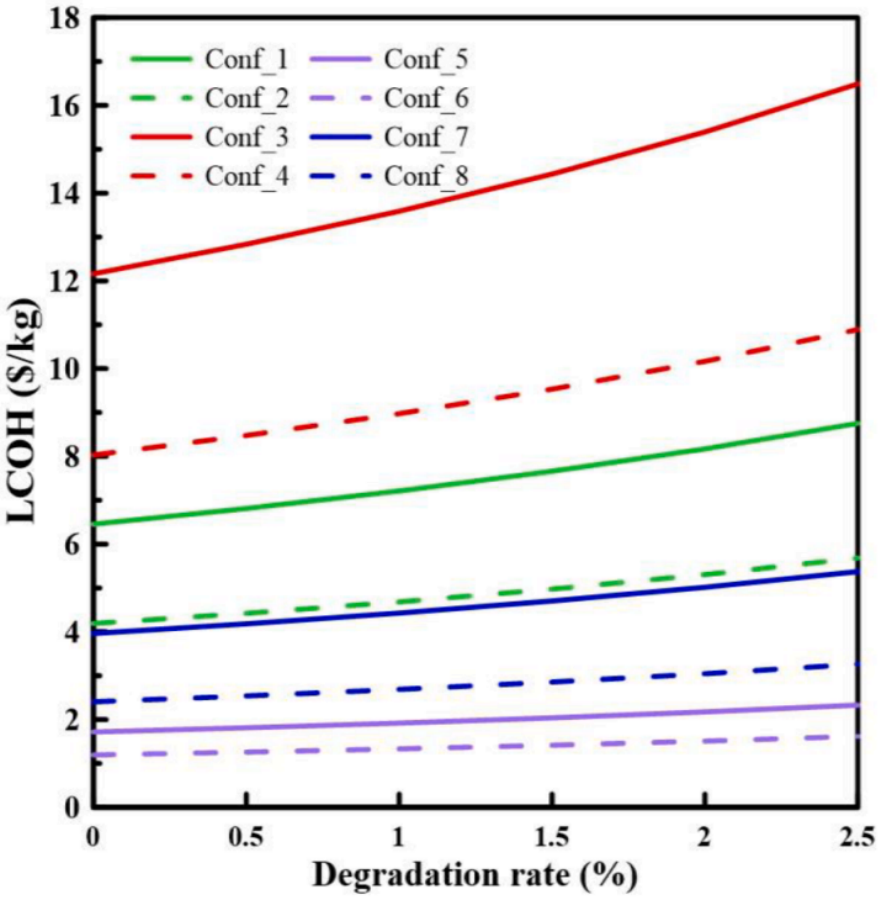

Figure 7.8: Trend of LCOCH for Nasser's work varying the degradation rate, with interest rate = 8.75% and inflation rate = 6.55%

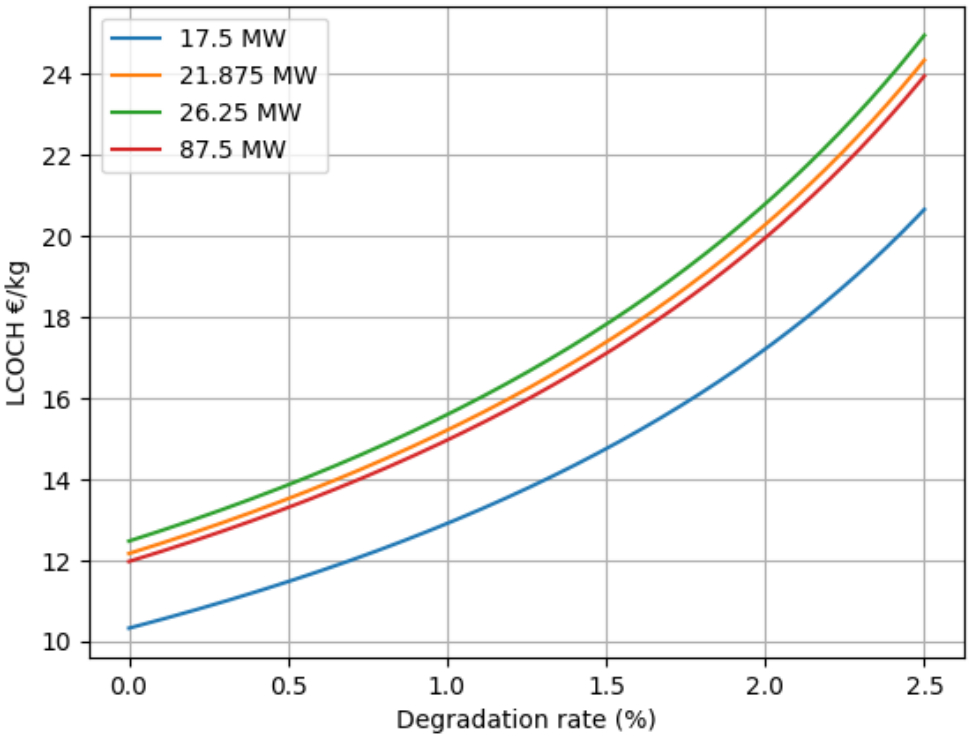

Figure 7.9: Trend of LCOCH varying the degradation rate, with interest rate = 8.75% and inflation rate = 6.55%

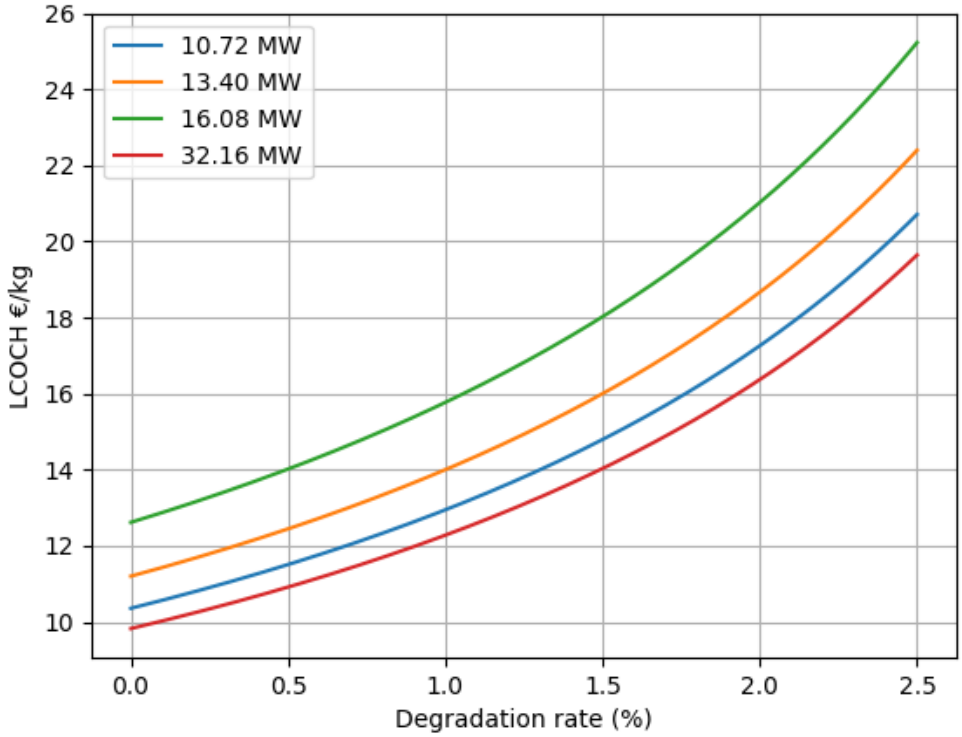

Figure 7.10: Trend of LCOCH varying the degradation rate, with interest rate = 8.75% and inflation rate = 6.55%

In the end it is possible to see the plots equivalent to Fig. 5.10, Fig. 5.11, Fig. 5.20 and Fig. 5.39 for unit 1:

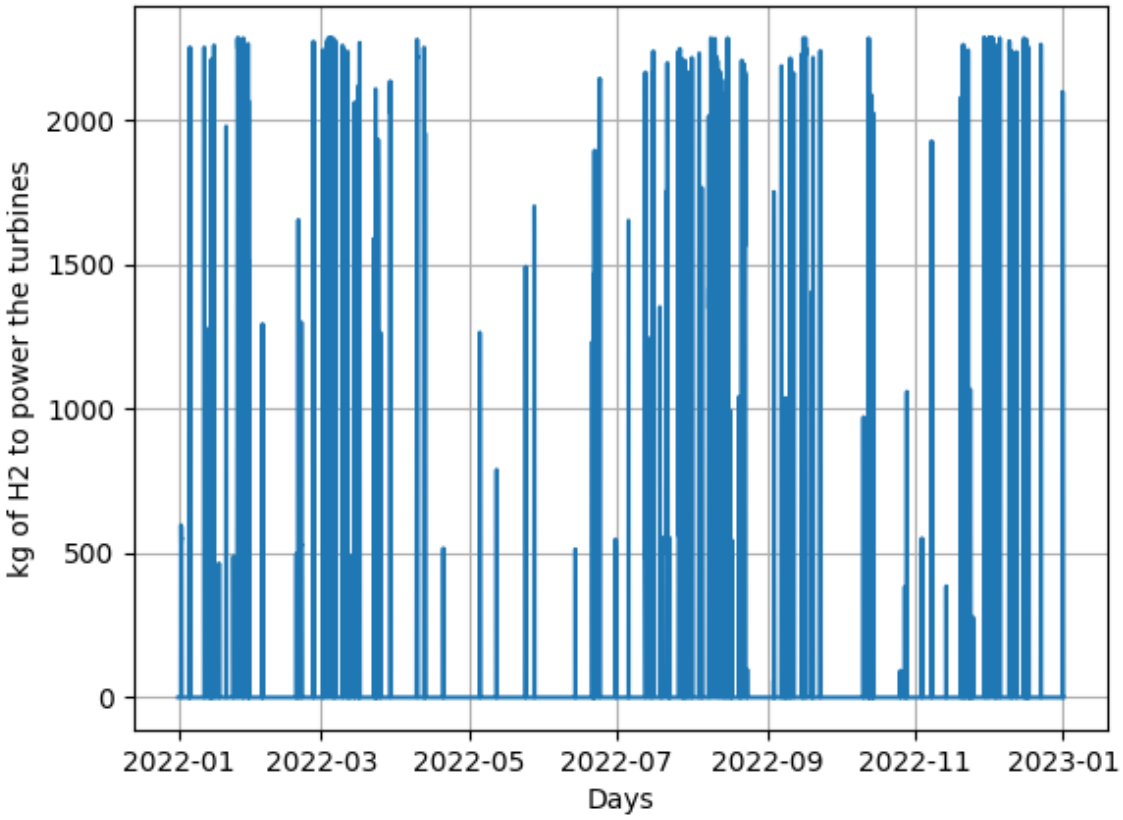

Figure 7.11: H_2 required for the repurposed turbine operation of unit 1, every 30 minutes

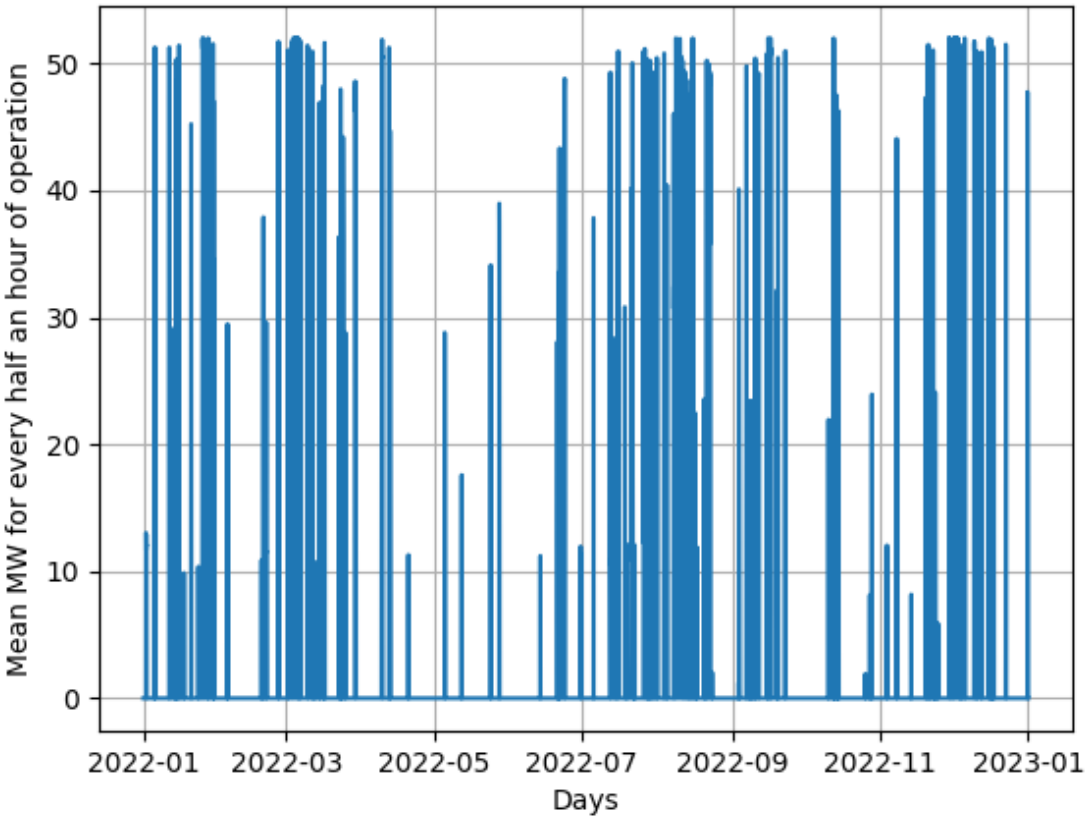

Figure 7.12: MW_e output of the repurposed turbine of unit 1, every 30 minutes

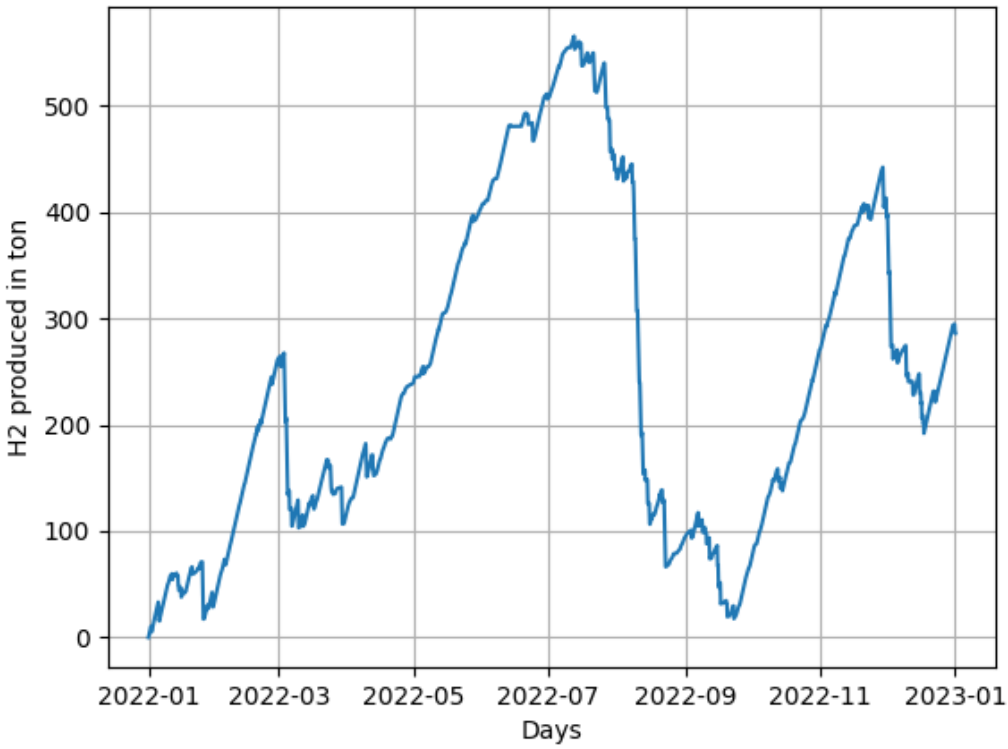

Figure 7.13: Cumulative difference of H_2 production and consumption for unit 1 with PEM power of 21.875 MW

Figure 7.14: Cumulative difference of H_2 production and consumption for unit 1 with SOC power of 13.4 MW

Acknowledgments

Completing this thesis has been a challenging yet incredibly rewarding journey, and I am deeply grateful to those who have supported me throughout.

First and foremost, I would like to thank my supervisors, Professor Paul Leahy and Professor Anna Stoppato, for their unwavering support, insightful guidance, and patience throughout this process. Their advice helped me refine my ideas and stay on course.

I would also like to extend my gratitude to the H-Wind team, who welcomed me and made me feel part of the group. In particular Quang Vu Dinh and Nithiya Streethran, for their constructive feedback and thoughtful suggestions during the development of this research.

I am especially grateful to my colleagues and friends, with whom I shared my university and high school studies. Their companionship made this journey easier and much more enjoyable.

I'd also like to thank the friends I made during my Erasmus experience, particularly the fellow Italians, the volleyball team and the people I bonded with during my Irish trips. I hope to see you again soon!

To my family, especially my parents Mirna and Andrea, I owe more than words can express. Thank you for your unconditional love, patience, and belief in me; your support has been my greatest strength throughout this academic journey.

Finally, to all those who have inspired and supported me along the way, whether named here or not, your contributions are deeply appreciated. This thesis would not have been possible without you.

Thank you all for helping me reach this point.

Tommaso

Bibliography

[1] Siemens gas turbine running 100% H2.
https://renewablesnow.com/news/siemens-energy-team-demonstrates-gas-turbine-running-on-100-hydrogen-836941/
https://www.engie.com/en/news/hyflexpower
https://www.siemens-energy.com/global/en/home/press-releases/hyflexpower-consortium-successfully-operates-a-gas-turbine-with-.html
https://resources.sw.siemens.com/en-US/case-study-b-b-agema.

[2] European Union. Horizon 2020 project.
https://wayback.archive-it.org/12090/20220124080607/https://ec.europa.eu/programmes/horizon2020/what-horizon-2020.

[3] European Union. European hydrogen bank.
https://ec.europa.eu/commission/presscorner/detail/en/IP_24_2333.

[4] Multiphly. 2.6 mw soc electrolyzer.
https://multiplhy-project.eu/Pages/News/RENEWABLE-HYDROGEN-PROJECT-%E2%80%9CMULTIPLHY%E2%80%9D-WORLD%E2%80%99S-LARGEST-HIGH-TEMPERATURE-ELECTROLYZER-FROM-SUNFIRE-SUCCESSFULLY-INSTALLED.aspx.

[5] Bloom energy. 4 mw bloom electrolyzer.
https://www.bloomenergy.com/bloomelectrolyzer/.

[6] PEM Shell. 10 mw project.
https://balkangreenenergynews.com/shell-launches-europes-biggest-pem-electrolyzer-for-green-hydrogen/.

[7] PEM Siemens. 8.75 mw project.
https://www.pv-magazine.com/2022/09/16/the-hydrogen-stream-siemens-commissions-8-7-mw-electrolyzer-in-germany/.

[8] Antonio Escamilla, David Sánchez, and Lourdes García-Rodríguez. Techno-economic study of power-to-power renewable energy storage based on the smart integration of battery, hydrogen, and micro gas turbine technologies. *Energy Conversion and Management: X*, 18:100368, 2023.

[9] Bord na Móna. Mountlucas wind farm.
https://www.mountlucaswindfarm.ie/the-wind-farm/.

[10] SSE Thermal. Rhode power station.
https://www.ssethermal.com/flexible-generation/operational/rhode/.

[11] Sem-o. Settlement data.
https://www.sem-o.com/market-data/dynamic-reports/#BM-086.

[12] Keyu Jia, Chao Liu, Suhui Li, and Dongxiang Jiang. Modeling and optimization of a hybrid renewable energy system integrated with gas turbine and energy storage. *Energy Conversion and Management*, 279:116763, 2023.

[13] S. Shiva Kumar and Hankwon Lim. An overview of water electrolysis technologies for green hydrogen production. *Energy Reports*, 8:13793–13813, 2022.

[14] Xuan Liu, Gaoyang Liu, Jilai Xue, Xindong Wang, and Qingfeng Li. Hydrogen as a carrier of renewable energies toward carbon neutrality: State-of-the-art and challenging issues. *International Journal of Minerals, Metallurgy and Materials*, 29(5):1073–1089, 2022.

[15] Sandra Dermühl and Uwe Riedel. A comparison of the most promising low-carbon hydrogen production technologies. *Fuel*, 340:127478, 2023.

[16] Mohamed Nasser and Hamdy Hassan. Techno-enviro-economic analysis of hydrogen production via low and high temperature electrolyzers powered by pv/wind turbines/waste heat. *Energy Conversion and Management*, 278:116693, 2023.

[17] Torbjørn Egeland-Eriksen, Jonas Flatgård Jensen, Øystein Ulleberg, and Sabrina Sartori. Simulating offshore hydrogen production via pem electrolysis using real power production data from a 2.3 mw floating offshore wind turbine. *international journal of hydrogen energy*, 48(74):28712–28732, 2023.

[18] Hugo Groenemans, Genevieve Saur, Cortney Mittelsteadt, Judith Lattimer, and Hui Xu. Techno-economic analysis of offshore wind pem water electrolysis for h2 production. *Current Opinion in Chemical Engineering*, 37:100828, 2022.

[19] Malte Pfennig, Barbara Schiffer, and Tanja Clees. Thermodynamical and electrochemical model of a pem electrolyzer plant in the megawatt range with a literature analysis of the fitting parameters. *International Journal of Hydrogen Energy*, 2024.

[20] Siemens Silyzer. Silyzer 300 datasheet.
https://oapecorg.org/media/c28eb50d-a084-4fc2-bfc0-6b145196ebd8/-1206715591/%D9%86%D8%AF%D9%88%D8%A9%20%D8%A7%D9%84%D9%87%D9%8A%D8%AF%D8%B1%D9%88%D8%AC%D9%8A%D9%86/6_%20Dr%20Manul%20Kuehn.pdf.

[21] Pegah Mottaghizadeh, Mahshid Fardadi, Faryar Jabbari, and Jack Brouwer. Thermodynamic and Dynamic Analysis of a Wind-Powered Off-Grid Industrial Building Integrated With Solid Oxide Fuel Cell and Electrolyzer for Energy Management and Storage. *Journal of Electrochemical Energy Conversion and Storage*, 19(3):031003, 02 2022.

[22] Yongming Zhao, Huaqing Xue, Xu Jin, Bo Xiong, Renhe Liu, Yong Peng, Luyang Jiang, and Guohua Tian. System level heat integration and efficiency analysis of hydrogen production process based on solid oxide electrolysis cells. *International Journal of Hydrogen Energy*, 46(77):38163–38174, 2021.

[23] Aruna Chandrasekar, Damian Flynn, and Eoin Syron. Operational challenges for low and high temperature electrolyzers exploiting curtailed wind energy for hydrogen production. *International Journal of Hydrogen Energy*, 46(57):28900–28911, 2021.

[24] Anne Hauch, Rainer Küngas, Peter Blennow, Anders Bavnhøj Hansen, John Bøgild Hansen, Brian Vad Mathiesen, and Mogens Bjerg Mogensen. Recent advances in solid oxide cell technology for electrolysis. *Science*, 370(6513):eaba6118, 2020.

[25] Anne Hauch, Peter Gustav Blennow, Kim N. Dalby, Daniel Bovin Drasbæk, Thomas Heiredal-Clausen, Aiswarya Krishnakumar Padinjarethil, Giovanni Perin, Jeppe Rass-Hansen, Elena Marzia Sala, and Ramchandra Tiruvalam. The topsoe perspective: From electrode nanostructures to mw scaled soec systems. *ECS Transactions*, 111(6):1125, may 2023.

[26] Lateef A Jolaoso, Idris T Bello, Opeyemi A Ojelade, Abu Yousuf, Chuancheng Duan, and Pejman Kazempoor. Operational and scaling-up barriers of soec and mitigation strategies to boost h2 production-a comprehensive review. *International Journal of Hydrogen Energy*, 48(85):33017–33041, 2023.

[27] Jérôme Laurencin, D Kane, Gerard Delette, Jonathan Deseure, and Florence Lefebvre-Joud. Modelling of solid oxide steam electrolyser: Impact of the operating conditions on hydrogen production. *Journal of Power Sources*, 196(4):2080–2093, 2011.

[28] P Kazempoor and RJ Braun. Model validation and performance analysis of regenerative solid oxide cells for energy storage applications: Reversible operation. *international journal of hydrogen energy*, 39(11):5955–5971, 2014.

[29] Chaoyang Wang, Ming Chen, Ming Liu, and Junjie Yan. Dynamic modeling and parameter analysis study on reversible solid oxide cells during mode switching transient processes. *Applied Energy*, 263:114601, 2020.

[30] Tadeusz Chmielniak and Leszek Remiorz. Entropy analysis of hydrogen production in electrolytic processes. *Energy*, 211:118468, 2020.

[31] Paweł Trawiński. Development of real gas model operating in gas turbine system in python programming environment. *Archives of Thermodynamics*, pages 23–61, 2020.

[32] Sangjo Kim. Generating a virtual physical model through measurement data and reverse engineering: Applying a performance prediction model for an industrial gas turbine during start-up. *Applied Thermal Engineering*, 232:120927, 2023.

[33] Abhinav Anand Sinha, Tushar Choudhary, Mohd Zahid Ansari, and Anoop Kumar Shukla. Energy, exergy, and sustainability a novel comparison of conventional gas turbine with fuel cell integrated hybrid power cycle. *International Journal of Hydrogen Energy*, 47(80):34257–34272, 2022.

[34] Yousef Haseli, Ibrahim Dincer, and Greg F Naterer. Thermodynamic modeling of a gas turbine cycle combined with a solid oxide fuel cell. *International Journal of hydrogen energy*, 33(20):5811–5822, 2008.

[35] Donato Cecere, Eugenio Giacomazzi, Antonio Di Nardo, and Giorgio Calchetti. Gas turbine combustion technologies for hydrogen blends. *Energies*, 16(19), 2023.

[36] Nurettin Tekin, Mitsugu Ashikaga, Atsushi Horikawa, and Dr.-Ing. Harald Funke. Enhancement of fuel flexibility of industrial gas turbines by development of innovative hydrogen combustion systems. -, 04 2019.

[37] Guohui Song, Qi Zhao, Baohua Shao, Hao Zhao, Hongyan Wang, and Wenyi Tan. Life cycle assessment of greenhouse gas, ghg, and nox emissions of power-to-h2-to-power technology integrated with hydrogen-fueled gas turbine. *Energies*, 16(2), 2023.

[38] S Can Gülen, Raj Singh, and Pritam Banerjee. Hydrogen and gas turbines–a rational approach. In *Turbo Expo: Power for Land, Sea, and Air*, volume 86991, page V006T08A006. American Society of Mechanical Engineers, 2023.

[39] Reyhaneh Banihabib, Timo Lingstädt, Magnus Wersland, Peter Kutne, and Mohsen Assadi. Development and testing of a 100 kw fuel-flexible micro gas turbine running on 100 *International Journal of Hydrogen Energy*, 49, 07 2023.

[40] Charlotte Hussy. Electrolysis. https://ptx-hub.org/water-electrolysis-explained/.

[41] https://www.researchgate.net/figure/Plot-depicting-the-Butler-Volmer-equation-dependence-on-overpotential-ja-anodic-current_fig1_360805196.

[42] Andrea trovò. Energy storage engineering 2022-2023.

[43] A. Hauch and P. Blennow. Solid oxide electrolysis cells – interplay between operating conditions, fuel electrode overpotential and degradation. *Solid State Ionics*, 391:116127, 2023.

[44] Energy Education. Gas turbine. https://energyeducation.ca/encyclopedia/Gas_turbine.

[45] Jack Massih. An overview of brayton cycles. https://blog.softinway.com/an-overview-of-brayton-cycles/.

[46] A. Medina, J. M. Roco, and Antonio Hernández. Regenerative gas turbines at maximum power density conditions. *Journal of Physics D: Applied Physics*, 29:2802, 12 1996.

[47] Air Compressor Work. An overview of axial compressors. https://enggcyclopedia.com/2023/05/axial-compressor/.

[48] Air Compressor Work. An overview of centrifugal compressors. https://compressedair-intel.blogspot.com/2014/05/compressed-air-basics-part-11-other.html.

[49] Kawasaki Heavy Industries. Kawasaki launches world's first 1.8 mw class, 100 https://global.kawasaki.com/en/corp/newsroom/news/detail/?f=20230905_2781.

[50] Siemens. Silyzer 300. https://www.siemens-energy.com/global/en/home/products-services/product-offerings/hydrogen-solutions.html.

[51] Cantera organization. Cantera library. https://cantera.org/.

[52] Dmitry Pashchenko. Hydrogen-rich gas as a fuel for the gas turbines: A pathway to lower co2 emission. *Renewable and Sustainable Energy Reviews*, 173:113117, 2023.

[53] GasTurb organization. Gasturb software. https://www.gasturb.com/.

[54] Ian Halliwell. Preliminary engine design-a practical overview. In *34th AIAA/ASME/SAE/ASEE Joint Propulsion Conference and Exhibit*, page 3891, 1998.

[55] Günter Wilfert, Bernd Kriegl, Hermann Scheugenpflug, Jacques Bernard, Xavier Ruiz, and Serge Eury. Clean-validation of a high efficient low nox core, a gtf high speed turbine and an integration of a recuperator in an enviromental friendly engine concept. In *41st AIAA/ASME/SAE/ASEE Joint Propulsion Conference & Exhibit*, page 4195, 2005.

[56] Z. Abdin, C.J. Webb, and E.MacA. Gray. Modelling and simulation of a proton exchange membrane (pem) electrolyser cell. *International Journal of Hydrogen Energy*, 40(39):13243–13257, 2015.

[57] Y Wang, B Zu, R Zhan, Q Du, M Ni, and K Jiao. Three-dimensional modeling and performance optimization of proton conducting solid oxide electrolysis cell. *Fuel Cells*, 20(6):701–711, 2020.

[58] Multiphly data sheet. 2.6 mw soc electrolyzer. https://www.sunfire.de/en/hydrogen.

[59] A. Banerjee, Y. Wang, J. Diercks, and O. Deutschmann. Hierarchical modeling of solid oxide cells and stacks producing syngas via h2o/co2 co-electrolysis for industrial applications. *Applied Energy*, 230:996–1013, 2018.

[60] Nikolaos Skordoulias, Efthymia Ioanna Koytsoumpa, and Sotirios Karellas. Techno-economic evaluation of medium scale power to hydrogen to combined heat and power generation systems. *International Journal of Hydrogen Energy*, 47(63):26871–26890, 2022.

[61] Alex Badgett, Joe Brauch, Amogh Thatte, Rachel Rubin, Christopher Skangos, Xiaohua Wang, Rajesh Ahluwalia, Bryan Pivovar, and Mark Ruth. Updated manufactured cost analysis for proton exchange membrane water electrolyzers. Technical report, National Renewable Energy Laboratory (NREL), Golden, CO (United States), 2024.

[62] Cassidy Houchins, Brian D James, and Yaset Acevedo. Hydrogen storage cost analysis. *United States Department of Energy: Washington, DC, USA*, 2022.

[63] International Renewable Energy Agency. Hydrogen from renewable power. https://www.irena.org/-/media/Files/IRENA/Agency/Publication/2018/Sep/IRENA_Hydrogen_from_renewable_power_2018.pdf https://hidrogenoaragon.org/en/proyectos/sh2amrock-2/.

[64] Sustainable Energy Authority of Ireland. Energy price trends. https://www.seai.ie/data-and-insights/seai-statistics/prices/.

[65] European Union and Aragòn foundation. Sh2amrock project. https://cordis.europa.eu/project/id/101112039 https://hidrogenoaragon.org/en/proyectos/sh2amrock-2/.